Quaternary Evolution of the Drainage Systems in the Southern and Central North Sea Basin Deduced from High Resolution Reflection Seismic and Sedimentological Data

Kumulative Dissertationsarbeit

Ayobami Abegunrin

MARUM – Center for Marine Environmental Sciences,

Universität Bremen

zur Erlangung des Grades
-Doctor rer. nat.-

November 2022

Gutachter: Prof. Dr. Tobias Mörz (Universität Bremen, Germany)
Dr. Katrine Juul Andresen (Aarhus University, Denmark)

Advisor: Dr. Daniel A. Hepp (Niedersächsisches Institut für historische Küstenforschung, Wilhelmshaven, Germany)

Erste Version eingereicht am: 19 Juli, 2022

Tag der mündlichen Prüfung: 04 Nov. 2022

Überarbeitete Version eingereicht am: 21 Nov. 2022

Versicherung an Eides Statt

gem. §5 Abs. 5 der Promotionsordnung vom 15.07.2015

Ich, Ayobami Abegunrin, wohnhaft in Bremen, Germany,

versichere an Eides Statt durch meine Unterschrift, dass ich die vorstehende Arbeit selbständig und ohne fremde Hilfe angefertigt und alle Stellen, die ich wörtlich oder dem Sinne nach aus Veröffentlichungen entnommen habe, als solche kenntlich gemacht habe, mich auch keiner anderen als der angegebenen Literatur oder sonstiger Hilfsmittel bedient habe, und die zu Prüfungszwecken beigelegte elektronische Version der Dissertation mit der abgegebenen gedruckten Version identisch ist.

Ich versichere an Eides Statt, dass ich die vorgenannten Angaben nach bestem Wissen und Gewissen gemacht habe und dass die Angaben der Wahrheit entsprechen und ich nichts verschwiegen habe.

Die Strafbarkeit einer falschen eidesstattlichen Versicherung ist mir bekannt, namentlich die Strafandrohung gemäß §156 StGB bis zu drei Jahren Freiheitsstrafe oder Geldstrafe bei vorsätzlicher Begehung der Tat bzw. gemäß §161 Abs. 1 StGB bis zu einem Jahr Freiheitsstrafe oder Geldstrafe bei fahrlässiger Begehung.

Bremen, den 21.11.2022

Acknowledgements

I thank the Almighty God, who not only gave us the ability to make wealth, but also, the capacity and capability to acquire knowledge. My express gratitude goes to Prof. Dr. Tobias Mörz for given me the opportunity to further my academic pursuits under his tutelage. Special thanks to Dr. Daniel A. Hepp, who did not only co-supervise my work, but also critically read all versions of my drafts from a reviewer point of view. Financial support received from the Nigerian Petroleum Technology Development Fund (PTDF) and the German Academic Exchange Service (DAAD) went a long way in the realization of this milestone.

I am indebted to all my family members back in Nigeria: `Bunmi (mum) and siblings `Funmi, Opeyemi and Julius, my In-laws: Liz (mother), Priscilla and Paul for their unwavering love and support systems. To my nieces: Treasure, Gold and Flourish Adaramola, thanks for the beautiful memories. My mother, ´Bunmi, against all odds, sacrificed all in order to channel my path. I also remember my father, Elder Samson Ayofe Abegunrin, and Father In-Law, Elder Mattew Olunlade Ayoola, both of blessed memories. Grateful heart to Olatunde Salami who became a family far away from home. Many thanks to ´Seun Tanimomo, who took great delights in proof reading some versions of my manuscripts.

Unreserved gratitude goes to all members (both past and present) of the Marine Engineering Geology working group at MARUM for their support and an enabling working environment. Words are not enough to thank Dr. Olatunbosun Alao and Dr. Wasiu Odufisan, who at different times, saw me as a young prodigy, picked me up, mentored and engrained in me the genetics you see today. I am eternally grateful for all you did for me. I greatly acknowledged everyone who directly or indirectly contributed to this landmark achievement.

These acknowledgements will be incomplete if I fail to mention my dear wife, Oluwatobi Grace Abegunrin for her practical and emotional supports through both the good and bad times. In a special way, I say ´Herzlichen Dank´ for your kind understanding as I added the roles of a husband and father to the demands of study, work, personal developments and other related/unrelated commitments.

Executive Summary

The North Sea shelf is one of the classic regions for studying Quaternary depositional and erosional sedimentary structures formed by discharging melt-water from retreating ice sheets and fluvial processes during periglacial shelf exposure. This provides an avenue to unravel the complex interplay between shelf morphology, changes in hydrodynamic regime, sediment influx and climate-driven eustatic changes. The ongoing political energy transition has prompted an intense geo-survey and sampling of the North Sea floor largely by industrial organizations, various Federal agencies such as the German Federal Maritime and Hydrographic Agency (BSH), German Federal Institute for Geosciences and Natural Resources (BGR) as well as some scientific institutions. The wealth of acquired data in the course of these various commercial, governmental and scientific expeditions has led to an improved understanding of the Quaternary geology of the North Sea sub-surface. Using a combination of tidally corrected acoustic profiles, shallower and deeper sediment cores and cone penetration test (CPT) data acquired from the German North Sea sector, this doctoral thesis aimed at contributing to the ongoing understanding of the morphology, the development of the drainage systems and the palaeo-landscape of the North Sea shelf since the Last Glacial Maximum. It also aimed at refining the stratigraphy and the geotechnical properties of the highly competent shallow sand units in the southern North Sea.

The study unraveled the evolution, morphology and valley infill successions of the Elbe Palaeovalley (EPV). The EPV, located in the southeastern North Sea, occur as a shallow geomorphological trough spanning a length of about 210 km and width of about 40 km. The valley base is about 65 m below the present day sea-level. During the Marine Isotope Stage 2 sea level lowstand, this SE-NW oriented palaeo-drainage evolved as a braided fluvial system in a periglacial environment. Seismo-stratigraphic interpretation of the EPV infill successions revealed five major units. During deglacial sea-level rise, the EPV evolved into an estuary with tributaries, intertidal and subtidal flats. Towards the western flank of the EPV, the Palaeo-Ems, one of the known major tributaries that fed the southern head of the EPV was also identified and its overall course was seismo-stratigraphically described. The Palaeo-Ems river course was mapped as a buried, low gradient and meandering channel branching into two major pathways as it approaches a newly discovered delta flat at the western flank of the EPV. In its downstream direction, the Palaeo-Ems formed a unified depositional system with the early phase of the EPV. Based on available data, this study also shed light on the Palaeo Ems/EPV morpho-stratigraphic relationship for the first time. Ongoing sea-level rise since the early Holocene overwhelmed the adaptation capabilities of the joint system leading to the drowning of the whole drainage system.

By focusing on the less well understood, regionally dominant sand units which were deposited after the retreat of the last glaciers, this study also refined the stratigraphic units and geotechnical parameters of the uppermost 50 m below the sea floor within the German North Sea sector. Two sandy units, the Aeolian Member and the Upper Fluvial Member, were identified as dominant deposits in the late- to post-Saalian geology within the study area. In addition, a detail seismic analysis revealed the occurrence of a Saalian Buried Valley Member believed to comprise fluvial deposits. Based on the integration of seismic facies analysis with core and CPT data, a detailed geotechnical parameter set for each identified stratigraphic unit within the study area was developed and correlated with those of the neighboring North Sea sectors. The findings from this study complements and details Coughlan *et al*. (2018) geotechnical and stratigraphic framework of the study area as well as the stratigraphic framework recently developed by the BSH (2021). These deductions offer a new insight about the soil competency of the North Sea sub-surface which is key for various offshore commercial and economic activities within the region including but not limited to wind farm developments.

The findings from this study are thus crucial contributions in understanding the dewatering system and subsequently, the reconstruction of the palaeo-landscape development in the German North Sea sector since the Last Glacial Maximum. Lastly, the study contributes to an improved geotechnical understanding of the stratigraphy of the North Sea.

Zusammenfassung

Der Nordseeschelf ist eine der klassischen Regionen für die Untersuchung quartärer Ablagerungs- und Erosionsstrukturen, die während des Rückzugs der Eisschilde durch den Abfluss von Schmelzwässer und während periglazialer Umweltbedingungen auf dem unvergletscherten Schelf durch fluviale Prozessen entstanden sind. Deshalb bietet sich hier die Möglichkeit, das komplexe Zusammenspiel zwischen Schelfmorphologie, Veränderungen im hydrodynamischen Regime, Sedimentzufluss und klimabedingten eustatischen Veränderungen zu entschlüsseln. Die aktuelle politische Energiewende hat eine intensive Vermessung und Beprobung des Nordseebodens ermöglicht, die überwiegend von Seiten der Industrie, verschiedene Bundesbehörden, wie das Bundesamt für Seeschifffahrt und Hydrographie (BSH) und die Bundesanstalt für Geowissenschaften und Rohstoffe (BGR) und einige wissenschaftliche Einrichtungen durchgeführt wurde. Die Fülle der Daten, die im Rahmen dieser verschiedenen kommerziellen, staatlichen und wissenschaftlicher Expeditionen gewonnen wurden, haben wesentlich zu einem besseren Verständnis der Quatärgeologie des Nordseeuntergrundes beigetragen. Mit Hilfe einer Kombination aus gezeitenkorrigierten akustischen Profilen, flach- und tiefgründigen Sedimentkernen und Messdaten von Drucksondierungen (CPT) aus dem Gebiet der deutschen Nordsee, will diese Dissertation einen Beitrag zum Verständnis der Morphologie, der Entwicklung der Entwässerungssysteme und der Paläolandschaft des Nordseeschelfs nach dem Letzteiszeitlichen Maximum leisten. Außerdem sollen die Stratigraphie und die geotechnische Eigenschaften hochkompetenter flacher Sandeinheiten in der südlichen Nordsee verfeinert werden.

Die Studie entschlüsselte die Entwicklung, den morphologischen Aufbau und die Abfolge der Verfüllung des Elbe-Urstromtals (EPV). Das EPV, das sich in der südöstlichen Nordsee befindet, ist ein flacher geomorphologischer Trog mit einer Länge von etwa 210 km und einer Breite von etwa 40 km. Die Talsohle liegt etwa 65 m unter dem heutigen Meeresspiegel. Diese SE-NW-verlaufende Urstromtal, das ursprünglich als ein verflochtenes Flusssystem begann, entwickelte sich während des Meeresspiegeltiefstandes des Marinen Isotopenstadiums 2 in einer periglazialen Umgebung. Die seismo-stratigraphische Interpretation der Verfüllungsabfolgen des EPV ergab fünf Haupteinheiten. Während des warmzeitlichen Meeresspiegelanstieges entwickelte sich das EPV zu einem Ästuar mit Nebenflüssen und intertidalen und subtidalen Zonen. An der Westflanke des EPV wurde die sogenannte Ur-Ems, einer der belegten Hauptzuflüsse, die den Oberlauf des EPV im Süden speiste, identifiziert und ihr Gesamtverlauf seismo-stratigraphisch beschrieben. Die Ur-Ems konnte als ein heute vergrabener mäandrierender Flusslauf kartiert werden, der ein geringes Gefälle aufweist. Der Flusslauf verzweigt sich schließlich im Bereich einer neu entdeckten Deltaebene an der Westflanke des EPV in zwei Hauptarme. Flussabwärts gerichtet bildete

die Ur-Ems mit der frühen Phase des EPV ein einheitliches Ablagerungssystem. Auf der Grundlage der verfügbaren Daten, beleuchtet diese Studie erstmals die morphologisch-stratigraphische Beziehung zwischen Ur-Ems und EPV. Der kontinuierliche Anstieg des Meeresspiegels seit dem frühen Holozän hat die Anpassungsfähigkeit des gemeinsamen Systems überfordert, was zum Ertrinken des gesamten Entwässerungssystems führte.

In Hinblick auf die weniger gut bekannten, regional vorherrschenden Sandpakete, die nach dem Rückzug der letzten Gletscher abgelagert wurden, konnten mit dieser Studie auch die stratigraphischen Einheiten und geotechnischen Parameter der obersten 50 m des Meeresboden der deutschen Nordsee eingehender beschrieben werden. Für das Untersuchungsgebiet wurden dabei zwei Sandeinheiten, das sogenannte Aeolian Member und das Upper Fluvial Member, als dominierende geologische Ablagerungen der Spät- und Nachsaalezeit bestimmt. Zusätzlich deckte eine detaillierte seismische Analyse eine weitere Einheit auf, das sogenannte Saalian Buried Valley Member, welches mit fluvialen Ablagerungen verfüllt ist. Basierend auf der Integration von Bohrkern- und CPT-Daten in die seismische Faziesanalyse wurde ein detaillierter geotechnischer Parametersatz für jede identifizierte stratigraphische Einheit innerhalb des Untersuchungsgebiets entwickelt und mit den Einheiten der benachbarten Nordseesektoren korreliert. Die Ergebnisse dieser Studie ergänzen und verfeinern die geotechnischen und stratigrafischen Ergebnisse von Coughlan et al. (2018) im selben Untersuchungsgebiet sowie ein kürzlich vom BSH (2021) entwickelte Stratigrafie. Diese Ableitungen bieten einen neuen Einblick in die Kompetenz des Untergrundes der Nordsee, der für verschiedene kommerzielle und wirtschaftliche Offshore-Aktivitäten in der Region von entscheidender Bedeutung ist, einschließlich, aber nicht beschränkt auf die Entwicklung von Windparks.

Die Ergebnisse dieser Studie liefern somit einen entscheidenden Beitrag zum Verständnis des Entwässerungssystems und nachfolgend der Rekonstruktion der Paläolandschaftsentwicklung seit dem Letzteiszeitlichen Maximum im deutschen Nordseesektor. Nicht zuletzt trägt sie zu einem verbesserten geotechnischen Verständnis der Stratigraphie der Nordsee bei.

Thesis outline & contribution declaration

This section briefly outlines the structure of this thesis as well as a concise summary of the scientific findings that stemmed out of the PhD project. The three publications and one manuscript from this study are reprinted in full text as chapters 2 to 5. Chapter 2 is already published. A former version of the Elbe Palaeovalley manuscript (Chapter 3) was published in the cumulative thesis by Asli Özmaral (Özmaral, 2017). The current version of the manuscript has been extensively/carefully revised, brought up to the latest scientific standard and was successfully submitted for publication by the author of this thesis. This chapter has now been published. The revised version of the manuscript in chapter 4 is ready for submission for publication. The publication in chapter 5 was carefully revised, updated and submitted by the author of this thesis. The latter publication is also part of the cumulative thesis by Matthias Fleischer (in prep.). All the papers are either published or ready for submission in peer-reviewed journals.

The findings from these various studies focus on tidal correction on high resolution 2D seismic data and its application in understanding and unravelling the evolution of the drainage systems that developed in the German North Sea sector since the Last Glacial Maximum. The study also contributed to the revised stratigraphy of the German North Sea Quaternary deposits as well as its geotechnical characteristics. Each chapter and a detailed contribution of all co-authors are described as follows:

Chapter 1 encompasses a brief background to the study and study area, research objectives as well as the data base. Thereafter, an overview of the adopted methodology was also presented.

Chapter 2 devised a methodology for computing offsets i.e. variations from a reference datum, using a more precise differential global positioning system (dGPS) to account for the influence of water column height variations on seismic data acquired from the German sector of the North Sea. This chapter has been published in *Scientific Reports* as follows:

Abegunrin, A., Hepp, D. A., Mörz, T. (2020). **Correction of water column height variation on 2D grid high resolution seismic data using dGPS based methodology**. Scientific Reports 10: 18760. https://doi.org/10.1038/s41598-020-75740-z

Author contributions

T.M. conceived the basic idea of the methodology. D.A.H. was chief of the HE499 expedition during which the data sets used in this study were acquired, T.M. participated in the data acquisition. A.A. implemented the idea of

the methodology using the acquired data, wrote the full manuscripts and effected all corrections and contributions from D.A.H. and T.M. All authors contributed to the revised manuscript.

Chapter 3 employed a detailed interpretation of high-resolution seismic profiles and core data acquired from the German North Sea sector in unravelling the evolution, morphology and valley infill successions of the Elbe Palaeovalley and its hydrodynamic regime since the late Pleistocene. This chapter has been published in *Quaternary Science Reviews* as follows:

Özmaral, A., Abegunrin, A., Keil, H., Hepp, D. A., Schwenk, T., Lantzsch, H., Mörz, T., Spiess, V. (2022). **The Elbe Palaeovalley: evolution from an ice-marginal valley to a sedimentary trap (SE North Sea).** Quaternary Science Reviews 282, 107453. https://doi.org/10.1016/j.quascirev.2022.107453

Author contributions

The project was conceived by the authors. AÖ and HK led the multi-channel seismic and sediment echo-sounder data acquisition. AÖ carried out the seismic data processing and interpretation. MSCL core logging was done by AÖ and DAH while 14C dating samples were selected and treated by AÖ with the help and utilities provided by HL. TM and DH helped in developing an evolutionary conceptional model of events. All authors participated in the discussion of results. HL contributed a constructive internal first review with own additions. The full manuscript and its structural design were done by AÖ while AA provided some key amendments to some sections and also integrated recently published articles. AÖ and AA, at different times, effected all comments and contributions from all co-authors. AA revised the manuscript based on comments from the reviewers.

Chapter 4 employed a detailed interpretation of tidally corrected, high resolution 2D seismic profiles in tracking the overall course of the Palaeo Ems channel as well as its spatial and stratigraphic relationship with other palaeo structures within the study area with emphasis on the Palaeo Ems/Elbe Palaeovalley stratigraphic and morphologic relationship. This chapter is ready for submission to *Journal of Geophysical Research* as follows:

Abegunrin, A., Hepp, D. A., Mörz, T. **The Palaeo-Ems River in its Quaternary stratigraphic context**

Author Contributions

The project was conceived by the authors. D.A.H. head the HE499 sea cruise during which part of the data sets used in this study were acquired and T.M. participated in the data acquisition. A.A. carried out the data processing where applicable, interpreted the data sets, wrote the full manuscript and incorporated corrections and contributions from D.A.H. and T.M. All authors contributed to the revised manuscript.

Chapter 5 employed a combination of shallow seismic reflection surveys, ~50 m long sediment cores and cone penetration tests (CPT) data in refining the stratigraphic units and geotechnical parameters of the uppermost 50 m below the sea floor within the German North Sea sector. This chapter has been published in *Boreas* as follows:

Fleischer, M., Abegunrin, A., Hepp, D. A., Kreiter, S., Coughlan, M., Mörz T. (2022). **Stratigraphic and geotechnical characterization of regionally extensive and highly competent shallow sand units in the southern North Sea.** Boreas. https://doi.org/10.1111/bor.12595

Author Contributions

The project was conceived by MF, DAH, SK, MC and TM. MF and AA are involved in the data analysis, writing the full manuscript and implementing the comments and corrections from DAH, SK, MC and TM. All authors contributed to the revised manuscript.

Chapter 6 recapitulates the main conclusions deduced from this doctoral thesis alongside recommendations for future works.

Table of Contents

List of Figures

List of Tables

Chapter 1

Introduction

1.1. Background to the Study

In the last couple of decades, extensive high quality geophysical, core, paleoenvironmental and sedimentological data has been utilized by different scientists in understanding the former landscape appearances, dewatering systems, structural architecture and stratigraphy of the German North Sea sector and adjacent areas (Lutz *et al*., 2009; Hepp *et al*., 2012, 2017, 2019; Stoker *et al*., 2010; Stewart *et al*., 2013; Coughlan *et al*., 2018; Lohrberg *et al*., 2020; Papenmeier and Hass, 2020; Winsemann *et al*., 2020; Prins *et al*., 2019, 2020; Andresen *et al*., 2022). Shallow coasts such as the southern North Sea region are excellent palaeo-archives of past geological records and historical documentations which result from changing sea level. Prior to been submerged after the last glaciation and at a time of lower sea level than today, the North Sea areas are fertile lowlands more favorable for hunters and gatherers. The Quaternary period thus played an active role in sculpting the North Sea landscape as well as its palaeo-environmental conditions. The retreat of the ice sheets after the Last Glacial Maximum (LGM) resulted in the formation of palaeo-valleys and other comparable structures which did not only played a major role in the drainage system of the area but also hold a wealth of geomorphological, sedimentological and archeological information which are well preserved in them (Gaffney *et al.,* 2009, 2020; van Heteren *et al.,* 2014; Hepp *et al.,* 2017; Coughlan *et al*., 2018; Bailey *et al*., 2020).

In more recent times, an understanding of the distribution, orientation and composition of the various palaeo-structures is critical in modelling sub-surface sub-soil competency and the schematic development of palaeo-landscape architecture. These models are also important for various offshore commercial and economic activities within the region including but not limited to wind farm development, laying of submarine cables and pipelines, offshore sand mining and hydrocarbon engineering installations (BSH 2021; Weihrauch *et al*., 2009). The North Sea shelf has thus been subjected to various palaeo-reconstruction since the LGM. In this thesis, the German sector of the North Sea (Fig. 1.1) was investigated within the Marine Engineering Geology working group North Sea shelf project at MARUM – Center for Marine Environmental Sciences, University of Bremen, Germany. Subject of the thesis is to contribute to the current understanding as well as palaeo-reconstruction of the former landscape architecture and drainage systems of the German North Sea shelf since the LGM using tidally corrected seismo-acoustic and sedimentological data sets.

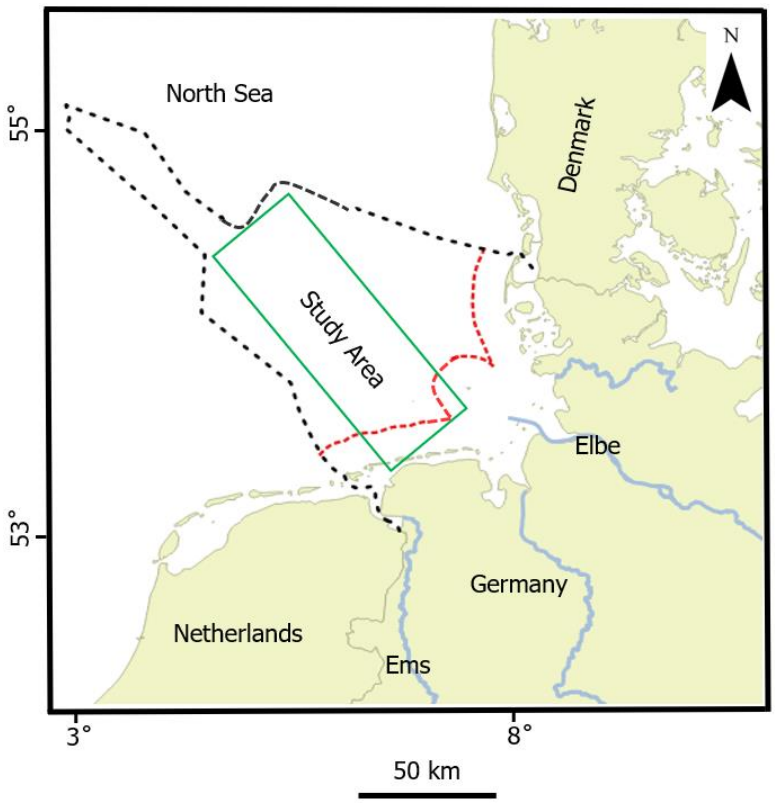

Fig. 1.1. Location of study area within the German North Sea sector. The black dash line is the German Exclusive Economy Zone while the red dotted line is the Territorial Waters (12 nautical miles). The study area is marked in green rectangle.

The findings from this study also reveals in detail the Pleistocene stratigraphy of an interval that is becoming increasingly important for geotechnical and engineering purposes as part of the ongoing energy transition.

1.2. Study Area – North Sea

1.2.1. Geological development of the North Sea basin

The North Sea is a shallow epicontinental sea situated in the northwest European continental shelf between the islands of Great Britain and the European. The water depth is generally <100 m with some deep patches ranging from about 200 m to 400 m occurring along the northern margin shelf edge and in the Norwegian Channel (Graham *et al*., 2011). The modern North Sea configuration is a result of successive filling of the NW-SE trending Mesozoic Central Graben (Ziegler 1990; Nielsen *et al*., 2009). The main rifting was followed by subsequent thermal cooling and subsiding structure provided accommodation space for sediment input from the Fennoscandia and central Europe (Huuse *et al*., 2001; Gołedowski *et al*., 2012). This subsidence continued during the Pliocene and Quaternary periods (Cameron *et al*., 1987; Rasmussen *et al*., 2005; Ottesen *et al*., 2014).

The pre-Quaternary geology of the North Sea basin can be followed back to the early Permian. During this time, the study area together with the central European basin system were almost entirely characterized by a low

topography (Maystrenko *et al*., 2008). The area has since experienced a minimum of four major tectonic cycles with its present-day geometry being a result of about 300 million years of sedimentation (Cameron *et al*., 1987; Pharaoh, 1999; Bradwell *et al*., 2008). The Caledonian (McCann 2008; Pharaoh 1999), Variscan (McCann, 2008; McCann *et al*., 2006) and Alpine (Littke *et al*., 2008) orogenic events represent key orogeny phases that shaped the development of the North Sea (Fig. 1.2). The late Permian phase was dominated with the deposition of more than 2000 m Zechstein evaporites at the basin depositional center (Ziegler 1990; Maystrenko *et al*., 2008). Clastic sedimentation coupled with predominantly chalk, coral reefs and shales deposition continued from the Triassic through to the Cretaceous. However, at the end of Jurassic, the sea retreated briefly causing a widespread unconformity as a result of a major sea level drop (Maystrenko *et al*., 2008). During these periods, extensional events resulted in the initiation, halokinesis and subsequent re-advancement of the evaporites. The Zechstein evaporites were thus remobilized in the course of their burial history and formed extensive salt diapirs in the southern and central North Sea areas (Jenyon 1988; Stewart and Coward 1995; Strozyk *et al*., 2017; Vejbæk 1997). These diapirs are variable in height and generally influenced subsequent deltaic deposition by either reducing the accommodation space over the crests or by adding accommodation space in the form of a syncline in between adjacent structures (Maystrenko *et al*., 2005). The Tertiary was in turn marked by post rift subsidence with the deposition of siliclastics derived from the adjacent continental areas (Cameron *et al*., 1987; Gatliff *et al*., 1994). From the middle Miocene to the Pleistocene, deposition of sediments in the southern North Sea was dominated by an east-west advancing Eridanos delta system (Fig. 1.3; Overeem *et al*., 2001). The development of this depositional system has been the subject of many scientific studies (Sørensen *et al*., 1997; Overeem *et al*., 2001; Kuhlmann 2004). This period was characterized by about 3000 m thick prograding deltaic sediments whose main feeder systems varied over time, stretching from Denmark through northern Germany and the Netherlands to England (Huuse 2002; Overeem *et al*., 2001; Michelsen *et al*., 1995, 1998). Extensive ice sheets during the Quaternary left behind a wide range of preserved landforms including glacio-tectonic thrust complexes and sediment accumulations reaching in excess of 1000 m in the deepest part of the Basin (Caston 1977; Gatliff *et al*., 1994).

1.2.2. Quaternary History of the North Sea

The North Sea Quaternary sediments overlay older and compacted sands deposited during the late Neogene/early Pleistocene (Cameron *et al*., 1987; Streif 2004; Kuhlmann *et al*., 2006). High degree of lateral and vertical complexity characterized this Quaternary cover resulting in facies assemblages which are localized and heterogeneous in nature. Lateral basin-wide correlation of individual Quaternary successions is therefore often

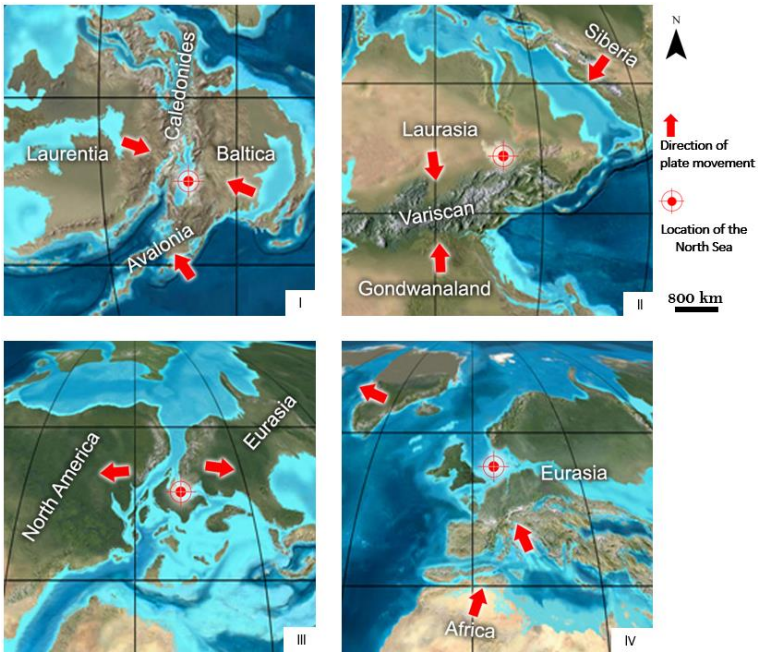

OROGENIC PHASE	REMARKS
CALEDONIAN (I) (510-390 Ma) Ordovician - Early Devonian	• Collision of Laurentia, Baltica and Avalonia • Predominantly compressional regime
VARISCAN (II) (380-250 Ma) Late Devonian – Permian	• Two-plate convergence (Laurasia and Gondwanaland) • All major continents collided to form Pangaea in Permian
KIMMERIAN (III) (240-120 Ma) Triassic – Early Cretaceous	• Breakup of Pangaea • Major rifting • Halokinesis in the North Sea
ALPINE (IV) (110 Ma - Present) Late Cretaceous – Holocene	• Regional subsidence • Inversion • Salt tectonics

Fig. 1.2. Plate tectonic evolution of the North Sea (Adapted from Frisch *et al*., 2011).

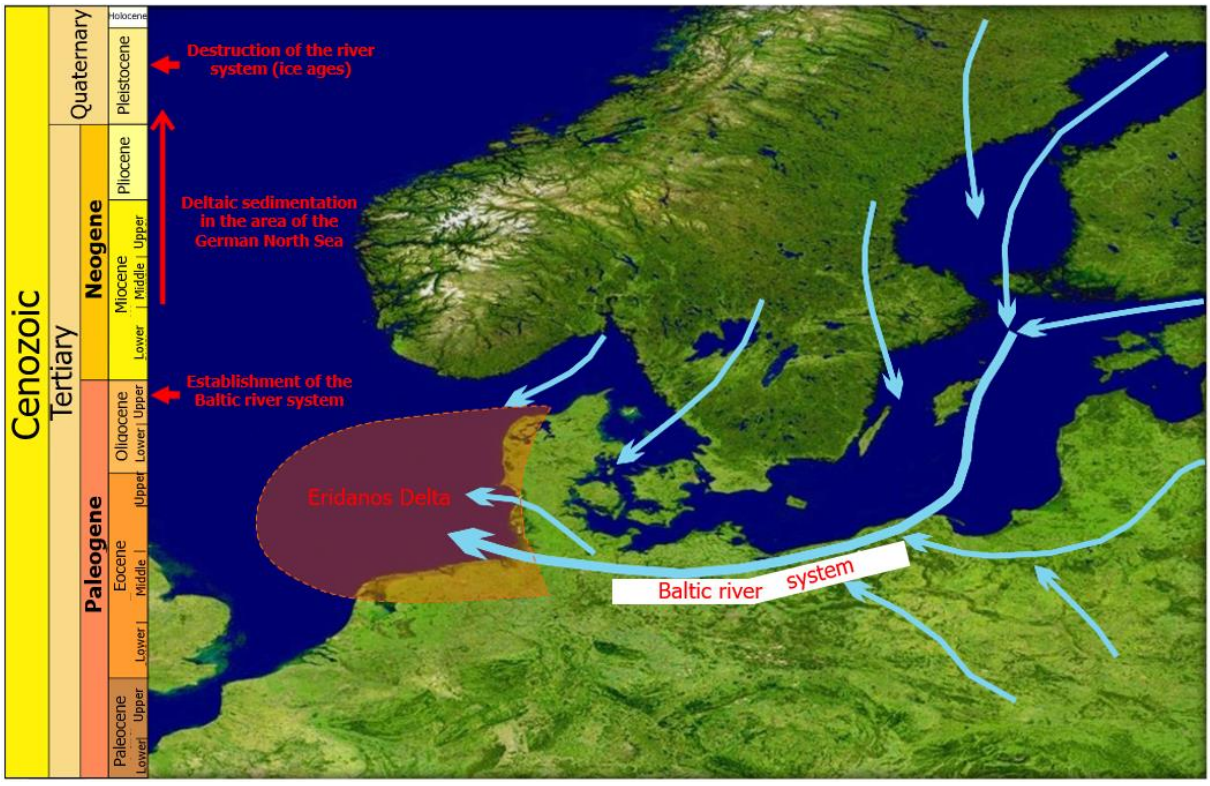

Fig. 1.3. Europe satellite image showing the Eridanos fluvio-deltaic system (GPDN 2022).

difficult due to the localized heterogeneity of each succession. The complex North Sea Quaternary deposits can thus be explained by understanding its history characterized by repeated ice advances which are separated by marine transgressions. Limited evidences of older glaciation episodes have been documented on- and offshore NW Europe based on studying of moraine fronts and tills (Gibbard 1988; Carr 2004; Graham *et al*., 2011; Lee *et al*., 2012; Buckley 2012, 2017). This was due to the fact that the onshore regions are particularly susceptible to subsequent glacial erosion while the offshore regions still remain under-studied (Bendixen *et al*., 2017). Traditionally, the Elsterian (MIS 12, oldest), Saalian (MIS 10 - 6) and Weichselian (MIS 5d – 2, youngest) glaciations represents the last known three major glaciation episodes that are widespread in the North Sea (Table 1.1; Gibbard and Cohen, 2008; Toucanne *et al*., 2009). The Weichselian glaciation however have the least southward extension and never extended as far south as the German North Sea sector (Fig. 1.4; Cameron *et al*., 1987; Streif 2004; Kuhlmann *et al*., 2006, Graham *et al*., 2011; Lee *et al*., 2012). Each glacial phase shows varying glacial intensity and a total of 6 major ice advances have been identified to reach the northern German lowlands. Two of these ice advances are in the Elsterian (MIS 12; Ehlers *et al*., 2011; Roskosch *et al*., 2015; Lang *et al*., 2018), three in the Saalian (MIS 6 and 8; Ehlers *et al*., 2011; Eissmann 2002; Lang *et al*., 2018) and the last one at the Last Glacial Maximum (MIS 2) during the Weichselian (Ehlers *et al*., 2011). During these glaciation periods, global marine waters are locked up in terrestrial ice with the sea level in the region of 110-130 m lower than that of the present-day (Cronin, 2012). These glaciation episodes are separated by warmer interglacial episodes (Holsteinian, Eemian and Holocene) which are marked by higher sea level and considerable transgression (Sindowski 1970; Streif 2004; Litt *et al*., 2007).

Based on current understanding of the North Sea, the complex late Saalian and Weichselian (MIS 6-MIS 2) history are now well understood while the Elsterian and early Saalian (MIS 12-MIS 10) are less well constrained chronologically although the North Sea area was generally believed to be repeatedly covered by large ice sheets during these periods (Graham *et al*., 2011; Lee *et al*., 2012; Moreau *et al*., 2012; Stewart *et al*., 2012). The Elsterian is represented by an unconformity (Table 1.1) occurring at a general depth of <50 m (Streif 2004) and also marked a major switch in sedimentation from non-glacial to predominately glacial deposition. This period is also dominated by extensive valley formation (tunnel valleys) which incised early Pleistocene and Tertiary deposits spanning a length of more than 100 km, width of 8 km and incised depth of about 500 m in some cases (Cameron *et al*., 1987; Wingfield 1990; Ehlers and Wingfield, 1991; Huuse and Lykke-Andersen, 2000; Lutz *et al*., 2009; Prins *et al*., 2020). The valleys are filled by relatively fine-grained meltwater sands with small quantities of basal gravels (Grube *et al*., 1986; Smed 1998; Ehlers *et al*., 2011), tills from the glacier base (Richter 1962; Ehlers *et*

Table 1.1. Simplified glacial history of the central North Sea showing the Quaternary glacial–interglacial stages (Bendixen *et al*., 2017).

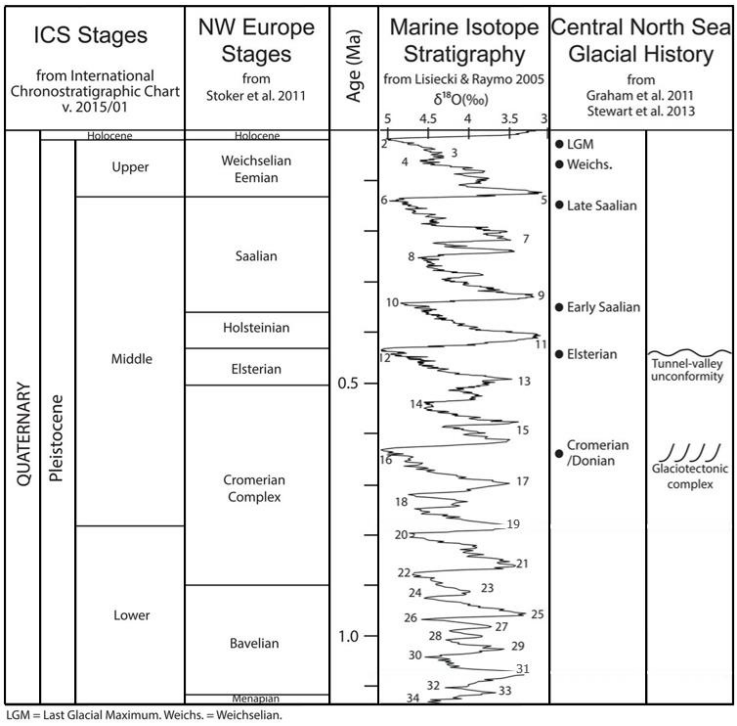

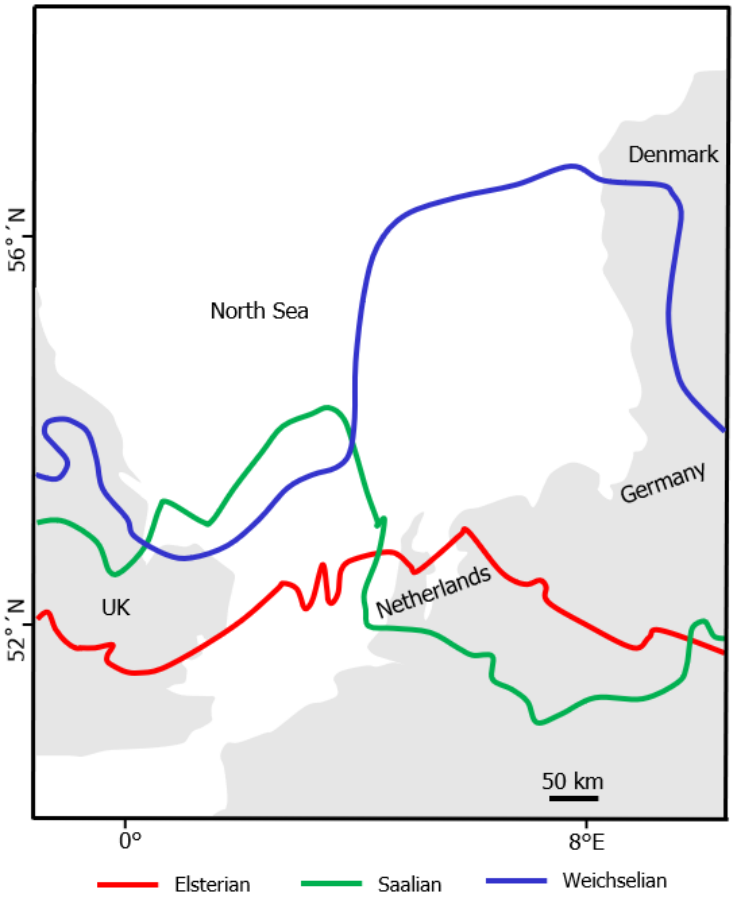

Fig. 1.4. Composite map showing the maximum extent of each of the major glaciation episode in the North Sea (modified after Ehlers and Gibbard, 2004; Emery *et al*., 2019).

al., 1984; Ehlers and Linke, 1989) and Lauenburg clay which provided the most useful stratigraphic marker from the Elsterian (Ehlers *et al*., 1984). In late Elsterian valleys, the stratigraphy infills revealed that the glacial deposits generally grade up into the marine and glaciomarine facies with arctic-boreal fauna of the early Holsteinian marine transgression. Offshore southern North Sea, Holstein deposits form a 25 m to a locally 40 m thick discontinuous unit of very fine, fine to medium-grained marine sand with bands of silt and clay with marine shells (Cameron *et al*., 1987). This period finished with climate deterioration at the onset of the Saalian (Hepp *et al.*, 2012). The subsequent Saalian complex was characterized by multiple climatic oscillations defining at least three Saalian advances with a minimum of one warm interglacial event in Northern Europe (Ehlers *et al*. 1984, 2011; Grube *et al*. 1986; Piotrowski 1994). Different depositional successions of Saalian age has also been identified and correlated across various parts of Northern Europe and their various extents and dynamics are well documented in literature (Ehlers 1990; Ehlers *et al*., 2011; Coughlan *et al*., 2018). The infill stratigraphy of the Saalian tunnel valleys are characterized by till of the first Saalian glacial sequence, meltwater sands that accumulated in vast outwash fans (Ehlers *et al*., 1984; Ehlers *et al*., 2004). While there is a limited information about the following Eem interglacial from offshore cores, Eemian deposits of varying thickness have been retrieved from various sites in the southernmost North Sea and adjacent areas such as the coast of Belgium. These Eemian deposits consists of shallow marine to intertidal fine- to medium grained, sometimes gravelly sands with shells, homogenous silty clays, sandy silts with characteristic foraminifera (Cameron *et al*., 1987; Konradi *et al*., 2005; Knudsen 1988; Somme 1979). During the Weichselian, intense climatic deterioration resulted in maximum glacial conditions between 29,000 to 21,000 years BP which led to about 130 m fall in sea level compared to present-day as well as about 600 km retreat of coastline (Graham *et al*., 2011). The southern North Sea areas at that time were left exposed as a periglacial terrain with lakes, dead ice hollows, meltwater valleys and channels, outwash cones and plains as well as moraines dominating the exposed plain (Streif 2004; Graham *et al*., 2009; Böse *et al*., 2012). This resulted in the deposition of brackish-marine silty clays, till and glaciofluvial sediments across the southern North Sea (Cameron *et al*., 1987; Carr 2004). A general amelioration of climatic conditions during the Holocene (about 11,700 years BP) was followed by a general rise in sea level in the North Sea and this continues to the present-day (Cameron *et al*., 1993). Limnic muds and peat layers occur locally at the base of Holocene sequences although brackish marine sediments overlain in some places an erosional contact with Pleistocene deposits (Vink *et al*., 2007). Fine to medium-grained shell-bearing shallow marine sands (Streif 2004) referred to as Mobile North Sea sands by Zeiler *et al*. (2000) dominated the uppermost interval of the modern sea-bed in the German sector of the North Sea.

The glacial ice sheet advances thus reshaped the landscape architecture and the near surface sediments of the North Sea through a number of deposition, erosion, and re-deposition processes leaving behind typical geological structures ranging from large structures (e.g. glacio-tectonic complexes, tunnel valleys, frontal moraines, sander plains) through medium size structures (e.g. drainage channels, basal moraines) to small scales structures such as fluvial channels (Pedersen 2014; Schack-Pedersen and Boldreel 2016; Bendixen *et al*. 2017). After the retreating of the ice sheets, dewatering river systems carved their courses in the sub-surface and singular glacial depressions served as lakes and swamps. Outwash plains are also formed by discharged meltwater from glaciers and are characterized by glacio-fluvial sediments. During the last interglacial period, marine transgressions again changed the landscape surface and filled the remaining topographical lows. These processes resulted in different environments characterized by highly heterogenous and complex sedimentary structures both laterally and vertically.

1.2.3. German North Sea Quaternary Techno-Stratigraphic Framework

The German sector of the North Sea, which is the study area for this doctoral thesis, is located in the southern North Sea extending between latitude 53° and 55°N and longitude 3° and 8°E (Fig. 1.1) with water depth of up to 60 m. It is flanked to the east and west by the Danish and Dutch North Sea sectors respectively and to the south by the German territorial waters (12 nautical miles; Fig. 1.1). Streif 2004 summarized the Quaternary geological development of the German North Sea coast and adjacent areas into three main stages which are (1) an early stage which can be distinguished by marine to fluvio-deltaic sedimentation during the early Pleistocene followed by (2) a phase characterized by repeated ice advances and alternating marine transgressions during the middle to late Pleistocene and then (3) a third stage whose onset was marked by the melting of the most recent ice sheet, development of modern day landscape elements and sedimentary environment at the beginning of Holocene.

Morphological features such as mega-scale glacial lineations, glaciotectonic thrust-fault complex and sub-glacial buried tunnel valleys from medium to late Pleistocene have been identified both on- and offshore German North Sea sector and adjacent areas (Huuse and Lykke-Andersen 2000; Pedersen 2000, 2005; Lutz *et al*., 2009; Hepp *et al*., 2012; Coughlan *et al*., 2018; Winsemann *et al*., 2020). Glaciotectonic complexes have a complex, multi-phase evolution controlled by both vertical and horizontal ice-bed coupling at ice margin (Huuse and Lykke-Andersen 2000; Pedersen 2000, 2014; Buckley 2012). Analysis of these glaciotectonic complexes has been used in determining the maximum extents of glaciers and ice sheets within the German North Sea and adjacent areas (Madsen and Piotrowski, 2012; Bendixen *et al*., 2017; Winsemann *et al*., 2020). Buried tunnel valleys on the other hand are over-deepened channels formed beneath or adjacent large continental ice-sheets (Ehlers and Wingfield,

1991; Ó Cofaigh, 1996; Huuse and Lykke-Andersen, 2000; Kluiving *et al*., 2003; Lutz *et al*., 2009). They are widespread across the North Sea as well as the rest of Northern Europe and contain thick records of glacial and interglacial deposits (Ehlers and Linke, 1989; Piotrowski, 1994; Huuse and Lykke-Andersen, 2000). The buried tunnel valleys are seen on geophysical profiles as anomalies which can be mapped over large areas and also interpreted in terms of their correct stratigraphic position (Huuse and Lykke-Andersen, 2000; Kristensen *et al*., 2007; Lutz *et al*., 2009; van der Vegt *et al*., 2012; Hepp *et al*., 2012; Lohrberg *et al*., 2020; Prins *et al*., 2020). These buried tunnel valleys and other comparable geological structures has helped in understanding the German North Sea stratigraphy and as well as that of the adjacent areas. Multiple ice advances coupled with various marine inundation resulted in sediment accumulations of more than 1 km thickness thus making the German sector of the North Sea a major sediment repository (Caston 1979; Gibbard *et al*., 1988).

The Quaternary stratigraphic framework of the German North Sea sector since the middle Pleistocene has been recently revised by Coughlan *et al*. (2018) and a summary is given in Table 1.2. Based on the study by Coughlan *et al*. (2018), the oldest sediments belong to the Basal Sands Formation which is Neogene in age. This was followed by the Lower Sands Formation. The Lower and Middle Tunnel Valley Formations, both of which are sub-divided into Upper and Lower Members, overlies the Lower Sands Formation and are subsequently separated from the overlying Peelo Formation (Upper and Lower Members) by the Middle Sand Package Formation. This was followed by fine grained clay with silt and sands of the Lower Marine Formation. Overlying this interval are sediments deposited in a lacustrine-like setting which are referred to as the Lacustrine Formation. Above this Lacustrine Formation are Till Member and Upper Member of the Drente Formation. The Middle Marine Formation and thick sand package of the Upper Sand Formation overlies the Drente Formation. Above this are the Limnic Fluvial Formation made up of variety of sediments and the Buried River Valley Formation. The upper 15 m referred to as the Upper Marine Formation is composed of fine sands and silts with shell remnants which was sub-divided into the Lower Member and the Mobile Sands Member.

1.2.4. Relative sea-level changes in the southern North Sea

Three shelf regions of the world are famous for large areal exposures during low glacial sea levels: North Sea (Doggerland), Alaska-Aleuten-Siberia (Berlingia) and Java-Borneo-Sumatra (Sundaland). During the glacial periods, the physical mass of ice sheets depressed the lithosphere and subsequent deglaciation during the inter-glacials together with recent increase in greenhouse gases/global warming (Marcott *et al*., 2013; Moossen *et al*., 2015; Behre 2007) has resulted in changes in the global relative sea level.

Table 1.2. Revised stratigraphy of the German North Sea sector (After Coughlan *et al*., 2018). See same for detailed description of units and nomenclature.

Period	Unit Code		Formation Name	Member Name	Description
Holocene	I	a	Upper Marine Formation	Mobile Sands Member	Fine to medium sands
		b		Lower Member	Fine to medium muddy sands with shell components
	II	a	Buried River Valley Formation	Upper Member	Silty, muddy sand with some organic silts
		b		Peat Member	Peat
Weichselian	III	a	Limnic Fluvial Formation	Channel Member	Muddy fine - sands
		b		Lower Member	Fine - grained calcareous clay and silt with fine sand
	IV		Upper Sands Formation		Fine to medium sands with gravel at base
Eemian	V		Middle Marine Formation		Fine - grained, clayey deposits with shells
Saalian	VI	a	Drente Formation	Upper Member	Fine to medium sands with gravel layers
		b		Till Member	Till
Late Holsteinian - Early Saalian	VII		Lacustrine Formation		Mud with humic and clay layers
Holsteinian	VIII		Lower Marine Formation		Shelly organic mud with peat -clay and clay layers
Elsterian	IX	a	Peelo Formation	Upper Member	Stiff clay with cm scale fine sand layers
		b		Lower Member	Well sorted sands with gravel layers
	X		Middle Sand Package Formation		Heterogeneous sands
	XI	a	Middle Tunnel Valley Formation	Upper Member	Clays and other fine - grained sediments
		b		Lower Member	Coarse sands and well-sorted gravel
	XII	a	Lower Tunnel Valley Formation	Upper Member	Laminated silts and clays
		b		Lower Member	Coarse - grained sands
Early Pleistocene – Pre -Elsterian	XIII		Lower Sands Formation		Well-sorted sands
Neogene	XIV		Basal Sands Formation		Heterogeneous sands

Subsequent re-adjustment of the earth crust to its initial isostatic equilibrium was attributed to glacial isostatic adjustment (GIA) and this also has a regional influence on sea level changes. The Northern Hemisphere ice sheets for instance were mostly deglaciated between early- to mid-Holocene and global mean sea level (MSL) was approximately 60 m below the present-day level at the Younger Dryas/Holocene transition (Smith *et al*., 2011). Also, the Scandinavia and adjacent southern Baltic region are believed to still be undergoing GIA own to the Weichselian glaciation (Steffen and Kaufmann, 2005) indicating such phenomenon as a result of waxing and waning of ice sheets during all the major glaciation episodes. Since the Last Glacial Maximum, several research efforts have aimed at reconstructing the global relative sea level variations using various sea level indicators such as fossil corals/micro faunas, peat deposits, wood from estuarine clays amongst others (Woodroffe and Murray-Wallace, 2012; Kiden *et al*., 2002; Vink *et al.*, 2007; Behre 2007; Steffen and Wu, 2011; Scheder *et al*., 2021).

However, factors such as tectonic/isostatic activities and coastal barrier systems have posed a great challenge to such research efforts (Kiden *et al*., 2002; Behre 2007) thereby making it difficult to represent changes in sea level by a common sea level curve especially the early- to mid-Holocene periods (Vink *et al*., 2007). Within the southern North Sea, Behre 2007 presented a new sea level curve (Fig. 1.5) spanning the last 10,000 years based on 118 dates obtained from basal as well as intercalated peats retrieved from Holocene sequence collected along the German coast. From the curve, seven sea level falls, each characterized by a distinct sea level decline, are recognized during the younger Holocene (Fig. 1.5). Behre 2007 estimated an average of 0.11 m/100yrs sea level rise in the last 3000 years. The consequences of such rise in sea level is a topical issue for both specialists, government agencies and the wider public. Shallow continental shelves and coasts as well as lowland regions are most vulnerable to sea level changes due to shifting of the coastline landwards. Furthermore, most river channels and incised valleys got drowned due to their inability to adjust their gradients to the fast-paced sea level rise (Hepp *et al.,* 2019). The Doggerland, which serves as a sort of paradise for Mesolithic people and fauna (Coles, 2000; Shennan *et al.*, 2000; Gaffney *et al*., 2007), is a classic example of submerged palaeo-landscape in the present-day North Sea region. The effects of changes in sea level thus cut across various dimensions ranging from ecological habitats through shaping and re-shaping of landscape to socio-economic implications on human livelihood (Church *et al*., 2010; Passeri *et al*., 2015).

1.2.5. The Oceanographic Conditions of the North Sea

In epicontinental embayments such as the North Sea, waves, currents and other oceanographic/meteorological conditions are key controlling factors inducing sediment motion and subsequent re-distribution within the basin (Wright 1995). The North Sea is known to be subjected to oceanic influences at its southern and northern ends as well as terrestrial inputs notably from important rivers such as the Elbe, Weser, Ems, Rhine, Meuse, Scheldt, Thames and Humber along its eastern and western shores (Fig. 1.6; Ellmer and Goffinet, 2006; Schieber 2016). This is coupled with pronounced seasonal changes in meteorological conditions (Lee 1980). These influences together with glaciers sculpt the shelf profile resulting in complexity in its present-day shape and topography. The processes behind sea shelf sediment transportation by tides, waves and wind-driven currents are complex and their relatively influence varies both in space and time (van der Molen, 2002; Neill *et al*., 2010; Ward *et al*., 2016). The German North Sea sector for instance experience high tidal influence compared to the German Baltic Sea (Backhaus 1989; Ellmer and Goffinet, 2006) with long-term transportation of sediments within this southern North Sea dominated by tidal currents aided by waves and wind-driven currents (van der Molen and Swart, 2001; van der Molen, 2002).

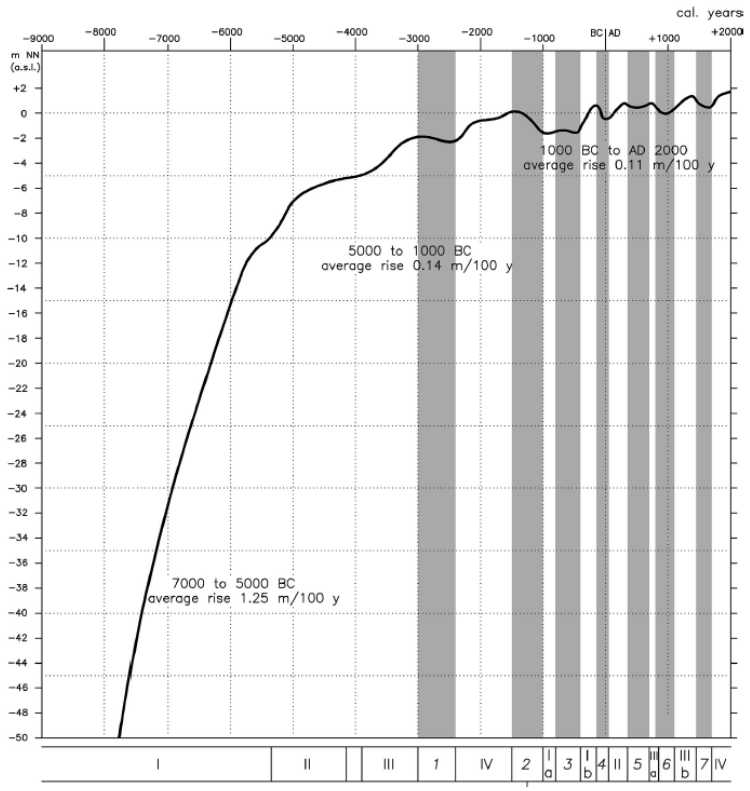

Fig. 1.5. Simplified new curve showing sea-level changes (mean high water level) in the last 10,000 years within the southern North Sea. Roman numbers: transgressions; Arabic numbers: regressions (for details about the curve, see Behre 2007).

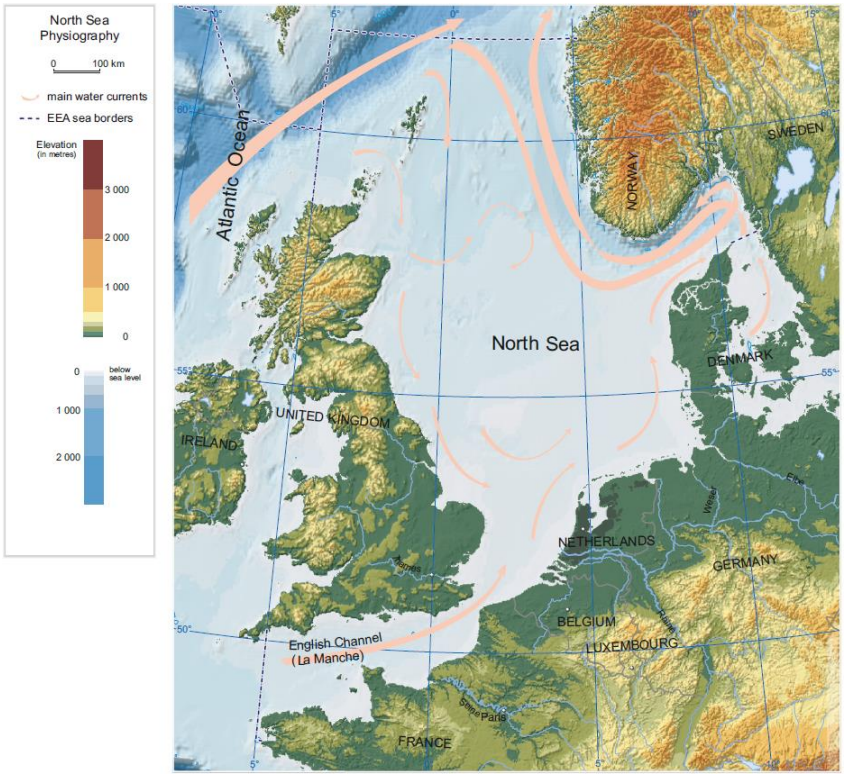

Fig. 1.6. Distribution of the main currents within the North Sea and adjacent areas (Source: European Environment Agency portal-https://www.eea.europa.eu/data-and-maps/figures/north-sea-physiography-depth-distribution-and-main-c).

Lateral transportation of clay- and silt-dominated sediments are generally ease by wind-driven circulation which occasionally interact with shallow sea beds. High wind pushing of sea water towards the coast may result in storm surges which can move and rework fine sediments either as bedload or suspension. The combination of these storm surges and tidal currents could result in large sediment transport (Nittrouer *et al*., 2007; Schieber 2016). Within the southern North Sea (e.g. Middelkerke Bank), large flow transverse bedforms which are common features are believed to be modified by strong storm and tidal currents (Caston, 1972, 1981; Davis and Balson, 1992; Deleu *et al*., 2004). Under present-day conditions, strong near bottom currents (75 to 125 cm/s) and large tidal ranges (about 1 m to over 4 m) prevailed in the North Sea with current circulations moving counter clockwise (Fig. 1.6) with inflow through the north and lesser southwest channels (Mittelstaedt *et al*.,1983; Cameron *et al*., 1992).

1.3. Statement of Research Problem and Research Questions

The German North Sea sector has continued to be an area of intense economic activities in the recent past. This has facilitated a more robust understanding of the sub-surface geological structures and stratigraphy particularly the uppermost 50 m. A detailed knowledge of buried palaeo-structures, their stratigraphic infills as well as geotechnical characteristics is crucial for various offshore engineering activities including but not limited to wind farm installation especially in this period of ongoing energy transition. There is therefore a need to understanding the palaeo-drainage network that serve as dewatering systems for the retreating ice in the German North Sea sector as well as the geotechno-stratigraphy of the uppermost 50 m hence, this study.

The research questions that prompted this study include the following. These questions are addressed in chapters 2 to 5 and the conclusions are summarized in chapter 6 of this doctoral thesis.

- How can water column height variations which hamper the quality of geological deductions obtained from shallow offshore seismic data be corrected or minimized?
- What role does the Elbe Palaeovalley (EPV) played in dewatering the hinterland?
- What is the overall course of the Palaeo Ems, a tributary to the EPV, and its morphological relationship with the EPV?
- What is the infill stratigraphy of the EPV, Palaeo-Ems and other seismic scale structures within the study area?
- What is the stratigraphy and geotechnical properties of the under-represented uppermost 50 m of the German North Sea sector?

1.4. Data Base and Methodology

This study was based on several series of sub-bottom seismic profiles (SBP), multi-channel seismic (MCS) data and drilled cores acquired in the German North Sea sector during various sea cruises using the research vessel Heincke (see Fig. 1.7 for the various cruise lines). Additionally, grids of closely spaced Boomer, core and cone penetration test data from commercial surveys carried out between 2007 and 2010 were sourced in areas with now restricted access due to ongoing wind farm operations (Fig. 1.7). Data from Heincke cruises are stored in PANGAEA (https://doi.pangaea.de/10.1594/PANGAEA.931763) except for the geophysical profiles which are stored on local servers at the University of Bremen, Germany. The commercial data are also stored on local servers of the Marine Engineering Geology working group, MARUM – Center for Marine Environmental Sciences, University of Bremen, Germany. These data sets can be access on request.

1.4.1. Acoustic Data

The SBP were recorded with a ship mounted Innomar SES-2000 medium-100 model with an acoustic power greater than 247 dB (~ 5.5 kW). The SES2000 is a parametric echo sounder system in which two signals of different frequencies are transmitted thereby creating new frequencies when they interact as a result of the non-linearities in the sound propagation. The primary frequency is around 100 kHz and it is usually used for the detection of the sea floor. The secondary frequency, which constitutes the resulting frequency, is much lower than the primary and penetrates deeper into the sub-surface. The SES data provides a very high resolution of the uppermost 15 – 20 m below the sea floor. The collected data were converted to SEG-Y-files using the SesConvert tool.

The MCS data was acquired using the University of Bremen customly designed MaMuCS-System (MTU). The micro Generator Injector (GI) provides signal frequencies of up to 600 Hz which are recorded by a 32-channel streamer with a total length of 128 m. The GI GUN is a pneumatic seismic source, made up of two independent air guns within the same casing, used to control and reduce bubble oscillations. The first air gun is called the generator, as it generates the primary pulse and creates the bubbles. The second one is called the Injector, as it injects air inside the bubble. The Boomer data on the other hand were collected using a Geopulse 5813b Boomer (GeoAcoustic Ltd) single channel seismic system and provided high resolution images within the uppermost 15-25 m with a very high vertical resolution of about 0.2 – 0.5 m. This system was operated with an energy of 200 J and a 3 m single-channel streamer with 8 hydrophones. Acoustic data were recorded with the NWC software (Nautik Nord GmbH) with a shot rate of 3.5 shots per second and a 16-bit resolution.

Where applicable, the data sets were processed with the capability of the VISTA seismic processing software following the standard processing scheme.

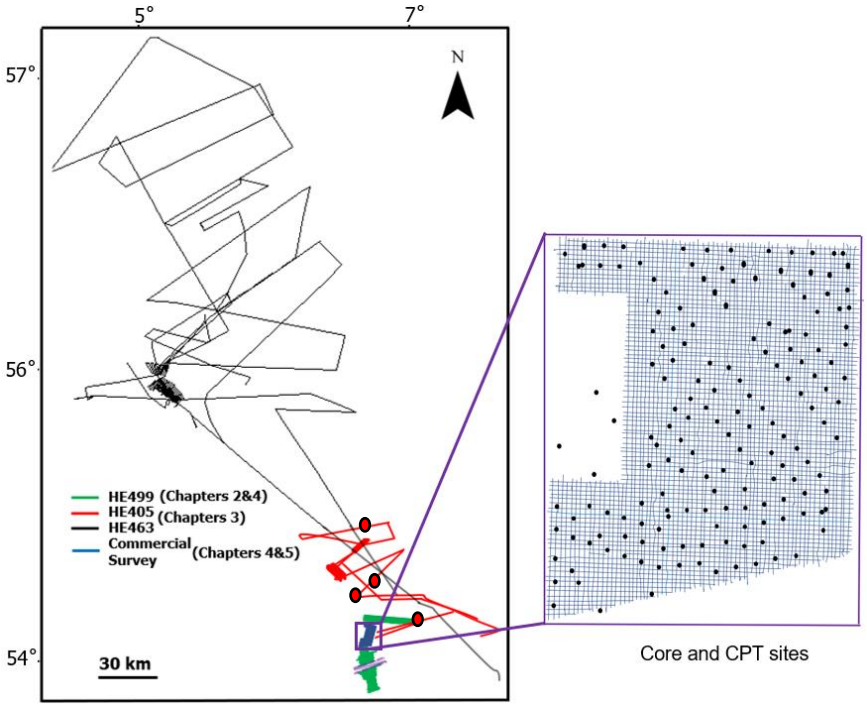

Fig. 1.7. Base map showing the available acoustic profiles, core and CPT sites for this study. Note that the red dots depict the core and/or CPT sites presented in this study (see Fig. 1.1 for location of the study area).

The calculations of exact positions of source and receiver, and their geometry relative to the GPS antenna were performed with the Wingeoapp 0.9.8 software (Hanno Keil). In order to obtain gathers that are reflected from common sub-surface midpoint, CMP-binning was performed along the MCS profiles. After CMP binning, dead and noisy channels were extracted and gun delay was corrected by applying bulk shift in time. On selected CMP gathers, the root mean square (RMS) velocities are interactively identified. The velocity model was subsequently used for the Normal Move-Out (NMO) correction. Vertical time shifts within CMP gathers due to movement of the ship and the sea surface were corrected by using the residual statics correction module of the Vista software. After stacking all CMPs, migration is performed as a final step. The Finite Difference (FD) migration method was employed as this method tolerates the possible errors in the velocity model. The processed data were then loaded into the IHS Kingdom Advanced software for conventional seismo-stratigraphic interpretation and analysis in a standard workstation. The interpretation procedures include identification and mapping of key seismic-scale stratigraphic surfaces and structures across profiles, correlation of surfaces with core samples at core sites and generation of maps where necessary. Time to depth conversation was done by linearly converting the two-way travel time values to depth values based on an average sound velocity of 1550 m/s, a value fitting well for the uppermost 50 m below the sea floor based on previous studies (Winsemann *et al*., 2000; Lutz *et al*., 2009). This

value also correlated well with the obtained values from the compressional P-waves velocities from multi sensor core logger and cone penetration tests data.

1.4.2. Sedimentological Data

A Geo-Corer 6000 vibro-coring system with a barrel length of 5.80 m was used in retrieving sediments samples from the uppermost sub-surface layers at selected locations during the FS Heincke expeditions in the German North Sea. The limitations in core length were balanced by a careful selection of coring sites and coring transects so as to penetrate deeper units at locations where they get closer to the surface. The cores were cut into 1-m segments and splitted laterally into two halves. Core imaging and visual descriptions were carried out onboard the research vessel while further analyses such as sample preparation for ^{14}C dating measurements and paleontology/palynology studies were performed in the laboratory onshore where necessary. The radiocarbon dating of selected core samples was done at the Poznań Radiocarbon Laboratory, Poland for the purpose of age determination. A standard GEOTEK multi sensor core logger (MSCL) was used for measuring physical properties such as compressional P-wave velocities, amount of magnetically susceptible material and attenuation of gamma rays at 1 cm and 2 cm intervals on half core sections. The cores were allowed to equilibrate to ambient room temperature before the start of measurements in order to ensure accurate measurement of parameters of interest.

Deeper cores (~ 50 m) were also acquired in areas with now restricted access due to the ongoing windfarm activities. These cores were recovered either from rotary flush drilling from the drill ships or percussion driver samplers operated from jack-up platforms during commercial surveys between 2007 and 2010. The cores were also cut into individual core section length of 1 m and were described offshore according to the soil classification scheme in DIN EN ISO 14688-2 (2020). The calcium carbonate test (Pedological mapping guide, KA5), dry and wet soil unit weight test at 0.5 m intervals (DIN 18125-2, 2011) and undrained shear strength of cohesive clayey and silty soils using a pocket penetrometer were also done onboard. The locations of all the cores available for this study is presented in Fig. 1.7.

1.4.3. Cone Penetration Test (CPT) Data

At a given location, the CPT was performed within an interval of 11-13 m depending on the ship or platform geometry and were chosen to convey the major geological structures. The CPT were conducted according to the procedure described by DIN EN ISO 22476-1 (2009) using either a downhole CPT operated from a drill vessel, or a top-driven CPT operated from jack-up platforms. The CPT tip resistance (qc) records the stress on the CPT steel cone during penetration and was used to derive the relative density of sands following DIN EN 1997-2 (2010). Tip resistance (qc) measurements obtained from CPT tests were used to characterize stratigraphic sequences and

to confirm identified sequences. Similar to downhole logging data, in-situ data like CPT allows for a more definitive characterization of lithostratigraphic units. The locations of all the CPT data available for this study is presented in Fig. 1.7.

These data sets were then integrated for a robust deductions and inferences of geological structures and palaeo-events.

Chapter 2

Correction of Water Column Height Variation on 2D Grid High-Resolution Seismic Data using dGPS Based Methodology

Ayobami Abegunrin[1*], Daniel A. Hepp[1] and Tobias Mörz[1,2]

[1]MARUM – Center for Marine Environmental Sciences, University of Bremen, Germany

[2]Geo-Engineering.org GmbH, Bremen, Germany

[*] Corresponding Author; E-mail: aabegunrin@marum.de

Published in Scientific Report **10:** 18760, https://doi.org/10.1038/s41598-020-75740-z.

Abstract

Variations in the physical properties of water column usually impede exact water column height correction on high-resolution seismic data, especially when the data are collected in shallow marine environments. Changes in water column properties can be attributed to variation in tides and currents, wind-generated swells, long and short amplitude wave-fronts, or variation in salinity and water temperature. Likewise, the proper motion of the vessel complicates the determinability of the water column height. This study provides a less time-consuming and precise differential Global Positioning System (dGPS) based methodology that can be applied to most types of high-resolution seismic data in order to significantly improve the tracking and quality of deduced geological interpretations on smaller depth scales. The methodology was tested on geophysical profiles obtained from the German sector of the North Sea. The focus here was to identify, distinguish and classify various sub-surface sedimentary structures in a stratigraphically highly complex shallow marine environment on decimeter small-scale. After applying the correction to the profiles, the sea floor, in general, occurs 1.1 to 3.4 m (mean of 2.2 m) deeper than the uncorrected profiles and is consistent with the sea floor from published tide corrected bathymetry data. The corrected seismic profiles were used in plotting the depth of the base of Holocene channel structures and to define their gradients. The applied correction methodology was also crucial in glacial and post-glacial valley features distinction, across profile correlation and establishing structural and stratigraphic framework of the study area.

Keywords: water column; variation; bathymetry; channel; profiles

2.1 Introduction

The physical properties of water column such as density, state of occurrence among others can change significantly over a short period of time. This poises a great challenge on seismic data acquired offshore as a series of

independent 2D or 3D seismic grid over time. These changes in the physical properties of water column may result in inaccurate interpretation of geologic features in the sub-sea floor particularly in cases where differences in depth on decimeter scale are critical for the relative stratigraphic classification of morphologic sub-surface structures. Changes in water column properties can be attributed to variation in tides and currents, wind-generated swells, long and short amplitude wave-fronts, variation in salinity and water temperature, pitch, tilt and roll of ship and/or combination of these factors. In nature, these factors could result in real or apparent variations in the water column. While the variation in tides and currents can influence the elevation of the sea surface, variation in salinity and water temperature can drastically affect the water sound velocity[1]. The effects of wind-generated swells during bad weather conditions has been stressed as a factor that can cause short wavelength incoherence in seismic data[2,3]. Accounting for the effects of these variations require offset and depth dependent timing corrections[4].

Real water column variations can be associated with either internal factors such as thermohaline stratification resulting from changes in water salinity and temperature or external factors caused by changes in water column level resulting from tides, shelf high water and surges due to big storms. Apparent water column variations on the other hand are small scale variations caused by external factors which may be associated with data acquisition like tilt, pitch, roll and shoaling of ship or effects of local wind action on the water surface. Detailed classes of the different ocean waves responsible for water column height variations exists in literature[5]. Long-period waves (storm surges, seiches and tsunamis) can have periods from order of minutes (tsunamis) to few days (big storm surges). Tides which are mostly semi-diurnal have period band between 12 to 24 hours, infra-gravity waves driven primarily by swells have a period range from about 20 s to 30 s up to a maximum of about 5 minutes. Wind sea and swell have a period band of 1 to 20 s. However, swell have small height and less intense dissipation when compared with wind sea. Capillary waves which have period of less than 0.1 s are the shortest period and first wave to be noticed when wind blows on the ocean surface[5] (Fig. 2.1).

Being a tidally influenced area, the German North Sea experience a larger tidal range when compared to the German Baltic Sea[6]. Tidal variations can induce lateral discontinuities on reflection seismic gathers[1] and this in turn hampers the areal-wide interpretation of geophysical profiles or makes it even impossible. A tidal correction, which is as exact as possible, is important for distinguishing various sub-surface morphological structures originating from different processes (e.g. formation of buried tunnel valleys, river valleys, or tidal channels) at different time scales and which on seismic profiles appear to be at similar levels due to erosional processes. These structures can therefore often be distinguished and interpreted only by precise analyses of their altitude in the sediment or their gradients.

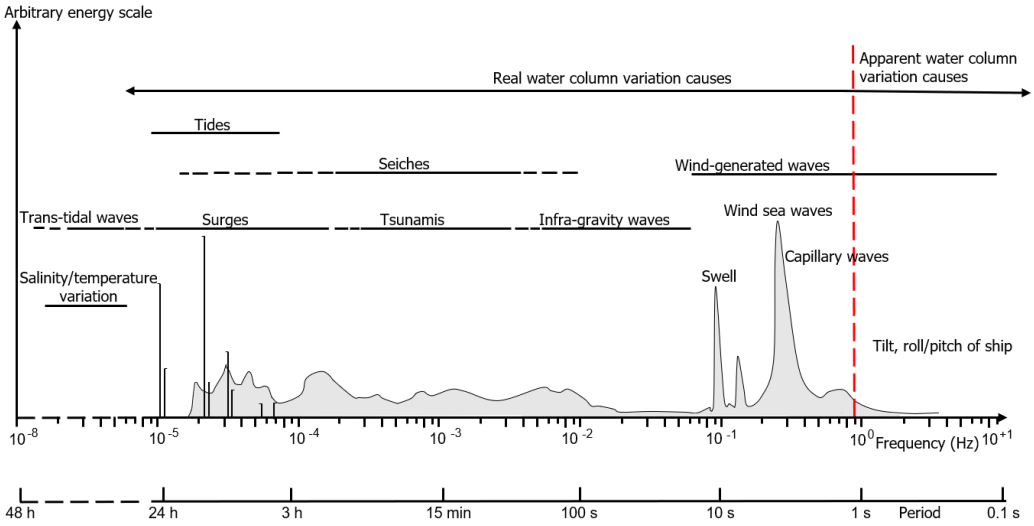

Figure 2.1. Frequency and period classification of water column height variation causes (Modified after Holthuijsen[29]). The red dash line depicts an arbitrary boundary between the real and apparent water column variation factors.

In some cases, high-resolution reflection seismic data acquired in shallow water include water column variations in the order of tens of meter relative to the mean sea level. This variation is often ignored by seismic interpreters[7,8] since a high-resolution deduction of the uppermost meter below the seafloor can be neglected for numerous purposes. Own to complex and high energetic sedimentary processes under glacial, post-glacial and marine conditions, morphological structures originally formed at different times and depositional horizons as well as different sizes and depth scales may now seem to be stratigraphically on the same depth level on seismic profiles. Thus, for example, a determination of the exact depth of valley and channel bases related to a consistent sea level, on decimeter scale, is crucial in distinguishing between different morphological structures, in determining the gradient of rivers or channels and understanding the effect of possible glacial rebound, salt rise and tectonic. This is required for Palaeo landscape reconstruction where it is assumed that the seismic profiles or blocks are acquired using a uniform datum reference.

Correcting for water column variations on seismic profiles requires a good understanding of the origin/cause of the variations in order to account for it in an appropriate procedure. Once obvious acquisition-related factors such as navigation, timing, source and receiver depth errors have been discarded, water-column variations or change in water velocity as a result of change in water salinity and temperature can be identified as the most likely cause of the problem[1]. In shallow water depth areas such as the German North Sea, change in velocity is considered insignificant. This is because there is a whole movement of the water column giving rise to a strong mixing of the water masses and thus preventing any form of thermohaline stratification. In such areas, variations as a result of tides and variations in the sea level due to possible bad weather condition related factors are key contributors to

statics observed on seismic profiles. Eliminating the effects of these statics will significantly improve the reflection strength and continuity of seismic data thereby increasing the accuracy of structural and stratigraphic interpretations[7].

This paper demonstrates the effectiveness of a differential Global Positioning System (dGPS) based methodology in correcting water column height variations using 87 ultra-high-resolution seismic profiles acquired from the shallow German North Sea sector as examples (Fig. 2.2). The adopted methodology used the mean sea level (MSL) as the datum to which the depth to sea floor was adjusted by adding and/or subtracting a profile length offset obtained from an empirical relation between the orthometric height, vessel height and ship draught.

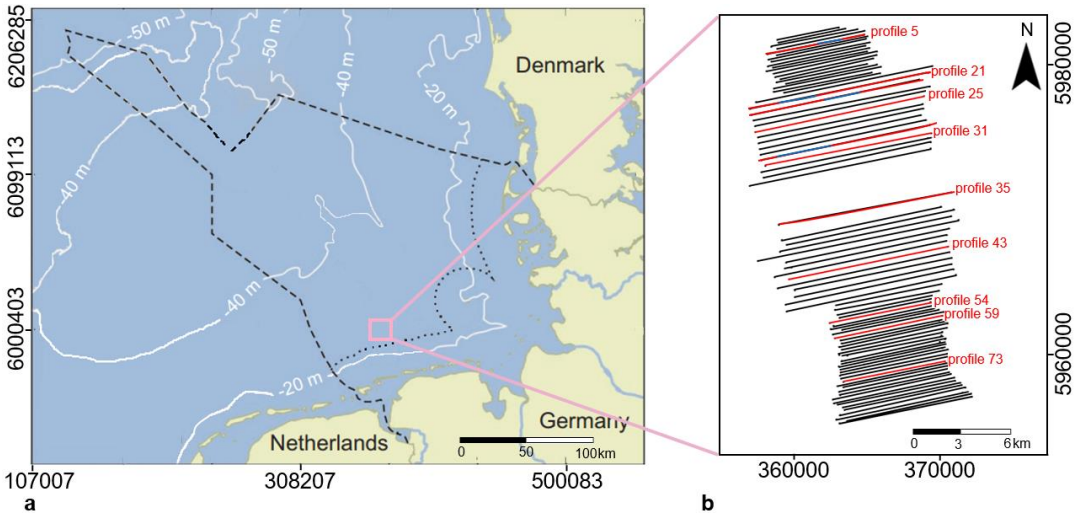

Figure 2.2. Map of the study area (a) north of the East Frisian Islands Norderney and Juist showing the location of the seismic profiles (b) acquired during RV Heincke expedition HE499 in 2017. Note: The black dash line is the German Exclusive Economy Zone, black dotted line is the Territorial Waters (12 nautical miles), white solid lines are bathymetry lines and black solid lines are SES geophysical profiles. The key geophysical profiles discussed in this study are the red solid lines while the blue parts represented the sections with prominent geologic features. Fig. 2.2a was modified after Hepp[16].

2.2 Tidal Correction in Literature and Practice

Tides in most cases are semi-diurnal characterized by two high and two low water levels per day and may cause long wavelength variations. The conventional method for tidal correction is by using predicted tidal tables recorded at nearby tidal gauge stations and this has been utilized in several studies: Balak[7] for example used tidal charts to compute water column variation in order of 0 – 5 m relative to the mean sea level for offshore seismic data acquired in the South Heera Field, India. The correction which was about 7 ms significantly improved the data quality and resolution. Despite the applicability of the tidal chart methodology in the entire German Bight area own to the availability of tide gauges and corresponding tidal correction charts[6], the use of this methodology suffers demerits. This method is very time-consuming as several tidal correction charts are required in a larger survey area since

each chart applies only to the local area around individual tide gauge. Also, the survey areas are often far from the tidal gauge stations commonly located along the coast and the accuracy, reliability and applicability of the tidal tables are limited and can therefore be questioned[6,1]. Furthermore, in shallow waters, sea storms and wind induced water level variations are not accounted for by tidal charts and their temporal shorter time interval effects can have larger magnitude than tides. In the last couple of decades, recent advances in technology have resulted in non-tidal table-based correction methodology. Xu[9] employed a non-linear inversion methodology to correct water statics from marine data set obtained from a deep-water environment. The procedure adopted involves automatic picking of relatively statics between sail lines and then eliminating it as a non-linear inversion problem using a priori constraint for final solution uniqueness. Lacombe[1] proposed a deterministic methodology for resolving water statics as a result of both acoustic velocity and water depth variations and demonstrated its effectiveness on seismic data acquired from the UK continental shelf. Water velocity effects were compensated by direct measurement of root mean square water velocity and arrival time of sea floor reflection at zero offset for each sail line. This was used in computing a spatially constant reference water velocity used in replacing the measured varying real water velocity. On the other hand, changes in water depth was accounted for by averaging dGPS data for the area and computing a mean for the survey from which a differential elevation is computed. Kim[3] presented a very simple bathymetry-based method for removing tidal effects on high-resolution seismic data acquired from the shallow-water area off the west coast of South Korea assuming a constant seawater velocity. The method used water column height variation computed by finding the difference between depth of the sea floor picked along each sail line and a reference bathymetry. This was then gridded and smoothed by averaging in order to generate the tidal variation for the survey area. The correction along each sail line was extracted from the smoothed grid. Wardell[8] developed a statistical approach in which tidal corrections are obtained from the redundancy of information contained in the first break in arrival times of the seismic data itself. Common offset spatial averaging was key in computing the correction which was applied to the recorded seismic data.

The general conclusions from the literature overview are that (1) the quality of seismic data acquired in marine environment may be impaired significantly by the state of water column which varies with tide and water sound velocity, (2) while the old method of using tidal correction tables obtained from tidal gauges may still be applicable, time consumption and the distance of the tidal gauge from the survey area in particular poises questions regarding the accuracy and reliability of this method for high-resolution seismic data, and (3) there is a need to develop an alternate tidal correction methodology which is as exact as possible to aid accurate interpretation of sub-surface structures and deducing their approximate depth of occurrence with respect to a fix datum.

2.3 Study Area and Data Base

The study area is located north of the East Frisian Islands Norderney and Juist between northings 5983000 and 5955000 and eastings 355500 and 373500 using the Europe ELD 1979 UTM Zone 32N Projection (Fig. 2.2). The study area is characterized by typical shallow sea shelf-sands, sandy or muddy tidal flats or marshes with an average water depth of 25 m dominated by lateral currents. Prominent landforms which constitute the costal landscape are low and small morainic hills flattened by various dunes and gradual movement of wet sediments during the last glaciation[10]. In terms of the geology, different generations of buried valleys spanning in age from Pleistocene to Holocene and each with its own complex origin, development history and infill stratigraphy has been described extensively in literature[11-18]. These valleys are separated by various regional, mostly sandy units of glacio-fluvial or aeolian origin. As oppose to the common NNW–SSE and NNE–SSW preferred axis orientations of the majority of Pleistocene tunnel valleys within the German North Sea, Hepp[15] identified and described a classical and rare E-W trend for a tunnel valley in the south eastern North Sea. Hepp[16] also gave a concise seismo-acoustical and sedimentological analyses of a tributary to the Elbe Palaeovalley (EPV) inferred to be the submerged Palaeo extension of the modern Ems River. This Palaeo Ems constitutes to the dewatering system that drained into the EPV within the area[19]. These earlier formed structures are overlain by Modern Mobile North Sea sands of varying thickness forming dunes or layers[18]. Behre[20] identified various generations of peat formations in Northern Germany associated with regressions which occurred as a result of decrease in the rate of sea level rise during the Holocene. Wetland systems consisting of tidal channels and coastal salt marshes among other structures constitutes other known features within the study area[21,22]. A detailed stratigraphic framework of the Quaternary deposit of the German sector of the North Sea is summarized in Coughlan[17].

The data used in this study consist of high-resolution seismic and co-recorded differential Global Positioning System (dGPS) data acquired along each of the seismic track lines. These data sets were acquired from the German sector of the North Sea during the RV Heincke expedition HE499 in October, 2017 (Fig. 2.2). The reflection seismic data were acquired using the ship mounted sediment echosounder Innomar SES2000 medium-100 model with an acoustic power greater than 247 dB (~5.5 kW). The SES2000 is a parametric echo sounder system in which two signals of different frequencies are transmitted thereby creating new frequencies when they interact as a result of the non-linearities in the sound propagation. The primary frequency is around 100 kHz and is used for the detection of the sea floor. The secondary frequency, which constitutes the resulting frequency, is much lower than the primary and penetrates deeper into the sea floor. The SES2000 medium-100 model used onboard during HE499 was in multi-frequency mode meaning that secondary frequencies of 4 kHz, 8 kHz and 12 kHz were generated at

alternate times. The ping rate was between 0.3 and 0.45 s per frequency and the high primary frequency restricted the aperture angle to 1˚. The collected data were converted to SEG-Y-files using the SesConvert tool. A grid comprising a total of 87 seismic profiles with an approximate east–west orientation was acquired in a north–south progression (Fig. 2.2). North – south profiles as well as sediment cores required for lithostratigraphic studies were not recovered due to extreme bad wave and weather conditions. The seismic profiles of the study area have an approximate spacing of 200 m and cover an area of about 321.60 km^2. The data were then subjected to the conventional seismic processing procedures. Heave, roll and pitch compensation was carried out onboard by the electronic beam steering depending on the external sensor data of the SES2000 system. The dGPS data were acquired at a sampling rate of 150 m along each sail lines using the Trimble SPS×61 GPS receiver onboard. The Trimble antenna ellipsoidal height was referenced to the Earth Gravitational Model 1996 (EGM 96). With respect to the dGPS quality, the Trimble antenna was shifted to an improved spot on RV Heincke in February, 2017 prior to the HE499 expedition in October, 2017. Additionally, tide corrected bathymetry data for the entire German sector of the North Sea was sourced from Geopotenzial Deutsche Nordsee (GPDN, https://www.gpdn.de/). The data which was published in 2013 was a compilation over a period of about 10 years. The tidal prediction table obtained for the year 2017 was also sourced from the German Federal Maritime and Hydrographic Agency (BSH). The Norderney gauge station where the tidal values were obtained is situated within close proximity to the study area. Conventional seismic processing and shot to shot high frequency static correction were carried out using the Reflex processing software while the IHS Kingdom Advanced software was used for seismo-stratigraphic interpretation on a standard workstation.

2.4 Methodology for the Correction

Tidal correction was carried out on the seismic echo sounder (SES) data using the technique illustrated in Fig. 2.3 with the mean sea level (MSL) been the reference for all corrections. The basic idea behind this methodology is to use a more precise information obtained exclusively from dGPS measurements in computing offsets from MSL to the water level. The ellipsoidal height (Fig. 2.3, a) along each of the sail lines were obtained from the dGPS data. In most cases in this study, the number of satellites from which these values were derived varies from 7 to 10 indicating a good data quality. The height from the reference ellipsoid to the geoid (Geoidal Height–b) which approximates the MSL was computed using the QuasiGeoid GCG2011 software obtained from the German Federal Office of Cartography and Geodesy. The geoidal height (b) was then subtracted from the ellipsoidal height (a) to obtain the height from the antenna to MSL (Orthometric Height–c). The research vessel has a height (d) of 16.35 m and average draught (e) of 3.93 m.

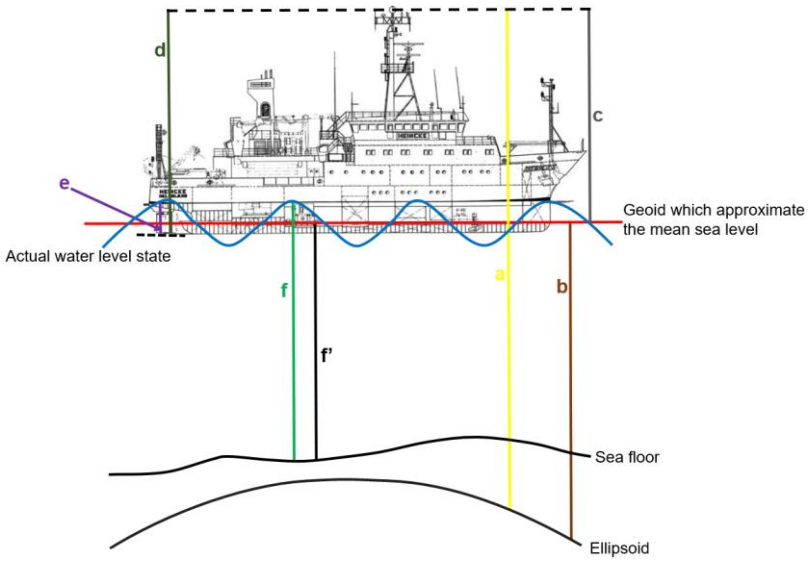

Figure 2.3. Adopted methodology for water column variation correction to determine the depth from the approximate mean sea level to the sea floor f˝; a = height between the ellipsoid and the dGPS antenna (Ellipsoidal Height); b = height between the ellipsoid and the approximate mean sea level (Geoidal Height); c = height between the approximate mean sea level and the dGPS antenna (Orthometric Height); d = ship height; e = ship draught; f = depth from the transducer to the sea floor, draught value was entered to the SES acquisition software; Research vessel image from RV Heincke configuration manual.

The draught was subtracted from the ship height and the resulting value was deducted from the orthometric heights to obtain the offset from the water surface to the MSL. The offset values calculated along each profile are converted to the unit of time (seconds) by multiplying by a water velocity of 1503 m/s and saved in xyz ASCII format. The water velocity was calculated using Leroy *et al.* 2008 equation[23] with an average temperature and salinity values of 14.5˚C[24] and 33 ‰, g/l[25] respectively for the month of October, 2017 when the survey was carried out. Bailey[26] used a simplified Leroy equation (Leroy 1968) to compute mean velocities for the months from May to October when a thermocline develops resulting in a 6 ˚C or 7 ˚C temperature difference and obtained a velocity of 1502 m/s. Both velocity values show good consistency over the study area. The offs*et al*ong each profile was then smoothed using a two-way zero phase filtering interpolation to eliminate outliers. The smoothed profile-length offsets represent the water column height variation for each seismic profile. The final smoothed offset/correction profile was loaded to the trace header of the SES data (f) as a total static for each profile using the Reflex software and the traces were shortened or elongated according to the sign convention of the static correction. By applying this correction to all SES data of the study area now eliminate the effect of tides and any other external influences assuming the MSL as the datum for all the acquired SES data (f˝). The adopted workflow is summarized in equation (1). The depth of the various geologic structures identified on the corrected seismic profiles were converted from the unit of time (seconds) to meters by multiplying half of the two-way travel time by a propagation speed of 1550 m/s assuming velocity homogeneity within the uppermost sub-sea floor. Since the base of the geologic structures

were rarely evenly level, the lowest depth range was selected from each seismic profile. Seismic facies analyses based on reflection strength, continuity and geometry was used in differentiating various lithostragraphical units.

$$f' = f - [c - (d - e)] \quad (1)$$

Where:

c = orthometric height
d = vessel height
e = ship draught
f = depth from the transducer to the sea floor
f′ = depth from mean sea level to the sea floor

2.5 Results

2.5.1 Water Column Variation Offsets

The offsets of the water level relative to the MSL which constituted the water column height variation for each seismic track line was computed using the procedures outlined above. For each seismic track line and shot, the computed offsets were calculated at an interpolated, equidistance dGPS positions. The estimated low and high water heights and the corresponding water column variation heights along each seismic track line are presented in Table 2.1. The tidal effects over the course of acquisition of each seismic profile were estimated from the tidal table recorded at the tidal gauge Norderney for the month of October, 2017 when the survey was carried out and also presented in Table 2.1. At the time of survey, the water level varies from about -2.3 m to 3.9 m relative to the mean sea level. The water column heights range from about 1.1 m to 3.4 m with a mean of 2.2 m. From the tidal table, it was observed that the average daily tidal height varies between 4.6 m and 5.4 m. However, the contribution of tidal variations to the whole water column height changes over the acquisition period of each profile which is typically between 35 mins and 90 mins varies from about 0.05 m to 1.20 m. This constituted in most cases less than 30% of the total variation. Representative examples of the estimated offset types were presented diagrammatically exhibiting three distinct patterns. The first group shows a more gentle variation with offset amplitudes of about 2.0 m along the profile (Fig. 2.4a-b). The second group showed a sinusoidal offset pattern (Fig. 2.4c-d) with an average amplitude of 1.5 m while the third group on the other hand were characterized by a marked fluctuation along profile length as shown in Fig. 2.4e-f. In addition, the plot of the estimated tidal influence revealed a near linear trend over the course of acquisition of each seismic profile (Fig. 2.4a-f). The approximate water column height variation for the study area as at the time of the survey was obtained by gridding and contouring the computed offsets for each seismic profile (Fig. 2.5). From the resulting map, it was observed that largest variation occurred near the coast towards the south while smaller variations were characteristic further away from the coast to the north.

Table 2.1. Estimated low water, high water and water column variation heights along each seismic profile.

Profile	Low water height (m)	High water height (m)	Water variation height (m)	Tidal height (m)*	Profile	Low water height (m)	High water height (m)	Water variation height (m)	Tidal height (m)*
01	−0.5	1.8	2.3	0.35	45	0.0	2.3	2.3	0.85
02	0.0	2.0	2.0	0.40	46	0.2	2.3	2.1	0.60
03	−0.1	2.5	2.6	0.40	47	−1.4	0.8	2.2	0.50
04	0.0	2.0	2.0	0.07	48	0.0	1.8	1.8	0.65
05	−0.3	2.2	2.5	0.20	49	0.0	2.3	2.3	1.10
06	0.0	1.6	1.6	0.30	50	−1.0	1.0	2.0	0.40
07	−1.0	1.9	2.9	0.40	51	−1.3	0.5	1.8	0.30
08	−1.5	1.0	2.5	0.40	52	−2.0	1.0	3.0	0.20
09	−0.1	2.0	2.1	0.20	53	−1.6	0.0	1.6	0.08
10	−1.0	1.3	2.3	0.05	54	−2.0	0.1	2.1	0.30
11	−2.0	0.5	2.5	0.10	55	−0.8	1.0	1.8	0.45
12	−1.0	1.0	2.0	0.40	56	−1.0	1.0	2.0	0.65
13	−0.3	2.0	2.3	0.60	57	0.0	2.2	2.2	0.60
14	−0.5	1.5	2.0	0.45	58	0.2	2.3	2.1	0.10
15	0.6	2.0	1.4	0.35	59	0.5	2.5	2.0	0.11
16	1.2	2.6	1.4	0.10	60	−0.8	2.1	2.9	0.20
17	0.6	2.0	1.4	0.10	61	0.0	1.8	1.8	0.20
18	0.8	2.5	1.7	0.20	62	1.5	1.9	3.4	0.30
19	0.3	2.4	2.1	0.40	63	−1.8	0.1	1.9	0.50
20	0.5	2.4	1.9	0.50	64	−2.2	1.0	3.2	0.55
21	0.2	1.4	1.2	1.20	65	−2.3	1.0	3.3	0.40
22	0.8	2.5	1.7	1.00	66	−2.3	0.9	3.1	0.35
23	1.0	2.5	1.5	0.37	67	−2.0	0.4	2.4	0.20
24	−1.4	0.3	1.7	0.39	68	−2.0	1.1	3.1	0.03
25	0.8	1.9	1.1	0.60	69	−0.5	2.0	2.5	0.08
26	0.2	1.9	1.7	0.80	70	−1.0	2.0	3.0	0.30
27	−0.8	0.4	1.2	0.20	71	0.0	2.0	2.0	0.15
28	0.5	2.1	1.6	0.10	72	−0.1	2.0	2.1	0.55
29	−0.1	2.0	2.1	1.00	73	0.5	2.4	1.9	0.45
30	−0.8	1.2	2.0	0.62	74	−0.5	2.6	3.1	0.80
31	1.5	3.9	2.4	0.56	75	−0.5	2.4	2.9	0.05
32	−0.8	1.8	2.6	0.55	76	−1.6	1.0	2.6	0.35
33	−1.0	1.9	2.9	0.52	77	−1.0	1.0	2.0	0.45
34	−0.2	2.0	2.2	0.90	78	−2.0	1.3	3.3	0.65
35	2.0	3.9	1.9	0.80	79	−2.0	0.5	2.5	0.55
36	−0.9	0.5	1.4	0.24	80	−1.5	1.5	3.0	0.40
37	−0.1	2.5	2.6	0.55	81	−0.2	1.5	1.7	0.05
38	0.3	1.8	1.5	0.80	82	−0.3	2.0	2.3	0.55
39	−0.7	0.9	1.6	0.80	83	0.6	2.8	2.2	0.55
40	1.5	3.4	1.9	0.10	84	−0.3	3.0	3.3	0.85
41	−0.7	1.0	1.7	0.20	85	0.3	2.8	2.5	0.35
42	0.2	2	1.8	0.52	86	0.0	2.9	2.9	0.24
43	1.1	3.2	2.1	0.35	87	−0.5	2.0	2.5	0.29
44	−1.0	1.0	2.0	0.57					

* Estimated tidal values obtained from the tidal table recorded at the tidal gauge Norderney for the month of October, 2017. Tidal prediction does not include the influence of wind and other factors on the sea level (Source: German Federal Maritime and Hydrographic Agency).

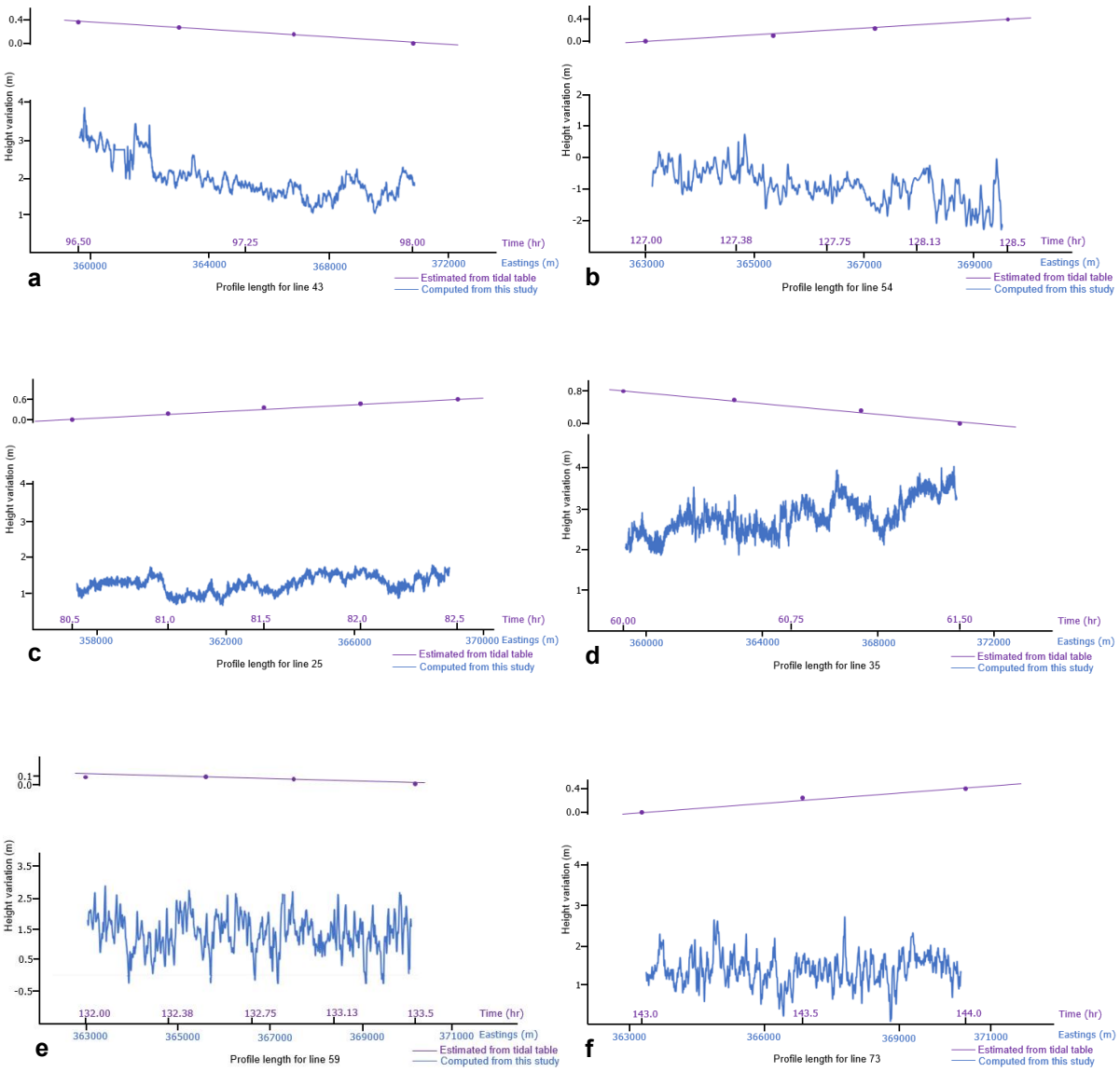

Figure 2.4. Representative water column variation curves showing a gentle variation (a and b), sinusoidal pattern (c and d) and marked fluctuations (e and f) along profiles (see Fig. 2.2b for location of the profiles).

2.5.2 Application of Methodology and Comparison of the Sea Floor from the Corrected Seismic with Existing Bathymetry Data

Having loaded the corrected seismic profiles into IHS Kingdom Advance software, the sea floor which is typically very distinct on seismic profile was interpreted. Fig. 2.6 shows a SES section for profile 31 after (a) and before (b) the correction for water column height variations and while the structural configuration within the profile was retained, the corrected profile occurs deeper than the uncorrected profile. This was evident as the sea floor picked from the uncorrected seismic profile occur shallower than that from the corrected profile (Fig. 2.6a).

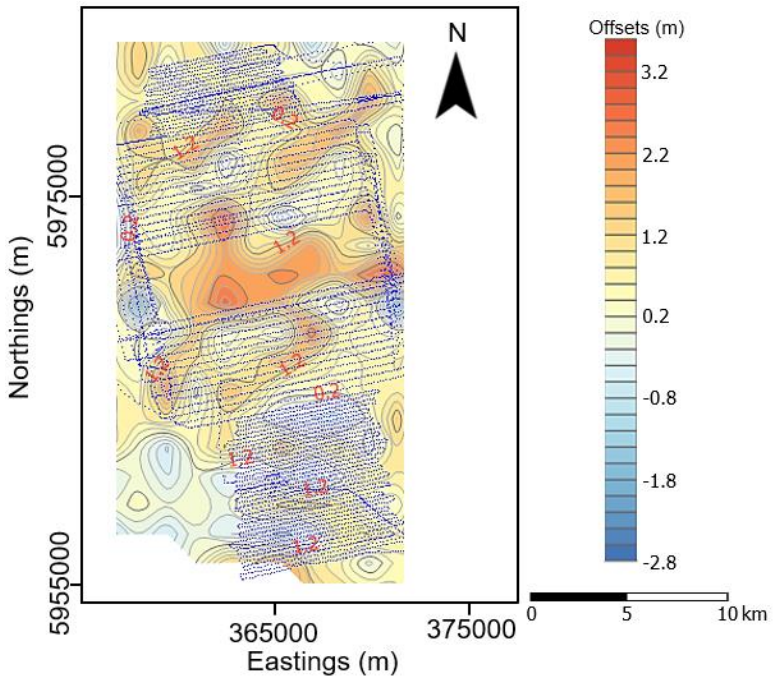

Figure 2.5. Estimated water column variation map over the study area. The blue lines depict the seismic track lines.

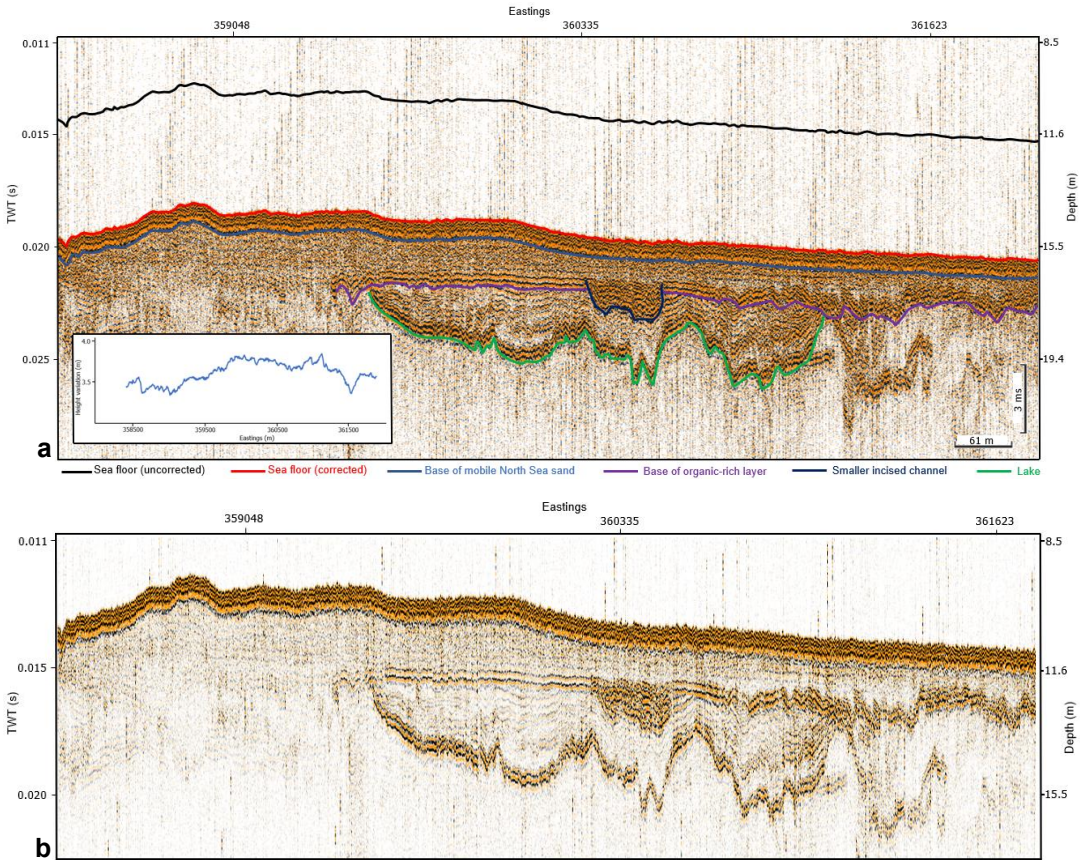

Figure 2.6. Profile 31 showing the location of the sea floor after (a) and before (b) tidal correction (See Fig. 2.2b for location of the profile). Note: The inserted map in (a) is the computed water column variation curve for the section shown. Color coding denotes key sub-surface features which are better identified and interpreted on the corrected and processed profiles.

The correction also improved the quality of sub-surface structural deductions from the seismic profile. The sea floor for profile 31 which was extracted from the gridded bathymetry data for the study area was then compared with the picked corrected sea floor. The depth of the sea floor from both the corrected SES and bathymetry profiles show an improved correlation with offset ranging from 0.5 m to a maximum of 2.0 m while the depth of the sea floor from the uncorrected SES profiles occur at a shallower depth with significant offsets (>3.0 m) from the published bathymetry profile (Fig. 2.7). Furthermore, the depth of the base of a younger channel below the sea floor before and after correction for water column height variation is shown in Fig. 2.8. It can be observed from Fig. 2.8 that the depth of the base of the channel plots as scattered points with no definite pattern on the uncorrected geophysical profiles (blue triangles). This implies that an attempt to develop a gradient study on an uncorrected dataset would fail. In contrast, an almost linear depth below MSL trend was observed for the same plot after tidal correction (black circles). This trend of the deepest point of the base of the channel course has a gradient of about 0.00211. Fig. 2.9e reveals the geometry of the younger channel and its stratigraphic relationship with other geologic features (Fig. 2.9a).

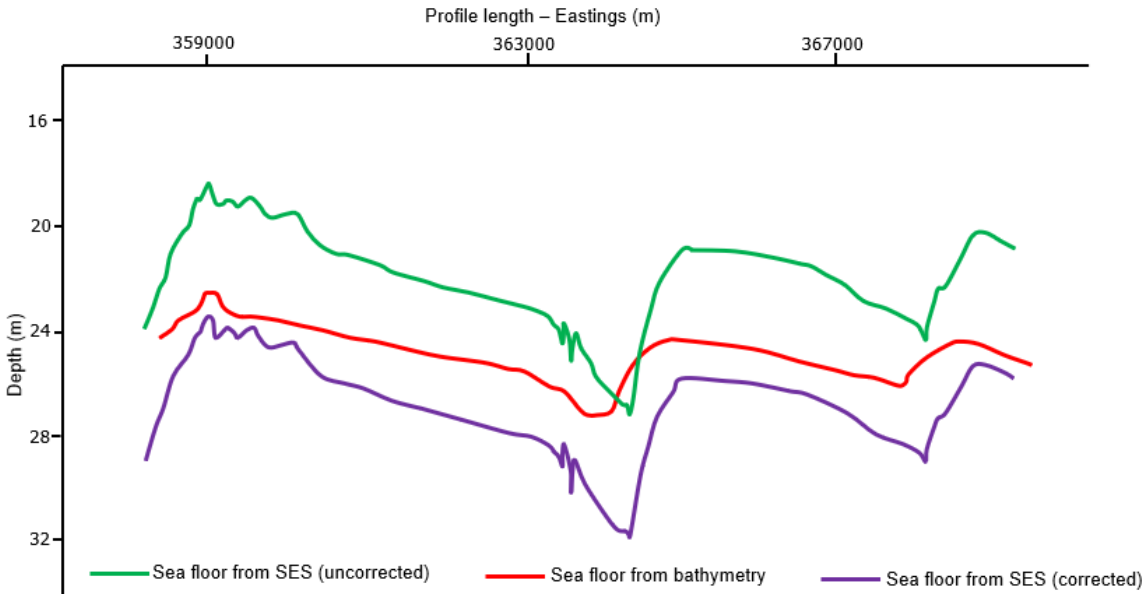

Figure 2.7. Comparison of the depth of the sea floor from uncorrected SES profile, water column height variation corrected SES profile and bathymetry for Profile 31 (See Fig. 2.2b for location of the profile).

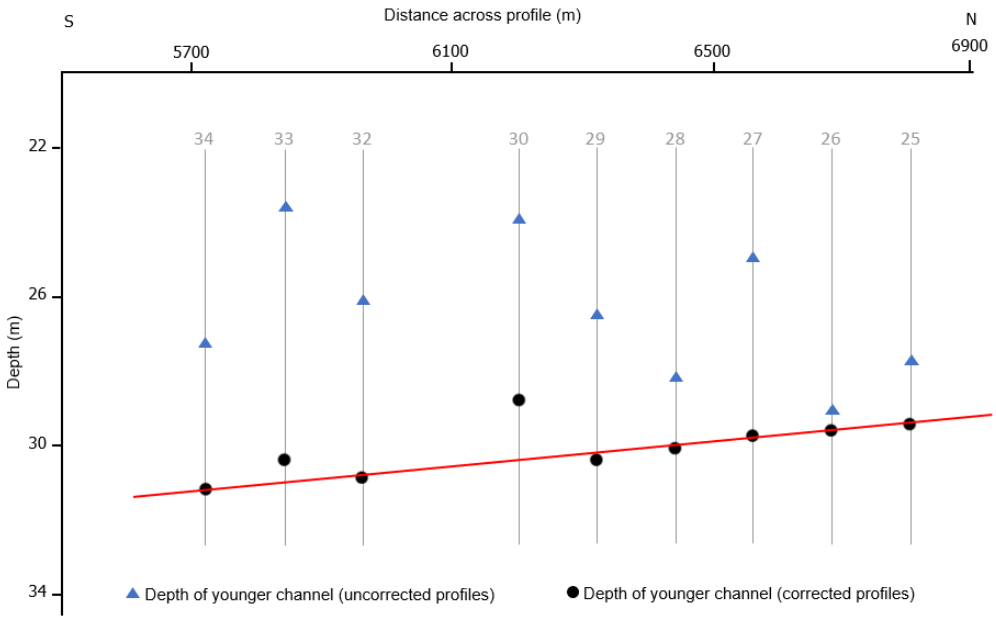

Figure 2.8. Depth of the younger channel below the sea floor along both the uncorrected (blue triangles) and corrected (black circles) SES profiles (See Fig. 2.9e for position of the channel base).

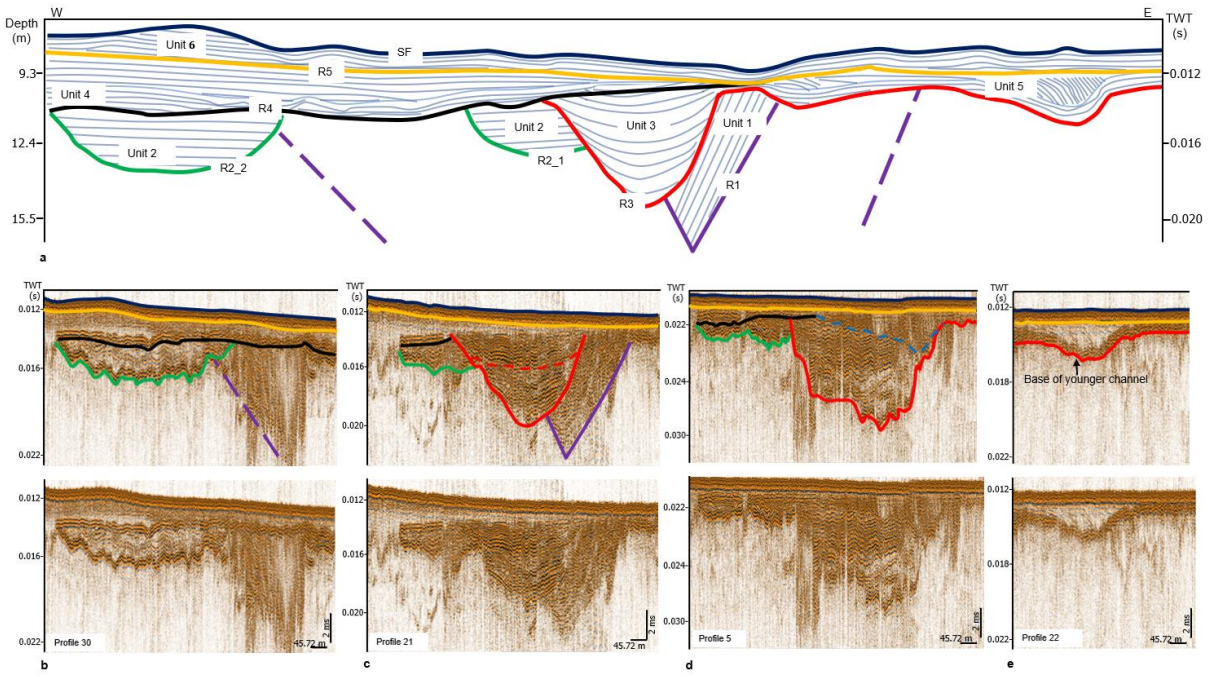

Figure 2.9. Seismic stratigraphy overview detailing the inter-relationships of different geologic structures over the study area. Major stratigraphic boundaries are highlighted in different colors while the infill sequences are shown in blue. The color lines marked distinct seismic reflectors interpreted as: Modern sea floor surface (blue; SF), base of Holocene sediments (yellow; R5), base of organic rich layer (black; R4), base of Palaeo Ems (red; R3), base of lake (green; R2) and base of the core of Pleistocene channel (purple; R1), (See the blue solid lines in Fig. 2.2b for location of the seismic sections).

2.5.3 Major Seismic Reflectors and Units

The schematic composite diagram illustrated in Fig. 2.9 covering an EW length of about 2.5 km and a resolved depth of approximately 30 m depicts six key seismic reflectors defining major structures and stratigraphic units. The infill seismic expression over the study area was deduced from the corrected profiles as seen in the inset Fig. 2.9b-e. Some of the major reflectors show former and modern landscape surfaces while other reflectors depict the bases of channels and valleys. Reflector R1 was interpreted as the lower boundary of the core of a tunnel valley capped above by reflector R3. These reflectors marked the lower and upper limit of Unit 1 and it belongs to the oldest geologic structure identified on seismic profiles within the study area. The internal reflector pattern of this unit displays a steeply inclined moderate amplitude, semi continuous to discontinuous internal reflectors (Fig. 2.9c). Reflector R2_1 was inferred to incised into the tunnel valley and belong to the same generation as Reflector R2_2 based on their approximate erosive depth, architecture and infill pattern. These reflectors defined Unit 2 bounded above by Reflector 4. Unit 2 in the study area appears in two forms expressed on seismic sections as a separate structure and a structure cut by reflector R3 of Unit 3 and it is younger than Unit 1. As evident from the separate structure, Unit 2 displayed a characteristic low to medium amplitude, semi-continuous to continuous internal reflectors unit. However, the base of this unit showed a high amplitude, continuous reflectors (Fig. 2.9b and c). The upper section of Unit 2 together with Reflector R4 often show a smaller secondary incised channel (Fig. 2.6). Reflector R3 is a major reflector that incised into the underlying Units 1 and 2 and extends to the eastern part of the study area. Its western extension however has been eroded by the overlying Reflector R4. Both Reflectors R3 and R4 define Unit 3 and this unit is younger than Unit 2 based on cross cutting relationship. The seismic pattern of the infill of this unit revealed a minimum of a two-phase poly infill (Fig. 2.9c). Seismic facies analysis of the poly infill revealed a strong amplitude and continuous reflector at the base which is overlain by a moderate amplitude and continuous reflector. In the northern part of the study area, Unit 3 show evident of smaller incisions at the upper boundary (Fig. 2.9d). The strong amplitude and continuous reflectors at the base of this unit extend to the eastern area and forms the base of younger structures (Fig. 2.9e). Lying above Reflector R4 is a strong amplitude and continuous reflectors defining Unit 4. The area extent of this unit to the east has been eroded by the overlying Reflector R5. The strong amplitude and continuous reflectors from the base of Unit 3 extends to form the base Unit 5. The classic internal pattern is a transparent unit characterized by low amplitude, continuous and dipping internal reflectors (Fig. 2.9e). In some areas, strong amplitude, continuous and dipping reflectors of this unit was observed to cut the upper area of Unit 3 (Fig. 2.9d). This indicates a relatively young age relationship for this unit with respect to Unit 3. Unit 6 is bounded below by Reflector R5. Reflector R5 separate recent

sediments above from the underlying older sediments across the entire region. Both reflectors R4 and R5 are erosional surfaces of former landscape within the area. Unit 6 is characterized by high amplitude and continuous smaller reflectors on seismic sections (Fig. 2.9b-e) and bounded above by Reflector SF which is the modern sea floor. None of these structures have an expression on the modern sea floor across the entire area as they were covered by the spatially distributed layer of Unit 6.

2.6 Discussion of Results

Differential Global Positioning System information was used to obtain water column height variation using the methodology depicted in Fig. 2.3. The computed offset values along the seismic profile (Table 2.1) revealed the genuine existence of water column statics. The computed water column variation ranges from about 1.1 m to 3.4 m with a mean of 2.2 m. From the tidal prediction table obtained from the Norderney gauge station for the month of October, 2017, the average daily tidal height varies between 4.0 m and 6.0 m for the period of the survey. Over the course of acquisition of each profile (60 – 90 mins), the tidal range varies from about 0.05 m to 1.20 m which is less than 30% of the total cause of the variation. This indicates that in shallow water areas where there is no thermohaline stratification, tides contribute only a fraction of the total cause of variations in the water column. The bulk of the variation in such areas can thus be attributed to pitch, tilt and roll of ship and local effects of wind-generated longer wavelength waves and swells which are not accounted for from the tidal gauge predictions.

Diagrammatic representation of the water column variation along each sail line revealed three distinct patterns described as those with gentle, sinusoidal and marked fluctuations patterns (Fig. 2.4a-e). The tidal variations along each profile behaves close to linearly as shown in Fig. 2.4a-e for the relatively short time periods of each sail line. This clearly shows the demerit of using predicted tidal tables only for correcting water column height variations for high-resolution seismic studies. This is because tidal tables do not consider the effects of acquisition related factors, influence of wind and waves on the survey vessel itself and other localized factors on the sea surface. In shallow water areas such as the area investigated, these non-tidal related factors can constitute more than 70% of the total statics. This high magnitude effects which cannot be account for based on tidal tables only can greatly degrade the quality of high-resolution seismic data. From the water column variation map generated for the study area for the survey period, high amplitude water column height variations attributed to amplification and shortening in wavelength caused by rapid shoaling toward the coast were observed towards the southern section while smaller amplitude water column height variations were observed in the northern section far away from the coast (Fig. 2.5). Another factor attributed to the high and low water column variation is the interplay between the water column and sea floor morphology. Towards the coast areas in the south, increased interaction between the

sea floor morphology and water column together with the coupling effects of long wavelength waves on the sea bed could result in the observed high amplitude water column variations while the low sea floor morphology-water column interaction could be responsible for the small variations in the northern areas.

The computed corrections along each profile loaded to the SEGY trace header of the SES data as a total static revealed that the corrected profile occurred deeper than the uncorrected profile (Fig. 2.6). While there is no significant discrepancy in the morphology of the sea floor before and after applying the correction, about 4.0 m difference exist in their depth of occurrence. The sea floor from the corrected profiles which in most cases occur deeper has been referenced to a consistent mean sea level datum. Fig. 2.7 depicts the interpreted sea floor along profile 31 from the uncorrected profile, corrected profile and bathymetry data. It was observed that the sea floor obtained from the bathymetry data was smoother than that of the SES data. Also, on the overall, the sea floor from the corrected profile showed a good consistency with that from bathymetry when compared to the sea floor picked from uncorrected profile. An offset ranging from 0.5 m to less than 2.0 m was obtained from the corrected profiles as opposed 2.0 m to over 3.0 m obtained from the uncorrected profiles. This revealed a better fit between the bathymetry and the corrected SES profiles and clearly indicates the presence of static effects on the seismic profiles during acquisition. The slight discrepancy between the interpreted sea floor from the corrected SES profile and the bathymetry can be attributed to major morphodynamic changes known to characterize the area as the bathymetry data was a compilation over a period of about 10 years and published in 2013. Series of survey carried out over time by BSH within the German North Sea corroborates the existence of intensive morphological changes of the sea floor. In addition, the bathymetry data points have a larger sampling points (data points are about 200 m apart in all directions) leaving out details which were captured in the SES (shot point to shot point distance of about 4 m along profile length). Both Fig. 2.6 and 2.7 re-iterated the importance of water column variation correction on seismic data for detailed sub surface interpretation as the SES profiles after applying the correction is not only corrected for static effects but also now referenced to a consistent mean sea level datum.

The stratigraphic position of the base of a younger channel on both uncorrected and corrected profiles was again used to demonstrate the importance of water column variation correction as shown in Fig. 2.8. Fig 2.8 depicts the depth of the deepest point of the base of the channel across profiles. From the depth of the base of this channel, it was possible to deduce the trend and gradient of the channel from the corrected profiles which was difficult to decipher from the uncorrected profiles. The channel course has a gradient of about 0.21% and this value together with the width-depth ratio of 2.60, sinuosity of 1.20, entrenchment ratio of 1.38, inferred channel material (sand), cross-section and plan view suggest a river type G5c based on Rosgen[27] natural river classification (see Fig. 2.9e

for the channel outline). A precise water column height variation methodology as described in this study is critical in shallow and very flat environment with small gradient. This implies that detailed geological interpretation such as gradient studies which can be used, for example, in the identification and classification of river systems and their underlying processes, areal-wide deduction of the approximate stratigraphic positions and trends of sub-surface morphological features will be obstructed on uncorrected geophysical profiles. In areas with complex geologic processes such as erosion and subsequent redeposition, the true stratigraphic position of geological features obtained from corrected seismic profiles is indispensable in distinguishing structures from different time scale (from glacial to post-glacial) and developing a relative stratigraphic model for the area.

Owning to the strong impact of erosion and re-deposition within the study area, glacial and post-glacial structures appeared on first sight indistinguishable as both structures now occur relatively at the same depth level below seafloor on seismic profiles (Fig. 2.9c, Units 1 and 3). Areal-wide interpretation of these morphological structures on the corrected geophysical profiles helped in distinguishing them based on their approximate true stratigraphic positions. This was difficult to determine on the uncorrected profiles because a structure can occur at different depth positions across profiles from the same area. This was evident from Fig. 2.8 as the same structure displayed an irregular depth positions across profiles. Also, a discrepancy of about 4 m (about 5.16 ms two-way travel time) existed between the sea floor picked from the uncorrected and corrected seismic profiles (Fig. 2.6). The implication of this observed discrepancy is that assuming a first-hand velocity homogeneity within the uppermost 30 m below the sea floor, a structure can occur at about ±4 m relative to its true stratigraphic position within a depth of 30 m. Therefore, distinguishing different sub-surface structures formed at different geological times in a tidally influenced complex shallow water area will be practically difficult if not impossible without a detailed shot to shot water column statics correction.

Seismic interpretation was carried out on both uncorrected and corrected seismic profiles and the relative stratigraphic position of the various identified morphological structures on the corrected profile is shown in Fig. 2.9. Six major reflectors and their corresponding stratigraphic units were identified in the study area based on seismic facies characteristics. The major reflectors depicted a marked change in impedance contrast as a result of change lithology and reflects the bases of geological structures as well as former and modern landscape surfaces. Based on the major reflectors and units, a local stratigraphy model for the study area was developed (Fig. 2.9a). Fig. 2.9a also revealed the relative stratigraphic relationship of major identified structures in the study area both in space and time. Due to the lack of sediment cores and other ground truth data, the lithology of each of the identified seismic stratigraphic units were inferred based on previous studies in the area[15-18,28]. The oldest sediment

belongs to a large tunnel valley defined by Unit 1. Comparable tunnel valley in the area described by Hepp[15], Lutz[28] and Coughlan[17] suggest that this unit is made up of glacio-fluvial sand deposited in the Pleistocene. This was followed by the infill Unit 2 defined by Reflectors R2_1 and R2_2. The horizontally stratified infill units defined by these reflectors are inferred to be the same based on their approximate erosive depth, architecture and infill pattern. Where the unit is well developed (R2_2), the infill is transparent to semi transparent interpreted to be made up of sandy materials mixed with some fine materials (clay/silt). Unit 3 which incised these earlier formed structures was interpreted to be the Palaeo Ems, the submerged extension of the modern Ems river described by Hepp[16]. The base of this unit which is similar to the base of Unit 2 based on seismic facies characteristics is composed of organic rich layer described as peat by Hepp[16]. Studies by Hepp[16] revealed that the peat in Unit 3 was overlain by intertidal or marine deposits of clays or silty clays. Careful examination of the internal architectural pattern of this unit revealed a minimum of a two-phase poly infill. Unit 4 then overlies these structures except for where truncated by later formed structures. The characteristics dipping reflectors of Unit 5 were then formed and are inferred to be composed of Holocene sand and/or a mixture of Holocene sand and silt. The whole area was covered by Unit 6 whose base is an erosive Reflector R5 that cut off the area extent of Unit 5 towards the eastern part of the study area. In comparison with the studies by Hepp[16] and Zeiler[18], this unit represents the widely distributed recent mobile North Sea sand deposits. This 2 – 3 m thick sand blankets the older structures within the study area. The sea floor within the study area was depicted as seismic reflectors SF.

2.7 Conclusion

The history of water column statics correction is a research topic with a long tradition which has received special attention in recent decades. Different methods exist for correcting variations in water statics observed on seismic reflection data as a result of changes in water depth due to tides, drastic effect of velocity, acquisition related factors and/or combination of these factors. The data set used for this study was acquired as a series of independent acoustic lines over time with water depth ranging from about 15 m to 35 m. Due to the duration of the acquisition, water column height variations was observed within the seismic surveys. Own to the shallow water depth within the study area, change in velocity as a result of change in salinity and temperature was considered insignificant. This was because there was a whole movement of the water column giving rise to a strong mixing of the water masses and thus preventing any form of thermohaline stratification. For this data set, correction for variations due to tide, variations in the sea level due to bad weather condition and variations due to other acquisition related factors were applied to the data set.

This paper presents a modern approach and easy recipe for correcting water column height variation using co-recorded information from dGPS especially in near shore, shallow and highly erosive marine shelf settings. The methodology was applied to the SES data acquired from the shallow-water area of the German North Sea where tidal influence and water column height changes has been documented. Variation in water column heights along profile length reached over 3.0 m with large corrections attributed to rapid shoaling occurring near the coast and interplay between the water column and sea floor morphology. The corrected profiles which are now referenced to a consistent MSL show improved quality when compared to the uncorrected profiles. The sea floor from the corrected profile occurred deeper and showed good consistency with the bathymetry data compared to the uncorrected profiles. It was possible to distinguish and classify different generations of valley/channel structures which are on apparently similar depth levels stratigraphically based on their small gradient using the corrected profiles and thus validating the applicability of this methodology. The correction and datum referencing also helped in developing the relative true stratigraphic model for the area investigated. The findings and methodology are especially important for further high-resolution sea level variation studies and can be used to directly compute water column statics required for improve quality interpretation derived from seismic data. The less time-consuming methodology can be applied to all sorts of reflections seismic data and requires only a small budget which is especially important for scientific data acquisition and processing.

Acknowledgements

This research was carried out by Abegunrin A. as part of a PhD project at MARUM – Centre for Marine Environmental Sciences, University of Bremen, Germany. Abegunrin A. was funded by the Nigeria Petroleum Technology Development Fund (PTDF) in collaboration with the German Academic Exchange Service (DAAD). The research benefitted from the Cluster of Excellence ‘‘The Ocean in the Earth System’’ and the BMWi project ‘‘Restrike-XL’’ (FK: 0324231B). IHS Markit are acknowledged for making a student license of the IHS Kingdom software available for this study. Geo-Engineering provided the basic idea of dGPS static corrections, helped with the Reflex software license and contacts to Authorities. Contributions from Connor Schulze were also appreciated.

Competing Interests

The authors declare no competing interest.

Chapter 3

The Elbe Palaeovalley: evolution from an ice-marginal valley to a sedimentary trap (SE North Sea)

Aslı Özmaral[a,b], Ayobami Abegunrin[a*], Hanno Keil[b], Daniel A. Hepp[a,c], Tilmann Schwenk[b], Hendrik Lantzsch[a,b], Tobias Mörz[a,b], Volkhard Spiess[b]

[a]*MARUM – Center for Marine Environmental Sciences, University of Bremen, D-28359 Bremen, Germany*

[b]*Faculty of Geosciences, University of Bremen, D-28359 Bremen, Germany*

[c]*Lower Saxony Institute for Historical Coastal Research, D-26382, Wilhelmshaven, Germany*

[*]Corresponding author: aabegunrin@marum.de

Address: Leobenerstrasse 8, 28359 Bremen, Germany.

Published in Quaternary Science Reviews 282, 107453. https://doi.org/10.1016/j.quascirev.2022.107453.

Chapter 4

The Palaeo-Ems River in its Quaternary stratigraphic context

Ayobami Abegunrin[1*], Daniel A. Hepp[1,2] and Tobias Mörz[1,3]

[1]MARUM – Center for Marine Environmental Sciences, University of Bremen, Germany

[2]Lower Saxony Institute for Historical Coastal Research, D-26382, Wilhelmshaven, Germany

[3]Geo-Engineering.org GmbH, Bremen, Germany

[*] Corresponding Author; E-mail: aabegunrin@marum.de

Abstract

The Palaeo-Ems is one of the major tributaries feeding the Elbe Palaeovalley (EPV) and formed an important part of the drainage system that dewatered parts of the continental NW Europe unglaciated hinterland. In this study, detailed interpretation of high-resolution 2D seismic grid was utilized in tracking the overall course of the Palaeo-Ems channel as well as its spatial and stratigraphic relationships with other geological structures within the study area. Fundamental revisions of the old mapping of buried tunnel valleys, lacustrine deposits and recent fluvial channels were also carried out. The last phase of the Palaeo-Ems occurs as buried, low gradient and meandering channel branching into two major pathways as it approaches the EPV western flank. In its downstream direction, the channel formed a unified depositional system with the early phase of the EPV thus contributing to the last terrestrial phase of the complex EPV evolution. The unified system was later drowned due to the fast rising sea-level which overwhelmed the adaptation capabilities of the joint system. For the first time, this study shed light on the Palaeo-Ems/EPV morpho-stratigraphic relationships which played a key role in the Holocene coastal landscape architecture of the German North Sea since the Last Glacial Maximum.

Keywords: Palaeo-Ems; Elbe Palaeovalley; coastal landscape; Doggerland, glaciation.

4.1. Introduction

In the last couple of decades, many research activities have aimed at reconstructing the lost palaeo-landscape architecture (Gaffney and Fitch, 2022; Andresen *et al*., 2022; Bailey *et al*., 2020; Lohrberg *et al*., 2020; Winsemann *et al*., 2020; van Heteren *et al.,* 2014; Gaffney *et al.,* 2020; Cohen *et al*., 2014; Spinney, 2008; Hepp *et al*., 2012; 2017; Husse and Lykke-Andersen, 2000) and stratigraphy (Fleischer *et al*., 2022; Prins and Andresen, 2021; Hepp *et al*., 2019; Coughlan *et al*., 2018; Phillips *et al*., 2017; Cotterill *et al*., 2017a, 2017b; Fitch *et al.,* 2005) of the North Sea Basin. The repeated glacial-interglacial and post-glacial reshaping of the Quaternary landscape of the

North Sea resulted in complex and heterogenous morphological structures. These structures which are now palaeo-archives of past environmental changes can be related to various geological processes aided by major climatic-driven eustatic changes. In general, the Quaternary North Sea sub-surface is dominated by glacio-fluvial sands which are not only hard to date but also difficult to distinguish from each other due to strong similarities in material and grain characteristics. Thus, localized structural elements such as buried tunnel valleys, river channels, moraines, dunes, peats and palaeo-soils are important seismo-stratigraphic elements used in unravelling the structural and stratigraphic frameworks. These frameworks provide a well-structured and topographically sculptured landscape of the North Sea.

While this study focused on the southern part of the German North Sea sector, buried tunnel valleys and other comparable geologic structures were formed during all the Quaternary glaciation periods in the North Sea and are dominant in the upper strata of the sub-sea floor. The abundance, distribution, orientation, size, morphology and inferred age of known buried tunnel valleys across the North Sea and other parts of northern Europe are well documented in literatures (Lohrberg *et al*., 2020; Ottesen *et al*., 2020; Prins *et al*., 2020; Prins and Andresen, 2019; Coughlan *et al*., 2018; Huuse and Kristensen, 2016; Stewart *et al.,* 2013; van der Vegt *et al*., 2012; Hepp *et al*., 2012; Lutz *et al*., 2009; Kristensen *et al*., 2007). These buried tunnel valleys, formed at ice sheet margins, were active under direct glacial conditions and their infills played a key role in reconstructing the offshore Quaternary stratigraphy of the North Sea (Fig. 4.1).

The Elbe Palaeovalley (EPV; Fig. 4.2a) for instance is a drowned river valley located in the southeastern North Sea with a width of about 40 km, length of approximately 210 km and water depth varying between 35 and 50 m. This valley extends from the south-west of Helgoland in a northwest-southeast direction through the whole German North Sea sector with an expression in the form of a shallow depression on the modern seafloor. Seismo-stratigraphic interpretation of the EPV infill revealed 5 major units which were ground-thruthed with core data (Fig. 4.3; Özmaral *et al*., 2022; Papenmeier and Hass, 2020). The EPV played a major role in the late Weichselian and early Holocene palaeo-drainage network of northwest Europe as the meltwater and sediment flux from these areas were collected by it through a network of palaeo-rivers (Pisarska-Jamroży, 2015; Ehlers *et al*., 2004).

Recent studies of these palaeo-valleys and other comparable natural archives have improved the understanding of the impact of sea level changes on coastal landscapes and re-organization of the drainage system of the North Sea (Andresen *et al*., 2022; Roberts *et al*., 2018; Hepp *et al.,* 2017; van Heteren *et al.,* 2014; Blum *et al*., 2013; Bourillet *et al*., 2003; Meijer, 2002; Blum and Törnqvist, 2000). Extensive high quality geophysical, drill core, palaeo-environmental and sedimentological data sets from scientific and commercial cruises have continued to improve

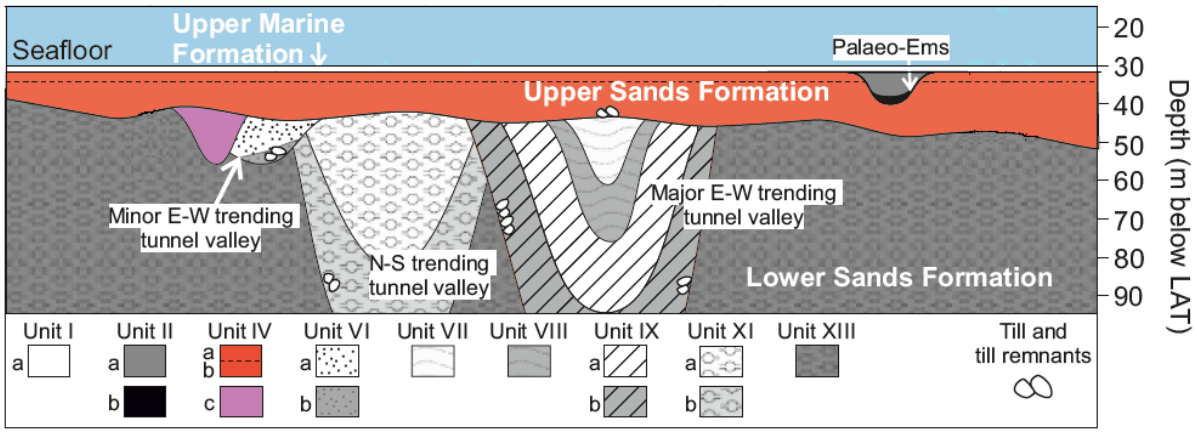

Fig. 4.1. Revised seismo-stratigraphic framework of the study area, modified after Coughlan *et al*. (2018) and Fleischer *et al*. (2022). See same for detailed description of units and nomenclature.

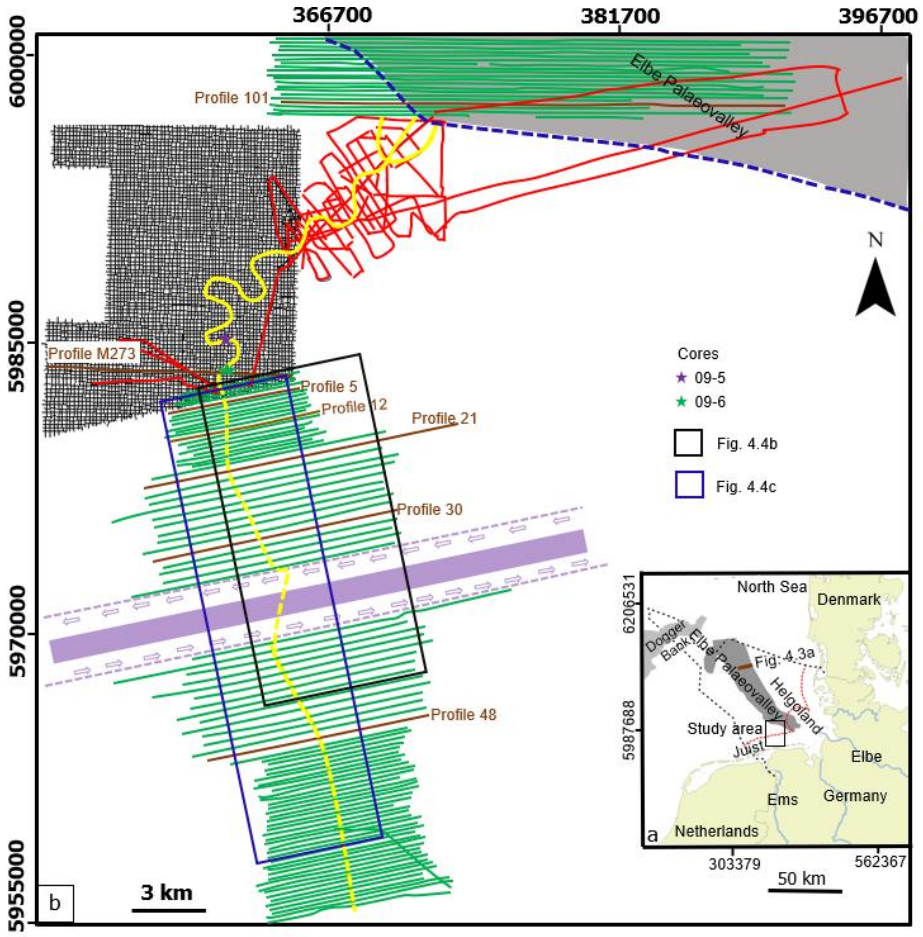

Fig. 4.2. Map of the study area north of the East Frisian Islands Norderney and Juist (a) within the German North Sea sector showing the location of the geophysical profiles (b). Note: The black dash line in (a) is the German Exclusive Economy Zone, red dotted line is the Territorial Waters (12 nautical miles), the green solid lines in (b) are geophysical profiles acquired during the RV Heincke expedition HE499 in 2017, the red solid lines are from 2013 HE403 RV Heincke expedition while the black solid lines are profiles from commercial surveys. The blue dashed line depicts the boundary of the Elbe Palaeovalley, the light purple area is the traffic separation scheme and the yellow line represents the documented river course (solid; Hepp *et al*., 2017) and hypothetical river course (dash line) of the Palaeo-Ems prior to the HE499 expedition. The key geophysical profiles discussed in this study are the brown solid lines. Purple and green stars mark location of cores 09-5 and 09-6 respectively.

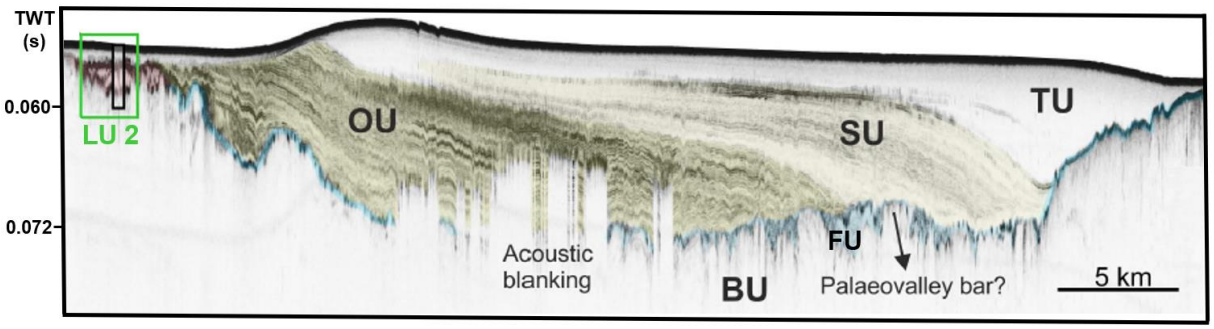

Fig. 4.3. Seismo-stratigraphic classification of the Elbe Palaeovalley infill after Özmaral *et al*. (2022). See the brown solid lines in Fig. 4.2a for location of the seismic sections. BU: Older Sediments; FU: Filled Unit; LU: Lower unit; OU: Oblique Unit; SU: Sigmoidal Unit; TU: Transparent Unit.

the understanding of palaeo-landscape structures in the North Sea. The result of one of such research efforts is a discovery of a tributary to the EPV, the now submerged palaeo-extension of the modern Ems River, which revealed the setting and evolution of the early Holocene landscape (Hepp *et al*., 2012). A small section of the river is seismo-acoustically and sedimentologically already well documented (Fig. 4.2b; Hepp *et al*., 2017; 2019) and a detailed deduction of its overall course is key in understanding the re-organization of the drainage system of the area since the Last Glacial Maximum (LGM). Based on this study, preliminary deductions from geophysical profiles obtained during the HE499 cruise in 2017 revealed that the linear course earlier defined for the Palaeo-Ems in the southern sector (yellow dash line in Fig. 4.2b, Hepp *et al*., 2017) is an artefact owing to an initial less dense seismic coverage. Furthermore, towards the downstream part of the river course, the nature of the river is not fully understood as studies by Hepp *et al*., 2019 revealed that the channel fans out into about three sub-channels forming a delta at the western flank of the EPV (Fig. 4.2b).

Understanding the palaeo-drainage networks of the North Sea is crucial for various reasons. In pre-historic times, coasts and river banks were a sought-after settlement area, because hunting and fishing offered a good livelihood there. At the same time, the flowing waters represented a natural network of paths through marshland, moorland, swamps and sometimes mark boundaries or territories (Warnke *et al*., 2014). Furthermore, the locations of the rivers are often preserved thereby holding relicts of the former landscapes and human habitation (Bailey *et al*., 2017, 2020; Coles, 1998; Flemming *et al*., 2017). A detailed knowledge of the palaeo-drainage stratigraphic infill is also important for various offshore geotechnical and engineering installations including but not limited to cable routing, wind farm development amongst others (Weihrauch *et al*., 2009; BSH 2021).

This study thus aimed at understanding the drainage systems of the palaeo-landscape at the North Sea shelf by answering the following distinct but closely related research questions. Firstly, what are the exact drainage pathways of the Palaeo-Ems at the western margin of the Elbe Palaeovalley as well as its southern connection to

the Modern Ems River? Secondly, what is the Palaeo-Ems/Elbe Palaeovalley´s spatial and stratigraphic relationship? What is the Palaeo-Ems spatial relationship with other glacial and post-glacial structures within the study area? The answers to these research questions will contribute to the morpho-stratigraphic reconstruction of the palaeo-landscape which developed after the LGM within the German sector of the North Sea.

4.2. Materials and Methods

4.2.1. Data Base

The study area is located north of the East Frisian Islands Norderney and Juist, within the southern part of the German North Sea sector (Fig. 4.2a). It extends between northings 5955000 m to 6000500 m and eastings 351700 m to 396700 m using the WGS84 UTM Zone 32N Projection and covers an area of about 1800 km^2 (Fig. 4.2b). The data sets available for this study consists of high-resolution seismic data (sediment echo sounder and Boomer data) acquired during the 2013 HE403 and 2017 HE499 cruises on the research vessel Heincke. Additional grids of closely spaced seismic profiles (Boomer data) and core data from commercial surveys carried out between 2007 and 2010 were sourced in areas with now restricted access due to ongoing wind farm operations as complementary data sets (Fig. 4.2b). These data sets are explained in detail in the following sub-sections.

4.2.1.1. Geophysical Data

A total of about 380 lines of both sediment echo-sounder (SES) and Boomer data constitute a dense grid of high-resolution 2D seismic data used in this study (Fig. 4.2b). The SES profiles were collected using a ship-mounted sediment echosounder Innomar SES2000 medium-100 model with an acoustic power greater than 247 dB (~5.5 kW). Differential Global Positioning System data were also obtained along each of the SES track lines. The SES data provide a very high resolution of the uppermost 15-20 m below the sea floor. The SES2000 is a parametric echo sounder system in which signals of new frequencies are created by the interaction of two transmitted signals of different frequencies owing to non-linearities in the sound propagation. On board of the research vessel Heincke used during the HE499 expedition, the adopted SES2000 medium-100 model was operated in multi-frequency mode and secondary frequencies of 4 kHz, 8 kHz and 12 kHz were generated at alternate times. The acquired acoustic data were digitally converted to the standard SEGY data format using the SesConvert tool and merged with differential GPS navigation. A total of 116 east-west profiles in a north-south progression which are between 200 m to 250 m apart were acquired and due to extreme bad wave and weather conditions at the time of the survey, north-south profiles and sediment cores required for ground truthing were not collected. About 80 SES profiles acquired during the HE403 expedition in 2013 were also made available for this study. These profiles were acquired in a similar manner as those from the HE499 expedition.

The Boomer data from the industrial survey were obtained using a single-channel seismic system operated using an energy of 200 J and a 3 m single-channel streamer with 8 hydrophones. The Boomer data produced a high-resolution image of the upper 15-30 m with a very high vertical resolution of about 20-50 cm. The data which were acquired in both the north-south and east-west directions were recorded using the NWC software (Nautik Nord GmbH) with a shot rate of 3.5 shots per second and a 16-bit resolution. A grid comprising of about 184 seismic profiles with a mesh width of approximately 200 m was acquired in total. Conventional seismic processing procedures were carried out specifically to meet the needs of high-resolution shallow-water seismic data with special emphasis on water-column static correction. Where applicable, water-column height variations caused by tides, weather and current were accounted for using procedures outlined by Abegunrin *et al*. (2020) prior to interpretation.

The processed data sets were then interpreted in a standard workstation. The seismic data were analyzed using the IHS Kingdom Advanced software for conventional seismic and stratigraphic interpretations. Key stratigraphic surfaces were identified based on detailed information observed from seismic sections which are marked by changes in impedance contrast. The identified surfaces were then mapped across the survey area based on amplitude strength, character and continuity. Channels and other seismic scale structures defined on the seismic sections were also identified and mapped. Due to the different acquisition parameters and degree of resolution, the SES data was gridded using the cubic spline gridding algorithm while the Boomer data was gridded using the flex gridding algorithm. The identified seismo-stratigraphical units and structures were then tied to core samples at core sites by linearly converting the two-way travel time to depth based on an average sound velocity of 1550 m/s, a value fitting well for the uppermost 50 m below the sea floor based on previous studies (Winsemann *et al*., 2020; Lutz *et al*., 2009; Hanno Keil, personal communication, February, 2021). This enables a direct integration of seismic and core data in ascertaining and correlating boundaries and lithology with seismo-stratigraphical units and structures. Channel sinuosity was obtained by taking the ratio of the length of the channel and the straight-line distance between the end points of the selected channel reach. The gradient was calculated by dividing the vertical difference in the depth of the channel base between two points by its horizontal distance.

4.2.1.2. Core Data

Sediment cores from commercial surveys carried out in 2009 within the vicinity of the seismic profiles using ship based rotary flush drilling and jack-up based high-quality percussion drilling, both with > 90% recovery, were made available for this study. Due to commercial restrictions, the cores selected for this study are coded 09-5 and 09-6 (Fig. 4.2b) and their exact locations are not provided in this study. The cores are recovered from water depths

between 28.7 and 31.1 m. The University of Bremen operated Geo-corer 6000 system with a barrel length of 5.80 m yielded sediment cores with a recovery rate between 85% and 97% for all encountered lithologies. The cores, either recovered in whole or segmented into 1 m sections, were immediately opened, photographed, visually described and documented on board and later further characterized in onshore laboratories. The core description includes but it is not limited to information on colour, lithology, sedimentary structures, grain size, bulk density and carbonate content.

Data integration was employed in defining the overall course of both the glacial and post glacial structures together with their relative age, morphological relationships and systematic infill stratigraphy.

4.3. Results

4.3.1. The Palaeo-Ems: An overview and infill stratigraphy

An overview of the Palaeo-Ems along its flow direction (downstream) is here presented. The northern course of the documented Palaeo-Ems river, west of the EPV (Fig. 4.2b), as well as the southern course towards the coast are hereafter referred to as the northern and southern extensions respectively. Within the southern extension, the southernmost area (about 20 km north of the Juist Island) was characterized by intense erosional activities and all the seismic profiles from this area are mostly featureless. From about 20 km north of the Juist Island, the Palaeo-Ems was identified and the overall mapped course span over 100 km in length (Fig. 4.4a). This channel course which runs from south to north was mapped on seismic profiles over an area of about 1800 km^2. The mapped course of the Palaeo-Ems channel presented in Fig. 4.4a depicts the last open phase of the river which was filled during subsequent marine transgression.

The channel has a sinuosity ratio of about 2.2 and shows evidence of lateral migration which resulted in abandoned courses over time (Fig. 4.4a). Fig. 4.5 depicts a gradient plot obtained from the depth of the deepest point of the seismically resolved base of the channel across profiles. From this plot, it was possible to deduce the trend and gradient of the channel in a south-north progression. The channel has a shallow gradient and dips gently at about 25 km (gradient of about 0.04%) before flattening out at about 37 km (Fig. 4.5). In the northern extension, the Palaeo-Ems can be sub-divided into two major pathways (P1 and P2), each subsequently sub-divided into at least three (P1) and two (P2) sub-paths (Fig. 4.4a). The major pathway P1 (black stars) appeared to be stratigraphically deeper than the major pathway P2 (green stars) as seen in Fig. 4.5. On seismic sections, the Palaeo-Ems was mapped as an asymmetrical channel characterized by both gentle and steep sides in areas where the seismic profiles cut its course perpendicularly (Figs. 4.6b and c). The channel width increases from about 1100 m to about 1700 m in a south-north progression. However, as seen in Fig. 4.6d, the width especially within the southern extension could be less than 300 m due to the effects of subsequent erosion.

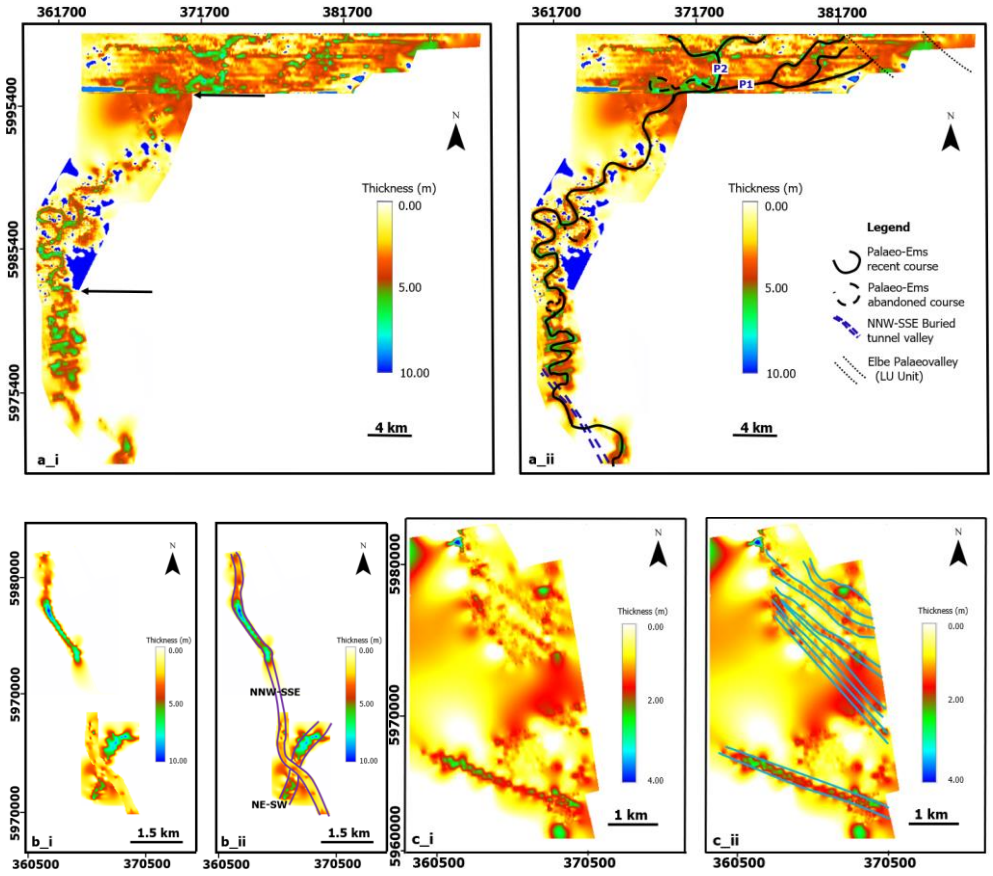

Fig. 4.4. Seismic interpretation of the Palaeo-Ems River (a), buried tunnel valley (b) and straight river channel systems (c). Note: The black arrow in Fig. 4.4a_i depicts the limits of the Boomer data from the SES data and both data are gridded using different gridding algorithms. Figs. 4.4a_i, b_i, c_i and Figs. 4.4a_ii, b_ii, c_ii represent gridded sections and gridded sections with interpretations respectively.

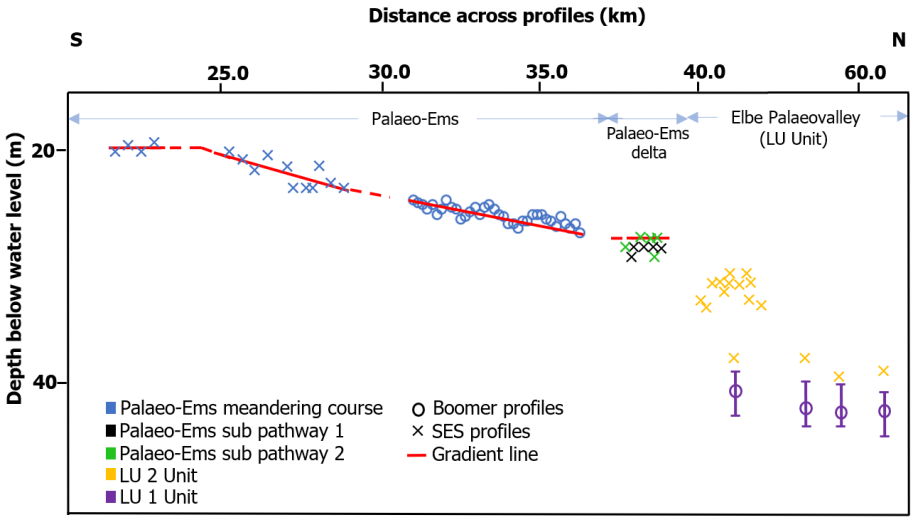

Fig. 4.5. Approximate base of the Palaeo-Ems channel mapped along the black line in Fig. 4.4 a_ii as well as the base of the LU unit of the EPV (see Fig. 4.8). Blue = Base of the Palaeo-Ems along the meandering course; Black = Base of the Palaeo-Ems along sub pathway 1; Green = Base of the Palaeo-Ems along sub pathway 2; Yellow = Base of the upper LU2 unit; Purple = Inclined base of the dipping LU1 unit. The star symbols depict estimated depth from SES profiles while the circle symbols depict estimated depth from Boomer profiles. Note: The purple vertical lines represent ranges while the circles denote mean values. The base of the channel was better imaged from the Boomer profiles due to lower frequency and deeper penetration depth.

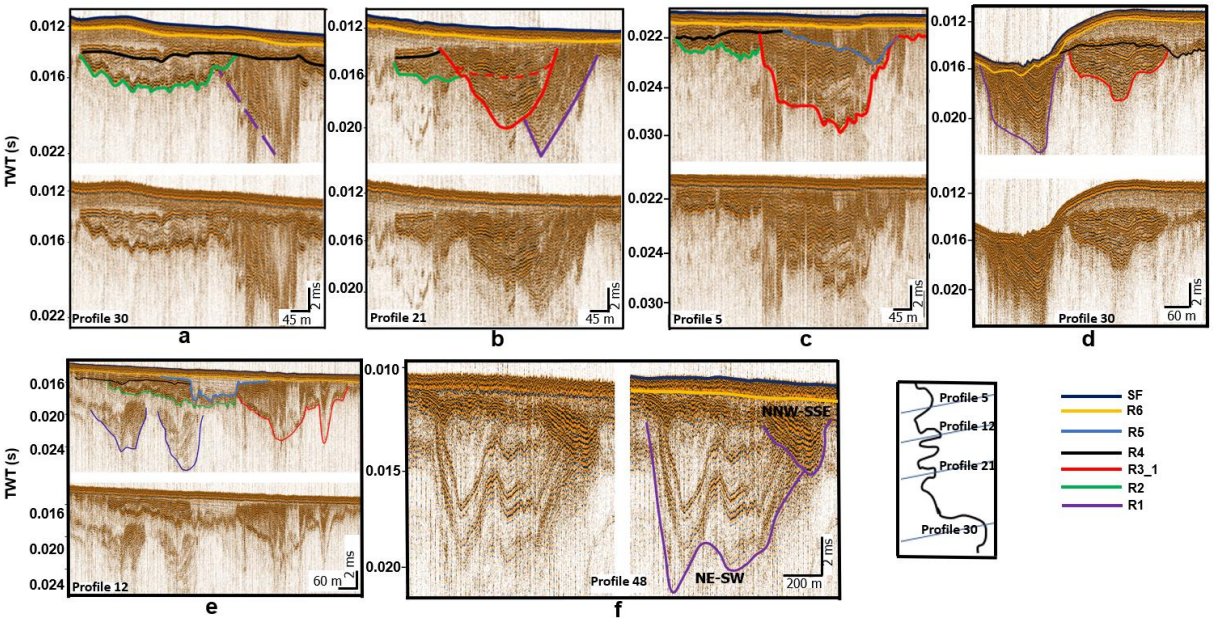

Fig. 4.6. Representative seismic sections showing the identified structures and their inter relationships within the study area (see the brown solid lines in Fig. 4.2b for location of all the seismic sections). Note: The purple colour: Buried tunnel valley, green colour: shallow depression structure, red colour: Palaeo-Ems, blue colour: straight river channel, black and yellow lines are the key seismic reflectors. R represents major seismo-stratigraphic surfaces and SF is sea floor.

Seismic facies analyses of the Palaeo-Ems infill show a minimum of a two-phase infill characterized by high-amplitude and continuous reflectors compared to the substrate in which the valley incised. The infill reflectors are undisturbed and parallel to each other (Figs. 4.6b, c and d). In some areas, the uppermost infill of the channel shows a characteristic secondary incision by younger structures (Fig. 4.6c). Based on the resolution of the seismic data, four seismo-stratigraphical units (Unit II, III, IV, V) were deduced from the base of the channel to the sea floor, while Unit I underlies the base of the channel (Fig. 4.7). In chronological order, Unit I which is characterized by low-amplitude and discontinuous reflectors corresponds to fine- to medium-grained sand. Unit II, which is defined by medium- to high-amplitude, semi-continuous to continuous reflectors, is composed of peat with some intercalated sand layers. Unit III is defined by medium-amplitude, continuous reflectors with a combined lithology of both silt and fine sand. Unit IV is predominantly fine sand seen on seismic sections as medium amplitude, semi continuous to continuous reflectors. Unit VI is characterized by high-amplitude, continuous reflectors and the lithology of this unit is fine sand with some pockets of medium-grained sand (Fig. 4.7).

4.3.2. Other identified structures and their seismo-stratigraphic infill

Within the study area, the Palaeo-Ems is accompanied by older and younger geological structures. These structures were mapped and described in order to avoid misinterpretation and false mapping which is typical in areas with complex generations of geologic structures.

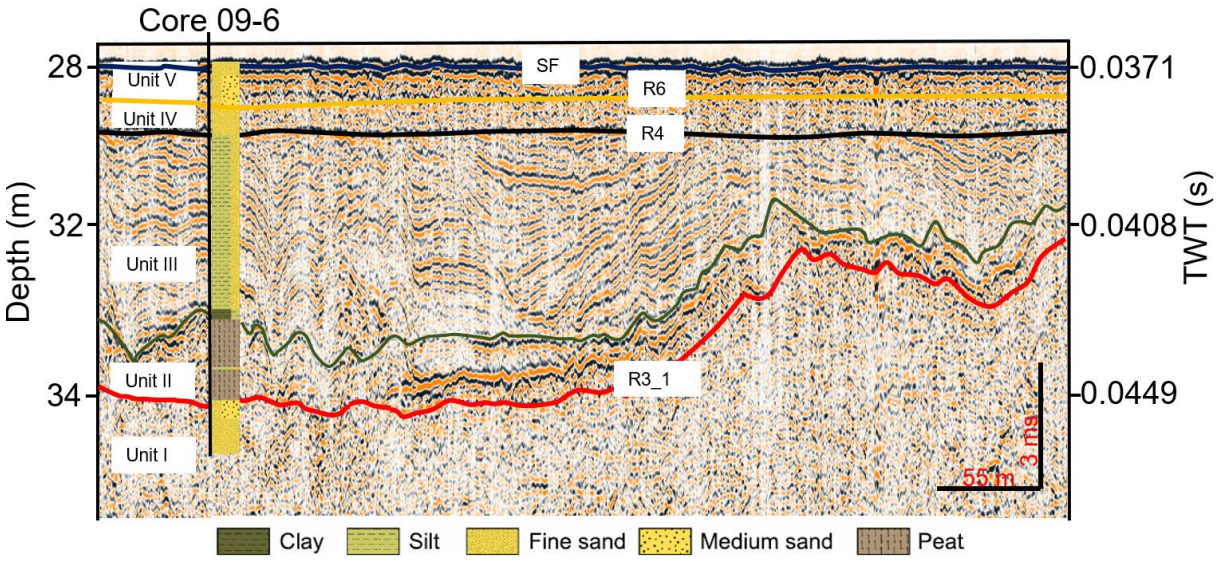

Fig. 4.7. Boomer profile M273 showing the super-imposition of core description on seimo-stratigraphic interpretation (see the brown solid line and green star in Fig. 4.2b for location of the seismic section and core site respectively). R represents major seismo-stratigraphic surfaces and SF is the sea floor.

The identified structures include buried tunnel valleys, shallow depression structure and straight channel structures. These structures as well as their seismo-stratigraphy are shown in Figs. 4.4b-c and Fig. 4.6. All identified structures are completely buried with no expression on the modern sea-floor. The oldest mapped geologic structures within the study area are the buried tunnel valleys which are characterized by steep dipping flanks and are more V-shaped. Two prominent generations of these buried tunnel valleys trending approximately in a NE-SW and NNW-SSE direction were identified (Fig. 4.4b). The seismic expressions of the valleys are depicted in Figs. 4.6b, d, e and f. The NE-SW valley is larger in size than the NNW-SSE valley. Furthermore, the NNW-SSE valley shows a cross-cutting relationship with the uppermost part of the NE-SW valley as seen in Fig. 4.6f. The NE-SW valley has a width of up to 800 m and a length of about 2.5 km while the NNW-SSE valley has an approximate mapped length of about 7.8 km and a width of about 300 m. The width and thickness of the NNW-SSE valley infill progressively become smaller from north to south (Figs. 4.4b and 4.6f). While the NE-SW valley was captured within the southernmost part of the study area at a depth below sea level of about 20 m, the NNW-SSE valley transcends the study area in an approximate north – south direction with an approximate depth below sea level of about 12 m in the south to more than 25 m further north. These depth values are based on the seismically resolved base of each of the valley generations and both valley generations extend beyond the area mapped in this study. In some areas, the NNW-SSE buried tunnel valley shows evidence of an incision by the Palaeo-Ems (Fig. 4.6b). Seismic facies analyses of the internal reflector pattern of the buried glacial valleys as seen in Figs. 4.6b, d, e and f revealed steeply inclined moderate-amplitude, semi-continuous to discontinuous reflectors.

Furthermore, west of the Palaeo-Ems, a shallow depression structure was identified as an adjoining structure to the Palaeo-Ems (green line in Figs. 4.6b, c and e) and also as a discrete structure (green line in Fig. 4.6a). Both forms of this structure have the same approximate erosive depth, architecture and infill patterns (Figs. 4.6a, b, c and e). Where the structure is well developed (Fig. 4.6a), the infill is defined by high-amplitude, continuous reflectors at the base overlain by a characteristic low- to medium-amplitude, semi-continuous to continuous reflectors. This structure has a cutting depth of about 15 m.

In addition, straight channel structures with a general NW – SE trend are also identified and mapped across the study area (Figs. 4.4c and 4.6c, e). In most cases, the course of these structures occurred as discrete channels while in some areas, they incised the upper parts of older structures such as the Palaeo-Ems (Figs. 4.6c and e). Where the straight channel structure is well developed, its infill reflectors displays a characteristic dip (Fig. 4.6e). The typical internal pattern of the its infill is a transparent unit defined by low amplitude, continuous and sometimes dipping internal reflectors (Fig. 4.6e).

4.3.3. The Palaeo-Ems/Elbe Palaeovalley stratigraphic relationship

For the first time, the Palaeo-Ems was also analysed in detail with respect to its spatial and temporal relationships with the Elbe Palaeovalley (EPV). The Palaeo-Ems constitutes one of the major tributaries towards the southwestern part of the EPV (Fig. 4.2b) where it fans out into two major and at least five minor pathways (Fig. 4.4a). Özmaral *et al*. (2022) and Papenmeier and Hass (2020) gave a comprehensive seismo-stratigraphic classification of the EPV infill. The Özmaral *et al*. (2022) classification sub-divided the EPV infill into 5 major intervals as shown in Fig. 4.3. These intervals from old to young are named Incised channel infills (FU), Transparent lenses (LU), Oblique Unit (OU), Sigmoid Unit (SU) and Transparent Unit (TU). The EPV incised older Pleistocene sediments denoted as BU. The LU units occurred as an in-channel aggradation in which two forms were identified: an inclined or dipping LU1 unit and an upper or shallower LU2 unit (Özmaral *et al*., 2022). Detailed seismo-stratigraphic interpretation of profiles within the study area identified units belonging to the LU2 unit of Özmaral *et al*. (2022) classification (Fig. 4.8). The acoustic units of the LU2 infill within the study area are defined by medium-amplitude, semi-continuous reflectors at the base overlain by a thin acoustically transparent interval. The upper boundary is represented by low-amplitude, semi-continuous reflectors (Fig. 4.8). The LU2 of Özmaral *et al*. (2022) and that identified in this study show consistency in terms of geometry, depth of occurrence and seismic facies characteristics (Figs. 4.3 and 4.8). On low-noise sections, the base of both the Palaeo-Ems and LU2 unit of the EPV are inseparable and their infills form a continuous unified depositional system (Fig. 4.8).

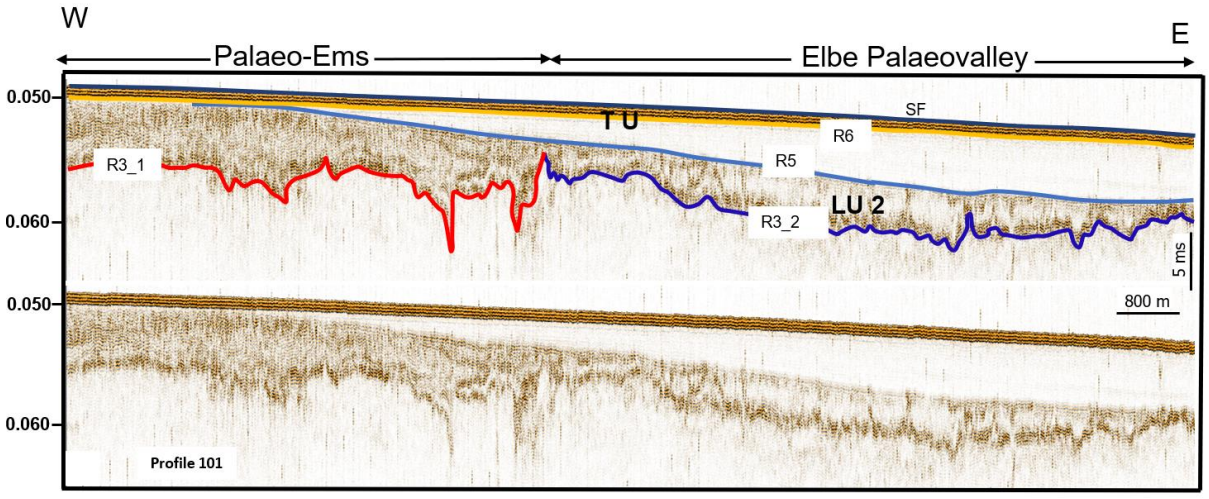

Fig. 4.8. Palaeo-Ems/Elbe Palaeovalley morphological relationship. R represents major seismo-stratigraphic surfaces and SF is sea floor. See the brown solid line (Profile 101) in Fig. 4.2b for location of the seismic sections.

The base of LU2 unit was also observed to be steeper than the base of Palaeo-Ems (Fig. 4.5). On some of the interpreted profiles, the Palaeo-Ems and the LU2 unit are directly overlain by the Transparent Unit (TU) (Fig. 4.8).

4.3.4. The Palaeo-Ems: Relationship with all identified geological structures

The spatial and stratigraphic relationship of the Palaeo-Ems with other identified structures within the study area is shown in Figs. 4.9 and 4.10 respectively. As seen in Fig. 4.9 (insert figure), younger structures show evidence of re-use of older structure's pathways. The Palaeo-Ems transcends parts of NNW-SSE valley while the straight structures incised parts of the older structures (Fig. 4.9). The oldest identified structures are the buried tunnel valleys bounded by seismic reflectors R1 and R3_1 (Fig. 4.10). This was followed by the infill unit of the shallow depression structure defined by reflectors R2_1/R2_2 and R3_1/R4. Next is the Palaeo-Ems channel (base reflector R3_1) which incised these earlier formed structures. As seen in Fig. 4.6b, the Palaeo-Ems incised the eastern part of the shallow depression structure. The Palaeo-Ems also incised more than 15 m of the NNW-SSE buried tunnel valley (Fig. 4.10) over an approximate length of about 4 km (Fig. 4.9). Reflector R3_2 marks the base of LU2 unit of the EPV and it is also a time equivalent with reflector R3_1. Evidences for this include similar age date, infill lithology and depositional settings (Table 4.1). Reflector R4 is a key stratigraphic surface representing a period of non-deposition/erosion that separate older structures from younger ones (Fig. 4.10). The top of LU2 unit is bounded by reflector R5 which also marks the base of the straight channel structure networks that sometimes incised the Palaeo-Ems (Figs 4.9 and 4.10). The straight channel structures as seen in Fig. 4.9 run roughly parallel to each other. All identified structures are overlain by laterally deposited units bounded by reflectors R4/R6, R5/R6 and R6/SF respectively.

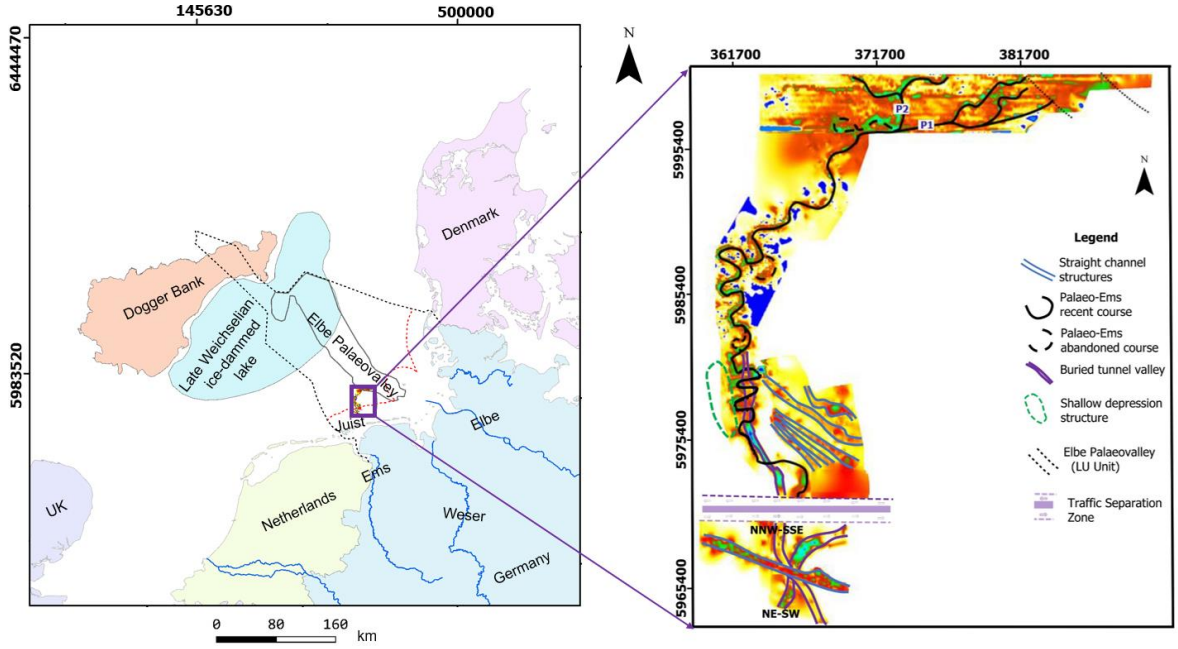

Fig. 4.9. Spatial relationship between the identified geological structures within the study area.

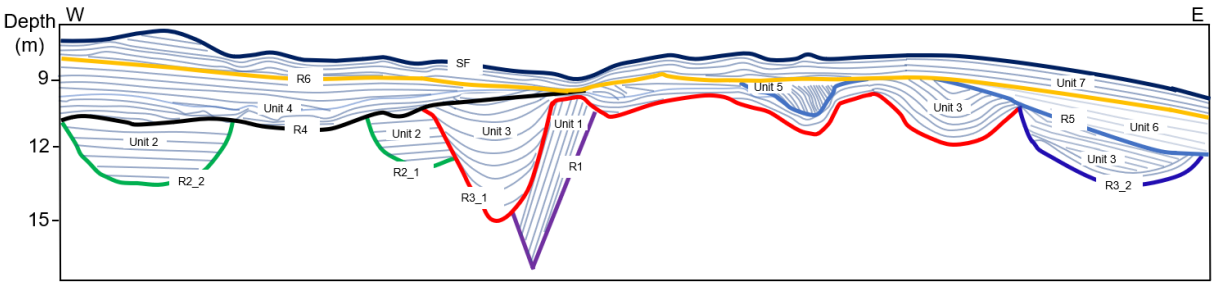

Fig. 4.10. 2D model showing the stratigraphic overview of various structures within the study area based on seismic sections presented in Figs 4.5 and 4.8.

Table 4.1. Classification of the Palaeo-Ems/Elbe Palaeovalley stratigraphic infill relationship

Palaeo-Ems				Elbe Palaeovalley			
R	Unit	Lithology/Thickness	Age (cal ka BP) Hepp *et al.*, 2019	Unit Özmaral et al., 2022	Unit Papenmeier&Hass, 2020	Age (cal ka BP) Özmaral et al., 2022	Lithology/Thickness
SF							
	V	fine to medium sand (30 cm)		TU	SU 4	<5.8	fine to medium sand (150 cm)
R6							
R4	IV	silty sand (106 cm)	7.48 – 9.29	SU	SU 3	8 - 5.8	silty clay (550 cm)
	III	clayey silty (256 cm)	9.29 – 9.47	OU	SU 2	10 - 8	fine sand with clay layers (600 cm)
	II	basal peat (81 cm)	9.69 – 11.44	LU2	not identified	11.20 -10*	basal peat overlain by stratified silty clay (200 cm)
R3_1				FU		LGM – 11.2	medium sand with clayey silt (200 cm)
	I	fine to medium sand (>62 cm)	>11.44	BU	SU 1	>LGM	fine sand (>100 cm)

* Age date was obtained from the basal peat; LGM: Last Glacial Maximum; R: Major seismic reflectors; SF: Sea floor

The sea floor (SF) consistently dips northward with depth to seafloor ranging from less than 15 m in the south to more than 35 m in the north.

4.4. Discussion

As revealed in Fig. 4.2b, Hepp *et al*. (2017; 2019) already described a part of the Palaeo-Ems course in terms of seismo-stratigraphy and sedimentology. The overall seismo-acoustic, sedimentologic characteristics and morphological relationships of the Palaeo-Ems in relation to other identified geologic structures within the study area are herein discussed.

The Palaeo-Ems is present as a buried meandering channel with no morphological expression on the modern sea floor. The meandering nature of the valley was attributed to low velocity of the flowing river, lithological composition and the shallow south-north gradient. The base of the Palaeo-Ems channel as imaged from high-resolution Boomer profiles corresponds to Unit II (Fig. 4.7) and it is made up of peat layers. All core samples taken along the channel course described by Hepp *et al*. (2017) penetrated the basal peat with an age of about 9-11 cal ka BP (Hepp *et al*., 2019; Table 4.1). Typically, the basal peat is overlain by clay, silty clay and sand of varying thickness denoted by units III, IV and V. A 10-20 cm shell agglomerate was also identified between units IV and V at some locations by Hepp *et al.* (2019). This valley infill was deposited in an environment that changed from freshwater to brackish and finally to marine conditions over a period of about 200 years as a result of a rapid rise (~2.5 m) in sea level during the early Holocene (Hepp *et al*. 2019). In general, the Palaeo-Ems channel incised sub-strata Pleistocene glacial and glacio-fluvial sediments/structures (Unit I).

The conceptual model presented in Fig. 4.10 depicts the stratigraphic relationships between the various structures within the study area. The Palaeo-Ems occurred in close relationship with other geological structures (Fig. 4.10) and these inter-relationships are also depicted in Fig. 4.9 (see Fig. 4.6 for seismic expressions). The oldest identified structures are the buried tunnel valleys (Figs. 4.6b, d, e and f) in which two generations with NE-SW and NNW-SSE orientations were mapped (Figs. 4.6f and 4.8). The widths and thicknesses of the buried tunnel valleys, which became progressively smaller in the southern part of the study area, were attributed to subsequent erosional processes. These buried tunnel valleys are bounded by seismic reflectors R1 and R3_1 (Fig. 4.10) and are comparable in size, length, orientation and morphology to other Pleistocene buried tunnel valleys mapped and described by Lohrberg *et al*. (2020); Stewart *et al.* (2013) and Lutz *et al*. (2009) in the southern North Sea and adjacent areas. The buried tunnel valleys are composed of mainly glacio-fluvial sands (Coughlan *et al*., 2018; Hepp *et al*., 2012) and incised into Neogene and late Palaeogene sediments (Lohrberg *et al*., 2020; Winsemann *et al*., 2020). While the exact processes responsible for the origin and formation of these tunnel valleys, which are widespread in the North Sea and northern Europe, remains contentious in literature (Winsemann *et al*., 2020; van

der Vegt *et al*., 2012; Huuse and Lykke-Andersen, 2000; O'Cofaigh, 1996), they are generally believed to occur roughly parallel to the direction of ice flow and serve as key conduits for meltwater discharge underneath the continental ice sheets (Özmaral *et al*., 2022; Stewart *et al*., 2013). The Palaeo-Ems incised about 15 m into the buried tunnel valleys emphasizing a younger age for the Palaeo-Ems. Furthermore, as shown in Fig. 4.9, the Palaeo-Ems shows evidence of re-use of the older buried tunnel valley pathways in some parts. Such re-use of older structures by younger glacial valleys or rivers which are usually expressed on seismic sections as complex valley infill architecture of multiple cut and fill structures are well documented in the North Sea (Prins and Andresen, 2019; Stewart *et al*., 2013; Lutz *et al*., 2009 amongst others). The low gradient of the Palaeo-Ems channel suggests a low velocity for the river with a moderate discharge. Further northwest of the Palaeo-Ems area, similar fluvial structures are known from the western part of the Dogger Bank as well as the north-eastern part of the EPV (Emery *et al*., 2020; Hepp *et al*., 2017; Fitch *et al.,* 2005). These structures exhibit close morphological similarities and time of development as the Palaeo-Ems. However, the advancing sea level of the North Sea resulted in an earlier drowning of these more northern river systems.

West of the Palaeo-Ems channel, another shallow depression structure was identified and mapped. This structure was referred to as lacustrine deposits owned to its characteristic architectural pattern and the near-horizontal seismic reflectors of its infill (Fig. 4.6a). The characteristic laterally stratified sediment successions of this structure as seen on seismic sections are similar to those of the late Weichselian ice-dammed lake identified north of the study area around the Dogger Bank area (Hjelstuen *et al*. 2018; Emery *et al.*, 2019; Özmaral 2017; Fig. 4.9). These lacustrine deposits are thus interpreted to be relicts of these late Weichselian ice-dammed lake which are believed to be present in the North Sea. The lacustrine deposits in this study occurred in two forms: as a discrete structure (Fig. 4.6a) and as an adjoining structure to the Palaeo-Ems (Figs. 4.6b, c and e). The discrete form is bounded below and above by reflectors R2_2 and R5 respectively while the adjoining structure was bounded by R2_1 and R3_1/R4 reflectors (Fig. 4.10). The composition of this structure was inferred from those of the pro-glacial lakes has been composed of sandy materials mixed with some fine sediments (clay/silt) (Hartmut Heinrich, personal communication, March 3, 2022; Özmaral 2017). Careful examination of the margin of the adjoining structure revealed that the Palaeo-Ems cuts the eastern side of this structure (Fig. 4.6b and c). This again shows that the Palaeo-Ems channel is younger than the lacustrine deposits. The Palaeo-Ems itself is bounded by reflectors R3_1 and R4 (Fig. 4.10). Seismic facies analyses of the channel infill revealed a minimum of a two-phase infill made up of peat-clay/silt sequences (Figs 4.6b; Hepp *et al*., 2019). Reflector R4 is a key stratigraphic surface representing a period of erosion and/or non-deposition (hiatus). This was followed by incisions of straight structures interpreted

as more recent fluvial river channel networks inferred to be infilled with sand and/or a mixture of sand and silt. In fact, the uppermost infill of the Palaeo-Ems as well as parts of the buried tunnel valleys were all incised by these fluvial river channels (Figs. 4.6c, e and 4.8). This indicates that the fluvial river channels are younger than the buried tunnel valleys, lacustrine deposits and the Palaeo-Ems channel which are also present within the study area. The fluvial river channels also occur as discrete structures with a general NW-SE trend (Fig. 4.9). This was followed by laterally deposited fine sand and silt separated from the overlying fine to medium mobile sand by reflector R6. This mobile sand is widely distributed throughout the North Sea (Zeiler *et al.*, 2000) and are referred to as the Upper Marine Formation by Coughlan *et al*., 2018 (Fig. 4.1).

Although studies by Özmaral *et al*. (2022) and Papenmeier and Hass (2020) detailed the evolution and stratigraphic infill of the EPV, this study for the first-time shed light on the Palaeo-Ems/EPV morphologic and stratigraphic relationship. The EPV, a now mostly buried geomorphological shallow trough, was the main drainage pathway for meltwater from the southern margin of the Scandinavian ice sheet as well as rivers draining the North European plain (Papenmeier and Hass, 2020; Özmaral *et al*., 2022; Figge 1983). The Palaeo-Ems on the other hand has been shown to be one of the major tributaries of this approximately 210 km long EPV situated in the southeastern North Sea (Hepp *et al*., 2017). While the Palaeo-Ems played a major role in the drainage network of the hinterland areas, its drainage pathways and morpho-stratigraphic relationship at the western margin of the EPV remained unknown. Based on this study, a detailed interpretation of high-resolution seismic profiles west of the EPV revealed that the Palaeo-Ems spatially sub-divided into two major pathways (P1 and P2) with each pathway branching out into smaller paths as it approaches the western rim of the EPV (Fig. 4.4a).

While the EPV itself is older than the Palaeo-Ems, detailed seismic analysis at the western margin of the EPV revealed that the Palaeo-Ems formed a unified depositional system with the EPV. In fact, the early infill sequence of the Palaeo-Ems was observed to coalesce with the LU unit of the Özmaral *et al*. (2022) EPV classification. Sediment cores revealed the presence of peat layers at the base of the Palaeo-Ems (Fig. 4.7) and LU2 unit (Özmaral *et al*., 2022) which are deposited in a wetland setting. Age dates by Hepp *et al*., 2019 and Özmaral *et al*. (2022) on these basal peats revealed similar ages in the range of 9.6 to 11.5 cal ka BP (Table 4.1). These similar ages corroborate the assumption that both the Palaeo-Ems and LU unit are contemporaneous. In addition, the similar infill lithology of silty clay and/or clayey silt and sand also points toward a simultaneous deposition (Table 4.1). This implies that the Palaeo-Ems constitutes not only part of the palaeo-drainage system that emptied into the EPV but also contributes to the shaping of the second phase (LU unit) of the EPV evolution at the earliest.

The Palaeo-Ems/EPV relationship can thus be explained by understanding their infill history and morphological patterns. The first phase of the EPV formation which is represented by the FU unit (Fig. 4.3; Özmaral *et al*., 2022) is a classic ice marginal valley infill formed as a result of water collected from the retreating ice. This FU unit formed a braided river system at the base of the EPV during periods of low sea level (Özmaral *et al*., 2022). Post-glacial sea-level rise led to a retreat in coastline and in-channel aggradation observed as LU unit by Özmaral *et al*. (2022). In-channel aggradation as a result of sea-level rise (Martin *et al*., 2009; Törnqvist 1994) can result in super-elevation of flowing river relative to the surrounding floodplain (Mohrig *et al*., 2000; Slingerland and Smith, 2004). The EPV drainage thus adapted to the new hydrodynamic regime during the post-glacial sea-level rise and maintained elevation relative to the sea-level (Özmaral *et al*., 2022). This possibly prompted the Palaeo-Ems river to change its course to different channels as observed at the western flank of the EPV (Fig. 4.4a_ii). As seen in Fig. 4.4a_ii, the different Palaeo-Ems pathways were attributed to hampering in its flow path leading to the development of a deltaic situation west of the EPV. This Palaeo-Ems delta formation is evident in the near-zero gradient seen on the gradient plot of the sub pathways (green and black symbols in Fig. 4.5). Morphological terraces initiated during the incision stage of the EPV are accompanied by valley widening during the subsequent valley infill stages (Özmaral *et al*., 2022). Such back-cutting and widening of the EPV are believed to be responsible for the subsequent capture of the Palaeo-Ems river by the EPV with the infill of the Palaeo-Ems corresponding with the last phase of LU unit (LU2) of Özmaral *et al.* (2022) classification. The steeper gradient of LU (yellow and purple symbols in Fig. 4.5) compared to that of the Palaeo-Ems is also believed to be as a result of the back-cutting and widening of the EPV. The infill of both the Palaeo-Ems and LU unit represents a last stage deposition prior to a full marine condition thus indicating a relatively young age for the joining event. Both the EPV and Palaeo-Ems systems were later drowned as a result of the fast-rising sea level overwhelming the adaptation capabilities of the joint system.

4.5. Conclusion

This study provides a new insight into the overall course of the Palaeo-Ems river as well as its stratigraphic relationship with other geologic structures particularly the EPV, using high-resolution seismic profiles. The overall morphology of the Palaeo-Ems was dictated by the topography of the area, underlying structures, intensity of fluvial activities and most of all, the sea-level rise as well as the relative timing of these events. In a south-north progression, the Palaeo-Ems occurred in most parts as a meandering river and became more linear towards the western margin of the southern part of the EPV. Over the course of its length, the river showed various abandoned pathways which supported intense fluvial activities at the time of formation. In addition, the Palaeo-Ems incised and re-used the pathway of the older Pleistocene structure in some areas. At the western margin of the southern

EPV, the river branched into two major and at least five minor sub-paths forming a large delta. It was deduced, based on available data for this study, that the younger Palaeo-Ems connected to the older pre-existing EPV structure and formed a unified system with the last stage of the EPV LU interval (LU2). This indicates that the Palaeo-Ems played a key role in shaping the early phases of the EPV evolution. Other mappable geologic structures include buried tunnel valleys, lacustrine deposits and fluvial river channels. In terms of its stratigraphic infill, the Palaeo-Ems is made up of a polyphased peat and clay/silt sequence. Above this Palaeo-Ems infill are laterally deposited silt and fine sand which are subsequently overlain by the fine- to medium-grained mobile sands of the Upper Marine Formation.

The relatively low gradient of the Palaeo-Ems was considered as the key factor responsible for its drowning as the river was unable to adjust to the prevailing rapid rise in sea-level which completely flooded the palaeo-landscape before 8.2 cal ka BP. Nevertheless, the Palaeo-Ems, a drowned predecessor of the modern Ems River, played a major role in the palaeo-drainage network of the hinterland areas and constituted one of the major tributaries in the southern part of the EPV. Together with other tributaries of the EPV, the Palaeo-Ems formed part of the drainage system that developed in the area since the Last Glacial Maximum and it is also significant to the early Holocene coastal landscape development of the German North Sea sector.

Acknowledgements

This study was jointly funded by the Nigeria Petroleum Technology Development Fund (PTDF) and the German Academic Exchange Service (DAAD). The study was carried out as part of a PhD project by Abegunrin A. at MARUM – Center for Marine Environmental Sciences, University of Bremen, Bremen, Germany. The Authors thanked Prof. Dr. Christian Winter for contributions which enriched this publication. IHS Markit are acknowledged for providing the academic license of the IHS Kingdom software used for this study. Sincere appreciation goes to all science and industry partners that contributed research data to the MARUM data base. Special thanks to Geo-Engineering.org GmbH, Bremen, Germany for providing access to industry data and contacts to Authorities. The efforts of ´Seun Tanimomo who proof-read the manuscript are also recognized.

Author Contributions

The project was conceived by the authors. D.A.H. head the HE499 sea cruise during which part of the data sets used in this study were acquired and T.M. participated in the data acquisition. A.A. carried out the data processing where applicable, interpreted the data sets, wrote the full manuscript and incorporated corrections and contributions from D.A.H. and T.M.

Competing Interests

The authors declare no competing interest.

Data Availability Statement

All data used for this study are available at the existing data base of the Marine Engineering Geology working group, MARUM – Center for Marine Environmental Sciences, University of Bremen, Germany and PANGEA (https://doi.pangaea.de/10.1594/PANGAEA.931763).

Chapter 5

Stratigraphic and geotechnical characterization of regionally extensive and highly competent shallow sand units in the southern North Sea

MATTHIAS FLEISCHER, AYOBAMI ABEGUNRIN, DANIEL A. HEPP, STEFAN KREITER, MARK COUGHLAN AND TOBIAS MÖRZ

FLEISCHER, M., ABEGUNRIN, A., HEPP, D. A., KREITER, S., COUGHLAN, M. & MÖRZ, T.: Stratigraphic and geotechnical characterization of regionally extensive and highly competent shallow sand units in the southern North Sea. Boreas. https://doi.org/10.1111/bor.12595, ISSN 0300-9483.

A detailed stratigraphic and geotechnical investigation of the uppermost 50 m below the sea floor was carried out for parts of the German North Sea sector using combined information from shallow seismic reflection surveys, 50-m long sediment cores and cone penetration tests covering an area of ~150 km². While most recent studies concentrate on unusual features such as buried tunnel- or river-valleys, this study focused on the less well understood, regionally dominant sand units deposited after the retreat of the last glaciers in this region. We identified two sandy units which dominate the late- to post-Saalian geology: (i) the Upper Fluvial Member, believed to be derived from deposition of the Weser, Ems and Elbe palaeo-rivers as well as other tributaries of the Elbe Palaeovalley in the northeast during the Saalian and (ii) the Aeolian Member, which correlates with periglacial deposits of Weichselian age. Additionally, a Saalian Buried Valley Member believed to comprise fluvial deposit was also identified. Key stratigraphic units within the uppermost 50 m below the sea floor were also identified and mapped. Detailed geotechnical properties were obtained for each of the individual stratigraphic units. The regional extent of the Aeolian and Upper Fluvial Members were documented in the region west of the Elbe Palaeovalley and south of the Dogger Bank where their geotechnical properties are important for foundation design. In conclusion, the study complements the established regional geotechno-stratigraphy and offers new and detailed public accessible information beneficial for offshore wind farm development within the region.

Matthias Fleischer, Ayobami Abegunrin (corresponding author: aabegunrin@marum.de), Daniel A. Hepp, Stefan Kreiter, and Tobias Mörz, MARUM – Center for Marine Environmental Sciences, University of Bremen, Leobener Str. 8, 28359 Bremen, Germany; Daniel A. Hepp, Lower Saxony Institute for Historical Coastal Research, D-26382, Wilhelmshaven, Germany; Mark Coughlan, UCD School of Civil Engineering, University College Dublin, 4 Dublin, Ireland and SFI Research Centre for Applied Geosciences (iCRAG), O'Brien Centre for Science East, University College Dublin, 4 Dublin, Ireland; *received 14th October 2021, accepted 15th June 2022.*

5.1. Introduction

The German sector of the North Sea is an area of active and intense wind farm construction and other commercial activities (Corbetta & Mbistrova 2015; Rodrigues *et al*. 2015; WindEurope 2018; Federal Maritime and Hydrographic Agency (BSH) 2021; Schupp *et al*. 2021). The present-day sea floor is the focus of a wealth of partly overlapping economic activities such as laying of submarine cables and pipelines, offshore sand mining, wind farm and hydrocarbon engineering installations, fish/sea farming, global transport as well as increasing natural protection areas (Hepp *et al*. 2017). Consistent wind yields coupled with improved technical know-how of foundation deployment has led to continued wind farm exploration activities. Wind turbines and associated transformation and installation infrastructure require a secure foundation on the seafloor. As a result, over the last 20 years, the uppermost 50 – 100 m of the sub-surface in the German North Sea sector has been the subject of extensive site specific geotechnical soil investigations for foundation design, installation risk mitigation and cable routing (Weihrauch *et al*. 2009; BSH 2021). The extensive data gained from these geotechnical site investigations aid geological research dealing with identification and correlation of stratigraphic units throughout the North Sea. In return, the wealth of obtained data has helped unravel a detailed knowledge and broader understanding of the three-dimensional regional sub-surface geology of the uppermost 50 – 100 m within the German North Sea sector (Coughlan *et al*. 2018; Lohrberg *et al*. 2020; Winsemann *et al*. 2020; Özmaral *et al*. 2022) which is crucial for future exploration of individual wind farms during the early stages of sub-surface investigation (Bot *et al*. 2005).

The Quaternary geology of the North Sea is complex and lithologically heterogeneous due to re-occurrence of multiple ice-sheet advances during the major glaciations of Elsterian, Saalian and Weichselian and multiple marine transgressions during the Holsteinian, Eemian and Holocene (Caston 1979; Long *et al*. 1988; Cameron *et al*. 1989; Ehlers 1990; Carr 2004; Streif 2004; Lutz *et al*. 2009; Graham *et al*. 2011). Despite this very variable depositional environment, Quaternary sub-soil models of the North Sea show horizontally extensive and regionally distributed sand units that were deposited after the early Saalian glacial ice advance (Sindowski 1970; Laban 1995; Rijsdijk *et al*. 2005; Coughlan *et al*. 2018; BSH 2021, Prins & Andresen 2021; Schaumann *et al*. 2021), the last known glacial ice advance to have reached this area prior to the Holocene inundation (Ehlers 1990). In the Dutch North Sea sector, Rijsdijk *et al*. (2005) distinguishes five large sandy formations of different geological settings using an integrated lithostratigraphic, seismostratigraphic and allostratigraphic approach as well as bounding discontinuities. However, despite being also readily identifiable in the German North Sea, the geology, origin and succession of these identifiable regional sand units is poorly understood. Coughlan *et al*. (2018) described about 22 m of this sand package (Upper Sands Formation) within the German North Sea sector (Fig. 5.1) which was

earlier grouped with the Limnic Fluvial Layer (Sindowski 1970). Also, BSH (2021) recognised this Upper Sands Formation of Coughlan *et al*. (2018) as Unit Ib.

From a civil engineering perspective, the geotechnical properties of this uppermost competent sand are highly relevant for wind turbine foundation design, installation and cable routing since the uppermost soil package has a significant influence on most foundation designs (Wiemann *et al*. 2002; Hinz *et al*. 2007; Wedel-Heinen *et al*. 2007; Germanischer Lloyd 2012; API RP 2A-WSD 2014; BSH 2014). Different kinds of foundations for which this soil package is important are presented as an example in Fig. 5.1. Note that 'soil' is used here strictly in the geotechnical sense synonymously with the term 'unlithified sediment'. Developing a plan for wind turbine foundations requires geotechnical design parameters for every geological unit in the influenced sub-surface.

The most common geotechnical design parameters used in these standards for foundation design are relative density, unit weight, cohesion, undrained shear strength, uniaxial constrained modulus and carbonate content. Some geotechnical parameters gained from grain size analysis, hand penetrometer tests on core material and cone penetration tests (CPT) are publicly available for parts of the German North Sea sector from the project 'Geopotenzial Deutsche Nordsee (GPDN)' (http://www.gpdn.de; Naumann *et al*. 2013; Schnabel *et al*. 2014). Naumann *et al*. (2013) and Schnabel *et al*. (2014) provided a basic sub-division of the sandy sub-soil in the documented areas based on geotechnical information, cores and seismic sections. Furthermore, the BSH recently compiled a geotechnical and geological model database for some part of the wind farm areas within the German North Sea sector (BSH 2021). However, a standardized regional stratigraphy with common geotechnical design parameters for each unit has not been established.

The overall stratigraphic framework of the present study area has been jointly revised with Coughlan *et al*. (2018). This present study thus builds on this established stratigraphic framework of Coughlan *et al*. (2018) by detailing the Saalian to Weichselian stratigraphy of a very well-studied wind farm area in the German North Sea sector using an integrated seismo- and litho-stratigraphic approach with emphasis on geotechnical relevant properties. It hence gives a detailed compilation of the geotechnical parameters for each of the identified stratum. High resolution seismic data detailing the uppermost 20 m below seafloor (m b.s.f.), lithological core information, *in-situ* CPT data and laboratory geotechnical parameters are the basis of this study. Geotechnical design parameters derived from CPT and laboratory tests for all units in the uppermost 50 m b.s.f. garnered from this study complement and detail the work recently published by Coughlan *et al*. (2018) and BSH (2021).

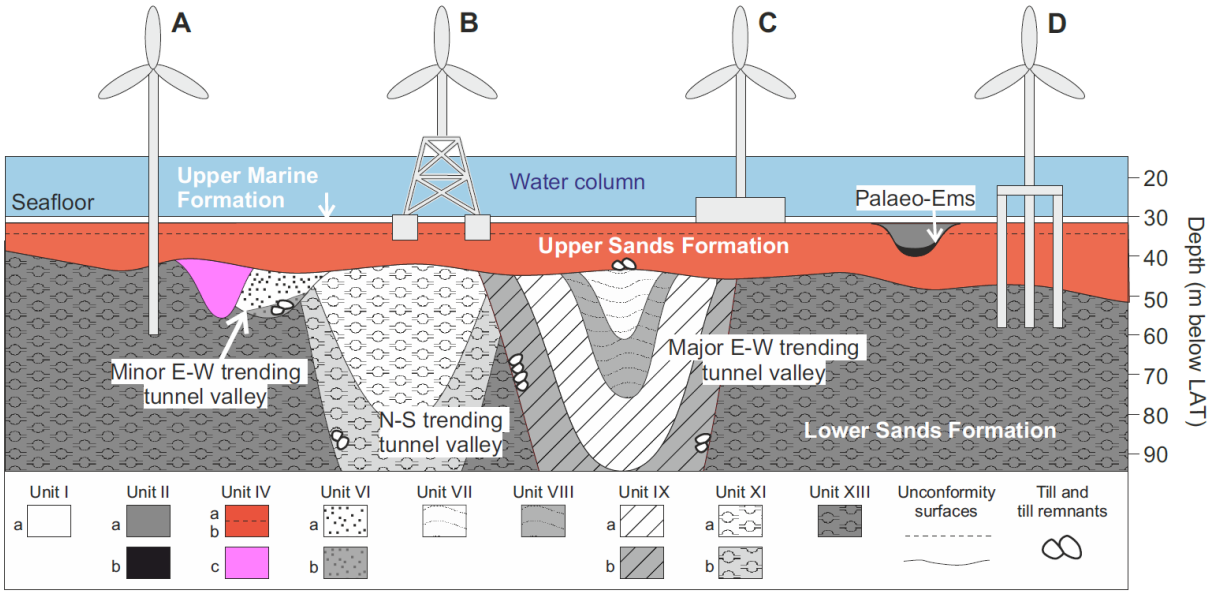

Fig. 5.1. Schematic overview of the stratigraphy and unit nomenclature in the study area, modified after Coughlan *et al*. (2018), see same for detailed description of units. The newly identified sub-units IVa/IVb and Unit IVc in this study are emphasized with red and purple shading, respectively. Superimposed are the different foundation types for offshore wind turbines: (A) Monopile, (B) Suction Bucket, (C) Gravity-based and (D) Tripod or Quadropod foundation.

By integrating the findings from this study with literature from the neighbouring North Sea sectors (e.g. Andresen *et al.* 2022), the results of this study are representative for a wider area within the North Sea and therefore offer new insights into the regional stratigraphy as well as new early planning opportunities for future offshore wind farm development within the region.

5.2. Study area

The study area comprises an area of approximately 150 km² of the southeastern German North Sea and it is situated about 40 km north of the Frisian Island Juist and west of the Elbe Palaeovalley (Fig. 5.2A). The Elbe Palaeovalley is a geomorphological shallow trough that transcend the entire German North Sea sector (Figge 1983; Papenmeier & Hass, 2020; Özmaral *et al.* 2022; Fig. 5.2A). Over the course of the Quaternary period, the depositional regime in the study area was subjected to different environmental conditions and processes linked to glaciations as well as sea level variations. Three widespread glaciation episodes, each characterized by multiple ice advances, have been identified in the North Sea and while the Elsterian and the early Saalian ice sheets covered the entire study area, the subsequent late Saalian and Weichselian ice advances did not reach the area (Oele & Schüttenhelm 1979; Ehlers 1990; Coughlan *et al*. 2018). During the Elsterian glaciation, valleys incised up to 500 m deep into Tertiary and Pleistocene deposits (Streif 2004).

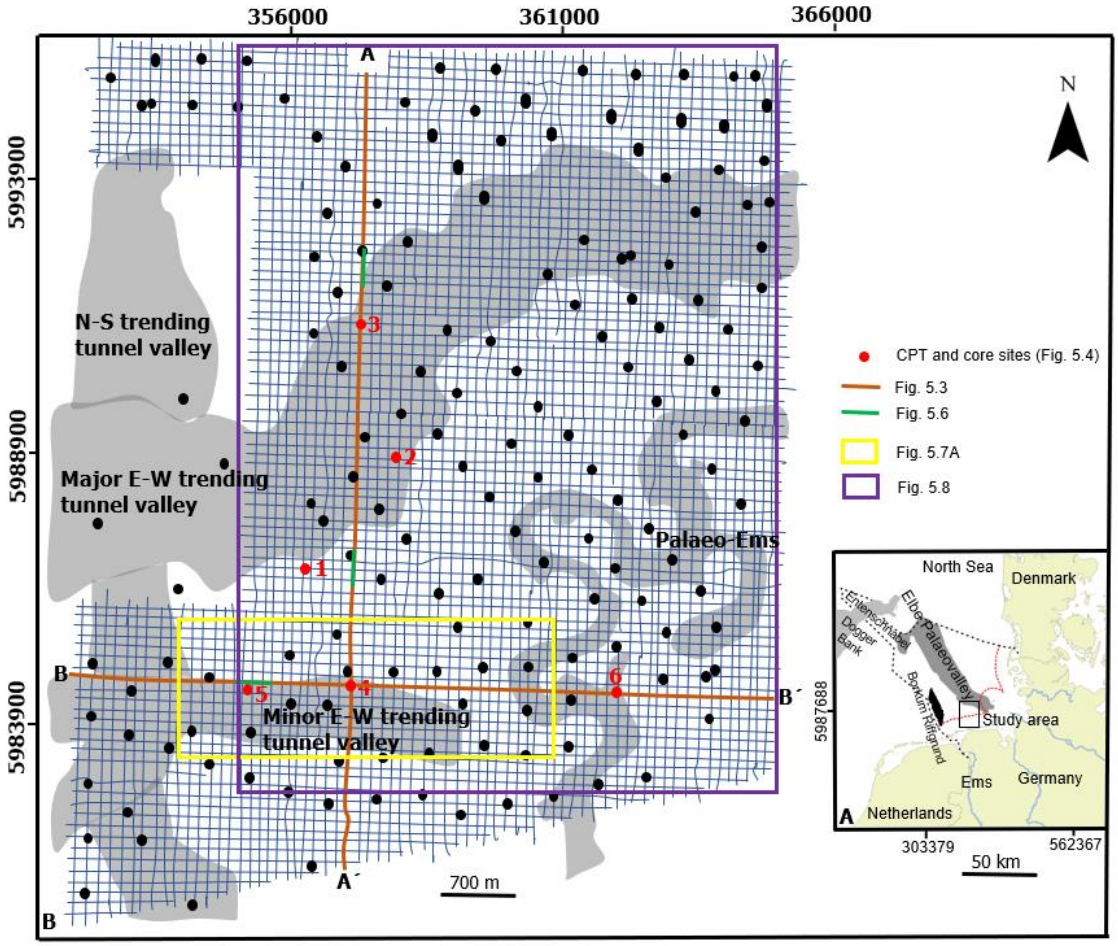

Fig. 5.2. A. Location of the study area within the German North Sea sector. B. Map of the study area with seismic grid shown as thin solid lines. The black dotted line in (A) is the German Exclusive Economy Zone, red dotted line is the Territorial Waters (12 nautical miles) while the brown solid lines in (B) indicate the two selected seismic sections shown in Fig. 5.3. Buried valleys are illustrated with grey shading and red filled circles show selected reference core and CPT sites. For complete morphology and description of the buried valleys outside the study area, readers are referred to Hepp *et al*. (2012, 2017).

Huuse & Lykke-Andersen (2000), Lutz *et al*. (2009), Hepp *et al*. (2012, 2019), Coughlan *et al*. (2018), Lohrberg *et al*. (2020), Ottesen *et al*. (2020), Prins *et al*. (2020), and Winsemann *et al*. (2020) amongst others gave a detailed seismo-stratigraphic interpretation of both the Elsterian and Saalian tunnel valleys as well as other comparable structures within the North Sea. The intercalated Holsteinian, Eemian and Holocene interglacial periods resulted in increased sea level and parts of the present-day coastlines were also inundated (Streif 2004). During these interglacials, former deposits were transgressionally/regressionally reworked, eroded and partly overlain by coastal peats, marine organic rich silts, silty clays and sands (Streif 2004).

After the last deglaciation, the sedimentary regime in the study area was dominated by proglacial and periglacial conditions (Caston 1979; Oele & Schüttenhelm 1979; Long *et al*. 1988; Laban 1995; Streif 2004; Graham *et al*. 2011). The geomorphology of the terrain at this time was characterized by lakes, kettle holes, meltwater valleys and channels, outwash cones and plains as well as moraines (Böse *et al*. 2012). Overall, the present-day seafloor

within the study area dips constantly northward with water depth within the study area ranging from about 26 m below lowest astronomical tide (LAT) in the south to more than 30 m below LAT some 15 km further north. A schematic overview of the refined stratigraphy of the uppermost 50 m b.s.f. within this area is shown in Fig. 5.1.

5.3. Material and methods

This study is based on seismic reflection data collected during five commercial surveys between 2007 and 2010, ~50 m long sediment cores from 40 sites and CPT data from 60 sites (Fig. 5.2B).

5.3.1. Shallow water seismic surveys

Seismic data were collected using a Geopulse 5813b Boomer (GeoAcoustic Ltd) single channel seismic system. The Boomer system provides high resolution images of the thin Holocene layers and shallow buried valley infills within the uppermost 15-25 m with a very high vertical resolution of about 0.2 – 0.5 m. The Boomer system was operated with an energy of 200 J and a 3-m single-channel streamer with 8 hydrophones. Acoustic data were recorded with the NWC software (Nautik Nord GmbH) with a shot rate of 3.5 shots per second and a 16-bit resolution. A layback correction was applied to correct for the streamer/source geometry behind the ship's differential global positioning system (DGPS) antenna. Noise was reduced using a band pass filter with 1200 - 4000 Hz limits. Several profiles were however filtered using a band pass width of 1200 - 6000 Hz. This was due to the perceived viable frequency of the data versus noise. A static correction was applied to eliminate swell effects using the sea floor reflection as a reference. The seismic grid was acquired in north-south and east-west directions with a mesh width of about 200 m (Fig. 5.2B). The seismic profiles were processed to zero phase data and increase in acoustic impedance is a peak and positive amplitude reflection. Seismic sections are presented here either as black and white-with-black denoting positive amplitude and white negative amplitude or in contrasted colour with orange denoting positive amplitude, black negative amplitude and white the zero-crossing.

5.3.2. Coring, Cone Penetration Testing (CPT) and offshore operations

Coring and CPT equipment were both operated from commercial drill ships as well as jack-up platforms. At a given location, both coring and CPT were performed within a lateral interval of 11-13 m depending on the ship or platform geometry. Sediment core and CPT sites are located along and/or <50 m away from the seismic lines. The reference sites and seismic sections shown in this study were chosen to convey the major geological structures (Fig. 5.2B).

Sediment cores were recovered using either: (i) rotary flush drilling applying a wireline-line operated push core sampler with a 53 mm or 72 mm inner diameter for sampling operated from a drill vessel, or (ii) a percussion drive sampler with 100 mm liner samples operated from jack-up platforms. The individual core section length is ~1 m and the recovery rates are between 85% and 97%. The cores were described offshore according to the soil

classification scheme in DIN EN ISO 14688-2 (2020). The calcium carbonate content was tested with 10% HCl solution and separated into six general categories ranging from no reaction to very strong effervescence according to the classification of the soil science mapping instructions (Pedological mapping guide, KA5). Dry and wet soil unit weight were determined at 0.5 m intervals following DIN 18125-2 (2011). The undrained shear strength of cohesive clayey and silty soils was measured onboard with a pocket penetrometer and a hand-held vane shear every 0.5 m or for every individual lithological layer.

The CPTs were conducted according to the procedure described by DIN EN ISO 22476-1 (2009) using either a downhole CPT operated from a drill vessel, or a top-driven CPT operated from jack-up platforms. The CPT tip resistance (q_c) records the stress on the CPT steel cone during penetration and was used to derive the relative density of sands following DIN EN 1997-2 (2010) (Table 5.1). Tip resistance (q_c) measurements obtained from CPT tests were used to characterize and confirm stratigraphic sequences. Similar to downhole logging data, in-situ data like CPT as independent datasets with superior depth accuracy allow for a more definitive characterization of lithostratigraphic units. The soil behavior type index (I_c) was computed using the principles outline by Robertson & Wride (1998). A full description of all the measured parameters for each core site is provided in Fig. S1.

5.3.3. Onshore laboratory tests

The sediment cores were sub-sampled onshore to determine additional lithological and geotechnical parameters of each unit in the study area (Table 5.2). Grain size distribution of 569 samples were measured following DIN 18123 (1996). The degree of sorting for sandy soil samples was determined from the standard deviation of the grain size distribution (Blott & Pye 2001). The calcium carbonate content was analysed for 240 soil samples according to the procedure described by Müller *et al*. (1994) using a LECO CS 200 analyser. The effective friction angle and effective cohesion were determined on 471 samples in direct shear tests (DIN 18137-3 2002). The uniaxial constrained modulus E_S was measured on 422 samples by oedometer tests (DIN 18135 1999). The number of tests in Table 5.2 documents the basis for obtaining the parameters presented in Table 5.3, which were used to characterize and differentiate between the identified units.

5.3.4. Stratigraphic correlation procedure

The stratigraphy of the offshore deposits was established by correlating seismo-stratigraphic units with CPT profiles and core lithology. In cases where there are discrepancies between seismo- and litho-stratigraphic surfaces, all available data were used for mutual calibration and complementing each other. The seismic sections were interpreted using bounding surfaces and truncations to identify key stratigraphic surfaces, but in this sandy environment with often nearly horizontal contacts, these distinctive features are often not very clear.

Table 5.1. Relative density derived from CPT tip resistance for quartz and feldspar sands (DIN EN 1997-2 2010) and relative density D_R (DIN EN ISO 14688-2 2020).

CPT tip resistance (MPa)	Relative Density Index	Relative density D_R (-)
0 – 2.5	Very loose	0.00 – 0.15
2.5 – 5.0	Loose	0.15 – 0.35
5.0 – 10.0	Medium dense	0.35 – 0.65
10.0 – 20.0	Dense	0.65 – 0.85
> 20.0	Very dense	0.85 – 1.00

Table 5.2. Number of tested soil samples with reference to seismic/lithological units in the study area.

Unit	Grain size measurement	Carbonate content (LECO CS 200)	Direct shear tests	Odeometer tests
I	58	9	6	6
II	16	13	15	14
IVa	28	10	27	24
IVb	89	15	83	67
IVc	3	-	-	-
VIa	86	41	58	58
IX/XI	122	92	118	118
XIII	167	60	164	135

Table 5.3. Compilation of geotechnical design parameters derived from offshore CPTs and onshore laboratory tests for each seismic/lithological unit within the study area. See Fig. 5.5 for median grain size d_{50} for the sandy units. * derived from CPT tip resistance.

Unit	Ia	IIa	IVa	IVb	IVc	VIa	IXa/XIa	XIII
Thickness (m)	<1 - 2	0 - 6	3 - 5	1 - 16	0 - 15	0 - 30	0 - >50	
Sediment type	Fine sand and partly silt, shell and organic material	Clay, silt and fine sand, varying organic content, peat layers	Fine sand	Fine to coarse sand	Fine to medium sand	Clay, silt and fine to medium sand	Very heterogeneous, clay to medium sand	Fine to coarse sand, seldom gravelly
Unit weight γ_s (kNm^{-3})	19.9-20.4	11.9-19.4	19.8-20.3	19.8-20.3	19.1-20.0	18.8-20.0	19.0-20.3	19.0-23.7
Friction angle ϕ' (°)	34-38	19-36	30-45	29-47	31 – 37	20-43	9-42	26-47
Cohesion c' (kPa)	–	0-75	–	–	–	0-51	0-146	–
Undrained shear strength c_u (kPa)	–	Cohesive infill sediments: <30	–	–	–	Cohesive infill sediments: 20 – 60	Cohesive infill sediments: 10 - 280	–
Uniaxial constrained modulus E_S (MPa)	<16	Granular infill sediments: <6.3	6-32	10-64	17-47	-	-	20-135
Carbonate content range (wt.-%) (Mean)	0.5 – 21 (7.4)	<12 (3.6), upward increase	<1 (0.2)	<1.7 (0.4)	0.5	<15 (2.7)	<23 (10.3)	<20 (2.5), upward increase
Tip resistance q_c (MPa)	<10	<6	10 - 25	30 – 60 (~40)	30 – 50 (~40)	<40	1 – 20	>60
Sleeve friction f_s	<0.1	<0.1	0.05 – 0.15	0.1 – 0.45	0.2 – 0.35	0.1 – 0.25	0.05 – 0.25	0.4 – 1.2
Friction ratio F_R	0.5 - 2	2 - 5	0.3 – 0.8	0.5 – 1.0	0.5 – 1.0	0.5 - 6	0.5 - 5	0.5 – 1.5
Soil behavior type index I_c	–	2.7 – 3.9	1.7 – 2.3	1.5 –2.0	1.6 – 2.1	1.9 – 3.5	1.8 – 3.9	1.3 – 2.1
Relative density D_R (-) *	0 - 0.6	–	0.6 - 0.9	>0.9	>0.9	–	–	>0.9

While seismic facies characteristics and first-order strong reflections, denoting marked impedance contrasts and hence major lithological changes, were employed in defining the key stratigraphic surfaces, the uncertainty introduced by this procedure in areas of low impedance contrast was compensated by the wealth of other available information sources such as CPT and sediment cores. These reflections were then mapped along profile length based on amplitude strength and continuity and their intersections on cross profiles were also traced.

CPT profiles were analysed and subsequently interpreted based on observed groups of repeating patterns in tip resistance values.

These patterns reflect major changes of sediment density and lithological changes (Lunne *et al.* 1997). Lithostratigraphic units from sedimentary successions deduced from cores were defined based on similarities in sedimentary properties (e.g. grain-size attributes, competence and visual characteristics). A direct correlation was then made between these lithostratigraphic units and CPT profiles using depth and log signature of the CPT profile against observed sediment composition.

Subsequently, the established lithostratigraphic units together with their CPT values were correlated to identified and mapped seismo-stratigraphic units. The units are named after the neutral roman numerals unit nomenclature previously published by Coughlan *et al*. (2018).

The dip and dip direction of buried valleys of interest were determined from two deepest points of neighbouring profiles. A mean P-wave velocity (Vp) of 1600 ms^{-1}, a value fitting well for the uppermost 50 m below the sea floor based on previous studies (Winsemann *et al*. 2020; Lutz *et al*. 2009), was used for depth conversion. This P-wave velocity value is roughly consistent with the Vp values measured along with the CPT data (Fig. S1) and enabled a robust approximation of depth of predominant lithologic units within the study area. Clayey to silty soils show a variety of P-wave velocities depending on the sand fraction, pore volume and consolidation state. Overestimated P-wave velocities of occurring clayey soil sections could lead to pull-up-effects. The authors are aware of this effect, it was however accepted because the cohesive sediment sections in the upper part of the stratigraphy are rare.

Area-wide contour maps showing the depth below the Lowest Astronomical Tide (LAT) were generated for the sea floor and seismic unit boundaries of interest. The sea floor contour map uses a basic bathymetry grid which was sourced from the BSH in 2012 and retrieved from the actual official nautical charts. Contour maps of seismic unit boundaries use depths obtained from seismic sections which are referenced to the bathymetric map grid hence showing depth below seafloor. The gridded data were interpolated using a cubic spline gridding algorithm within the IHS Kingdom software. The mean dip and dip direction of the individual boundary surfaces are determined from a least-squares flat regression plane through all data points in ArcGIS10.

5.4. Results

5.4.1. Seismic Stratigraphy and Unit Characterisation

Nine key seismo-stratigraphic surfaces defining eight major stratigraphic units were identified and mapped across seismic profiles (Fig. 5.3). The delineated stratigraphic units correspond to major seismic Units I, II, IV, VI, VII, VIII, IX, XIII as defined by Coughlan *et al*. (2018) (Fig. 5.1). The nine major seismic unconformities identified from Coughlan *et al*. (2018) are based primarily on shallow water multi-channel seismic (MCS) data. By focusing, in particular, on the very high-resolution single channel (Boomer) seismic data, this study identified new additional and distinct seismic stratigraphic surface subdividing Unit IV, as recognized by Coughlan *et al*. (2018), into Unit IVa and IVb. Additionally, a valley shaped sediment body was recognized beneath Unit IVb and was delineated as Unit IVc (Fig. 5.3). The new Units IVa, IVb and IVc are for the first time described in detail here, including their boundaries and internal seismic facies characteristics as well as a description of their geometry, lithology and geotechnical properties.

Furthermore, a brief description of the lithology and geotechnical properties of each unit within the investigated stratum is herein provided based on Coughlan *et al*. (2018), additional core and CPT profiles as well as laboratory tests. Where applicable, new inputs encompassing grain size distribution, carbonate content, and the most common geotechnical design parameters obtained from the additional laboratory tests for all of stratigraphic units within the study area are described here for the first time (Tables 5.2, 5.3). For a more detailed description and genetic interpretation of the previously identified units, readers are referred to Coughlan *et al*. (2018).

5.4.1.1. Strata underlying Unit IV

Unit XIII, the Lower Sands Formation (Coughlan *et al.* 2018), is the deepest identified unit in the study area (Fig. 5.3) and separated from the overlying unit by a strong reflection. Based on lithological analyses, the unit is composed of calcareous fine to coarse, sometimes gravelly sands (Fig. 5.4, Table 5.3) and are heterogeneous in nature. Samples taken from Unit XIII show a d_{50} (median grain size) of about 0.1 to 0.8 mm (Fig. 5.5B) and are moderately well to poorly sorted (Fig. 5.5C). The tip resistance of Unit XIII is higher than 60 MPa (Fig. 5.4, Sites 3, 4, 5, 6) and the soil behavior type index ranges from 1.3 to 2.1 (Table 5.3).

Unit IXa, the Upper member of the Peelo Formation, forms the upper infill of the major E-W trending tunnel valley (Coughlan *et al*. 2018; Fig. 5.3). It comprises heterogeneous, predominantly calcareous sediments of laminated clay to silty and sandy deposits with tip resistances in the range of about 1 MPa to about 20 MPa (Fig. 5.4, Sites 2 and 3). The soil behavior type index varies from 1.8 to 3.9 (Table 5.3).

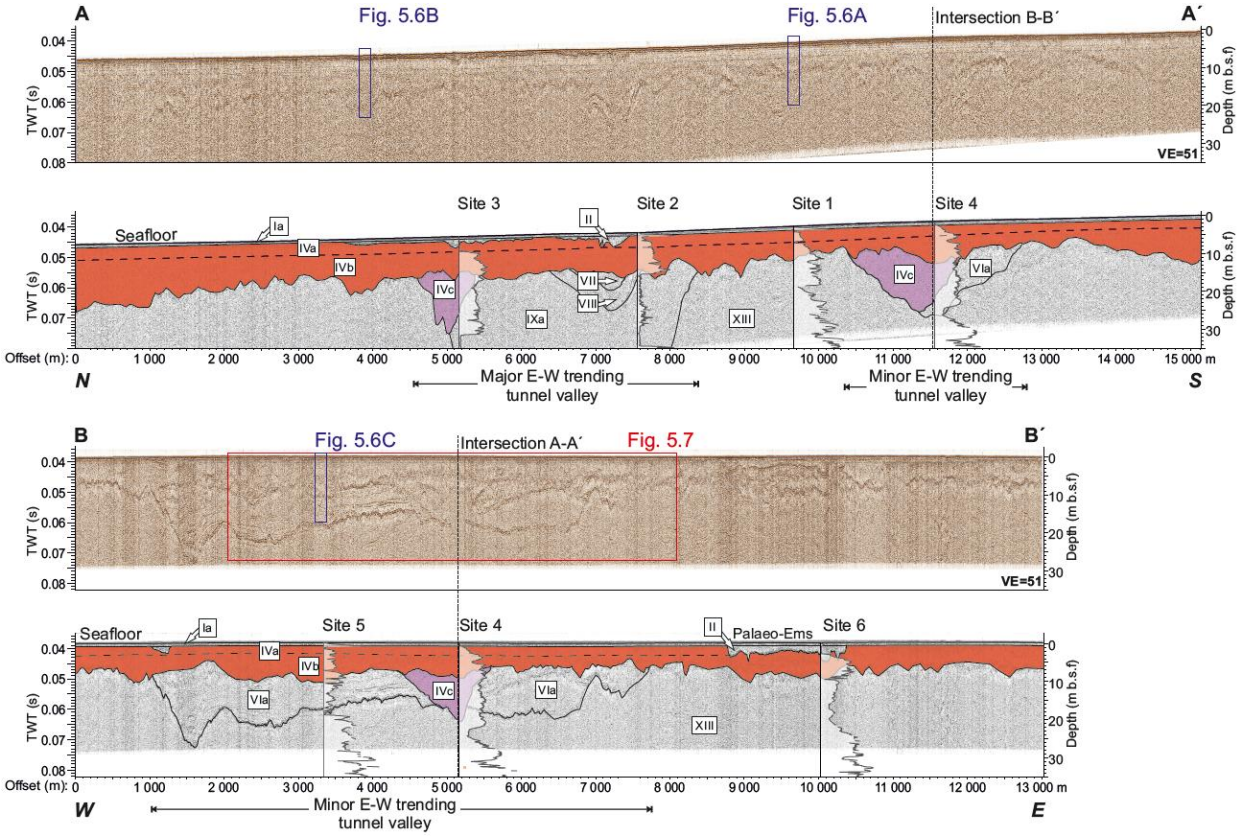

Fig. 5.3. Raw and interpreted seismic sections along profiles A-A' and B-B', see Fig. 5.2 for location. Seismic units are labelled with Roman numerals according to the stratigraphy of Coughlan *et al*. (2018). Units IVa/IVb and Unit IVc are emphasized with red and purple shading, respectively. TWT is the two-way-travel-time of the P-wave and VE is the vertical exaggeration of the profile. CPT tip resistances are projected on the seismic profiles and the locations of seismic details are marked with blue boxes (Fig. 5.6).

Unit VI, the Drente Formation, forms the infill of the minor E-W trending tunnel valley (Coughlan *et al.* 2018; Fig. 5.3). The Upper Member of the Drente Formation (Unit VIa; Fig. 5.3) comprises heterogeneous clays, silts and sands (Fig. 5.4, Sites 4 and 5) with varying tip resistances of up to 40 MPa (Fig. 5.4) and soil behavior type index range of 1.9 to 3.5 (Table 5.3). Moraine deposits at the base of the tunnel valley belong to the Till Member of the Drente Formation (Unit VIb, Fig. 5.4, Site 5). The base of the Till Member forms the early Saalian glaciogenic unconformity (Coughlan *et al*. 2018).

Unit IV

This study has identified three new stratigraphic units in the German North Sea, namely: Units IVa and IVb, previously grouped together as the Upper Sands Formation, Unit IV in Coughlan *et al*. (2018) and Unit IVc, which is restricted to buried valleys below Unit IVb.

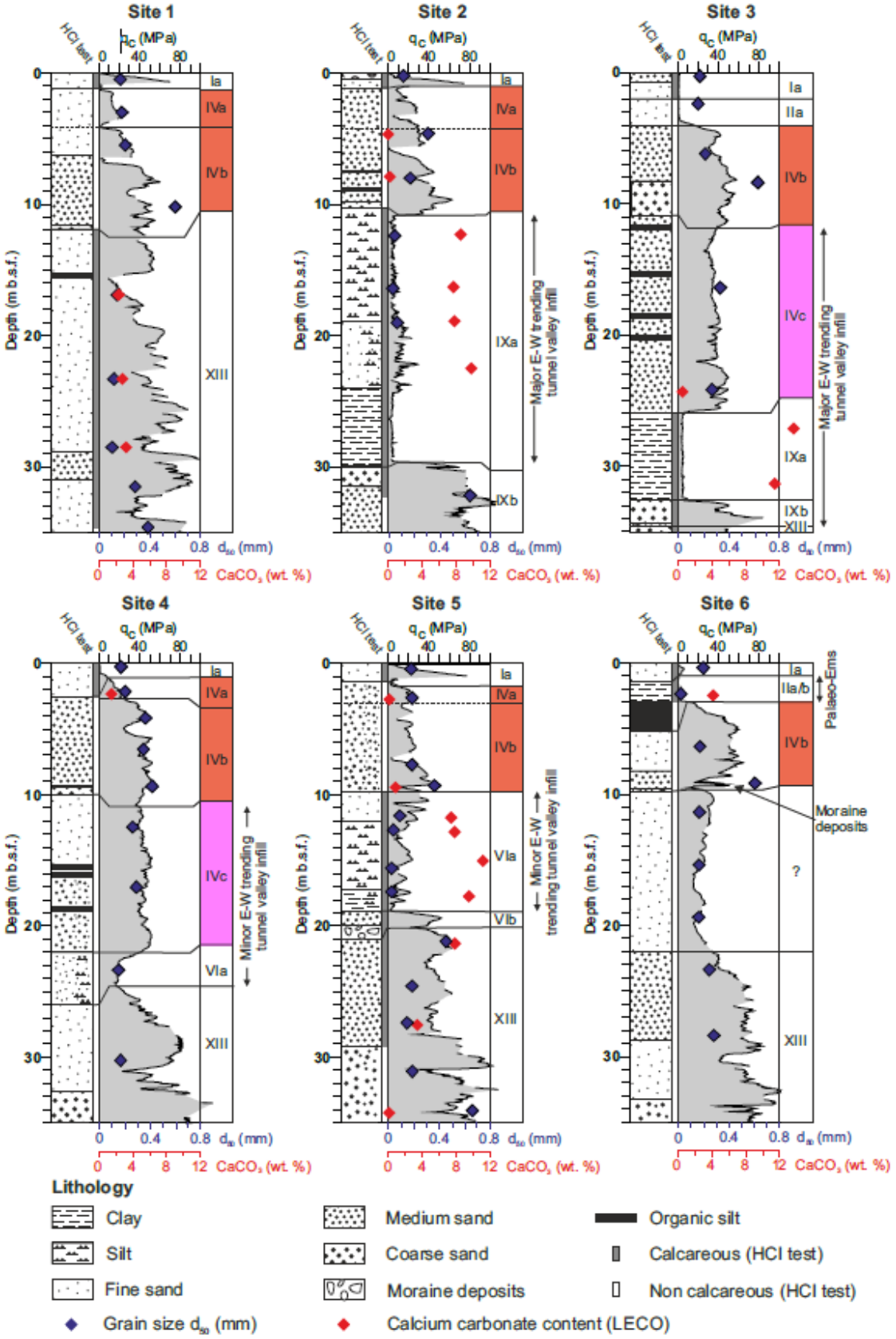

Fig. 5.4. Lithology, grain size d_{50} (black diamond), calcium carbonate content (red diamond), CPT tip resistance (grey-filled curve) and thickness of seismic Units for six selected sites; see Figs 5.2B and 5.3 for the location of the sites. The approximate thickness, in meters, of the seismic units is obtained from the related seismic profile.

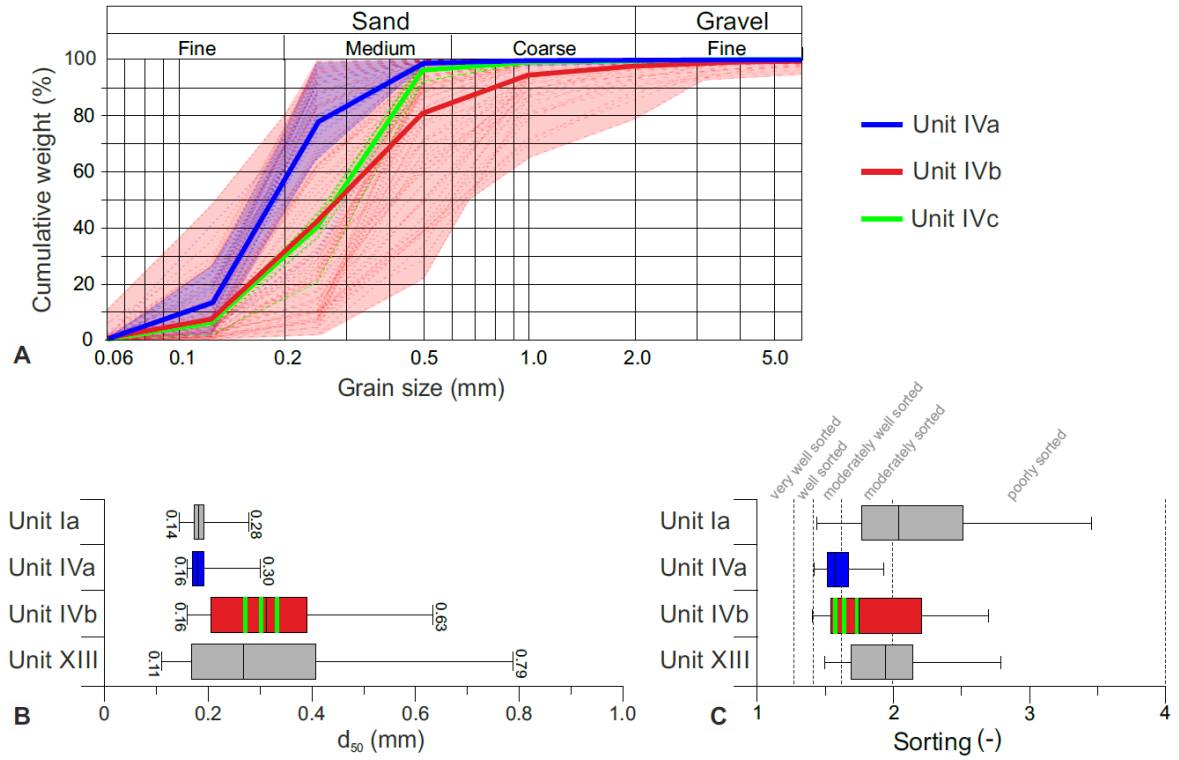

Fig. 5.5. A. Cumulative grain size distribution curve of the Aeolian Member (Units IVa, blue), the Upper Fluvial Member (Unit IVb, red) and Buried Valley Member (Unit IVc, green). B. Median grain size d_{50} and (C) sorting of Units Ia, IVa, IVb, IVc and XIII. The thin black lines in the boxes in (B) and (C) are the median, the box extension marks the first and third quartile and the whiskers show the 5 and 95 percentiles. The green bars indicate the d_{50} (Fig. 5.5B) and the sorting values (Fig. 5.5C) obtained from the grain size measurement of three individual samples of Unit IVc, respectively.

Unit IVc. – The unconformity marking the base of Unit IVc forms roughly V-shaped asymmetric valleys that truncate lower reflections (Fig. 5.3). The top of Unit IVc is truncated by the Unit IVb base unconformity. The unit has a maximum thickness of about 15 m and the width ranges between 0.5 and 2 km. Fig. 5.7A shows a representative Unit IVc-valley (purple colour) cutting the minor E-W trending tunnel valley in a N-S direction. Fig. 5.7B depicts a three-dimensional seismic interpretation of Unit IVc. The thalweg of Unit IVc is undulating with depth changing discontinuously between 45 m to 49 m below LAT along the valley thalweg. Another Unit IVc-valley cuts the flank of the major E-W trending tunnel valley (Fig. 5.3, Section AA').

On seismic sections, the internal signature of this unit shows a sigmoidal to chaotic facies. There are some internally stacked U-shaped and V-shaped channel-like structures outlined by high amplitude reflections which truncate lower internal reflections and similar structures (Figs 5.6A, 5.7B). However, these channel-like internal structures are discontinuous and can rarely be traced continuously over a considerable distance. In terms of lithology, Unit IVc is composed of fine to medium sands with some organic silt layer interbeds (Fig. 5.4, Sites 3

and 4). Samples taken from the sand intervals from these sites show a d_{50} of about 0.3 mm (Fig. 5.5A, B, green colour) and are moderately well sorted to moderately sorted (Fig. 5.5C). The tip resistance of Unit IVc is about 40 MPa (Fig. 5.4, Sites 3 and 4) corresponding to highly competent very dense sands ($D_R \geq 0.9$) and the soil behavior type index ranges from 1.6 to 2.1 (Table 5.3).

Unit IVb. - The base of Unit IVb is irregular, discontinuous and truncates the underlying Units VI, VII, VIII, IX and XIII of Coughlan *et al*. (2018) as well as Unit IVc (Fig. 5.3). Unit IVb directly overlies Unit XIII, the Lower Sands Formation in most of the area, except for where major and minor E-W trending tunnel valleys occur (Figs 5.3, 5.6). The base of Unit IVb (Fig. 5.8A) generally deepens from about 32 m below LAT in the southern part of the study area to a maximum of about 58 m below LAT at the northern boundary of the study area. The average dip of this surface which is shown in Fig. 5.8A is 0.049° in 349° direction. The deepest incisions of the Palaeo-Ems eroded parts of Unit IVb in the south-eastern part of the study area (Fig. 5.8A). Unit IVb has a variable thickness along profile length (Fig. 5.3, Section AA') which reaches a maximum of about 15 m in some sections. The combined thickness of this unit and that of the overlying Unit IVa is generally thicker towards the north (Fig. 5.8D).

Unit IVb is composed of fine to coarse sands (Fig. 5.4) and a wide range of d_{50}-values (Figs. 5.5A, 5.5B). 90% of the soil samples of Unit IVb have a d_{50} of about 0.2 to 0.6 mm. The sands of Unit IVb are moderately well- to poorly-sorted (Fig. 5.5C). The base of Unit IVb is often co-incident with reworked moraine deposits (Coughlan *et al*. 2018; Fig. 5.4, Site 6). Tip resistance values for Unit IVb are on average, about 40 MPa over the entire study area (Fig. 5.4) with highly competent, very dense sands ($D_R \geq 0.9$). Single sharp peaks in tip resistance at the base of Unit IVb occur when the CPT tip hits boulders or cobbles (Fig. 5.4, Site 6 at 9.5 m). The soil behavior type index ranges from 1.5 to 2.0 (Table 5.3). The seismic signature, grain-size distribution, median grain size and CPT values are very similar to the sands of Unit IVc.

The seismic facies expression of Unit IVb is sigmoidal to chaotic in nature, characterized by low to medium amplitude reflection strengths which are discontinuous to semi-continuous (Fig. 5.6). Similar to Unit IVc, the seismic profiles show internal mostly U-shaped stacked structures that are often observed near the base of Unit IVb (Fig. 5.7). In contrast to Unit IVc, the internal structures within Unit IVb are semi-continuous and can be locally traced from one seismic profile to the other. Five Unit IVb internal channels (1 – 5) were observed over the seismic coverage area and their three-dimensional representation are shown in Fig. 5.7. Four of these internal channels (1, 2, 3, 5) shown in green colour are directly located at the base of Unit IVb while the fifth one (4) in yellow colour cuts Channel 5. The Unit IVb internal channels have thalweg depths ranging from 35 to 40 m below LAT. These channels show infill thicknesses of up to 5 m.

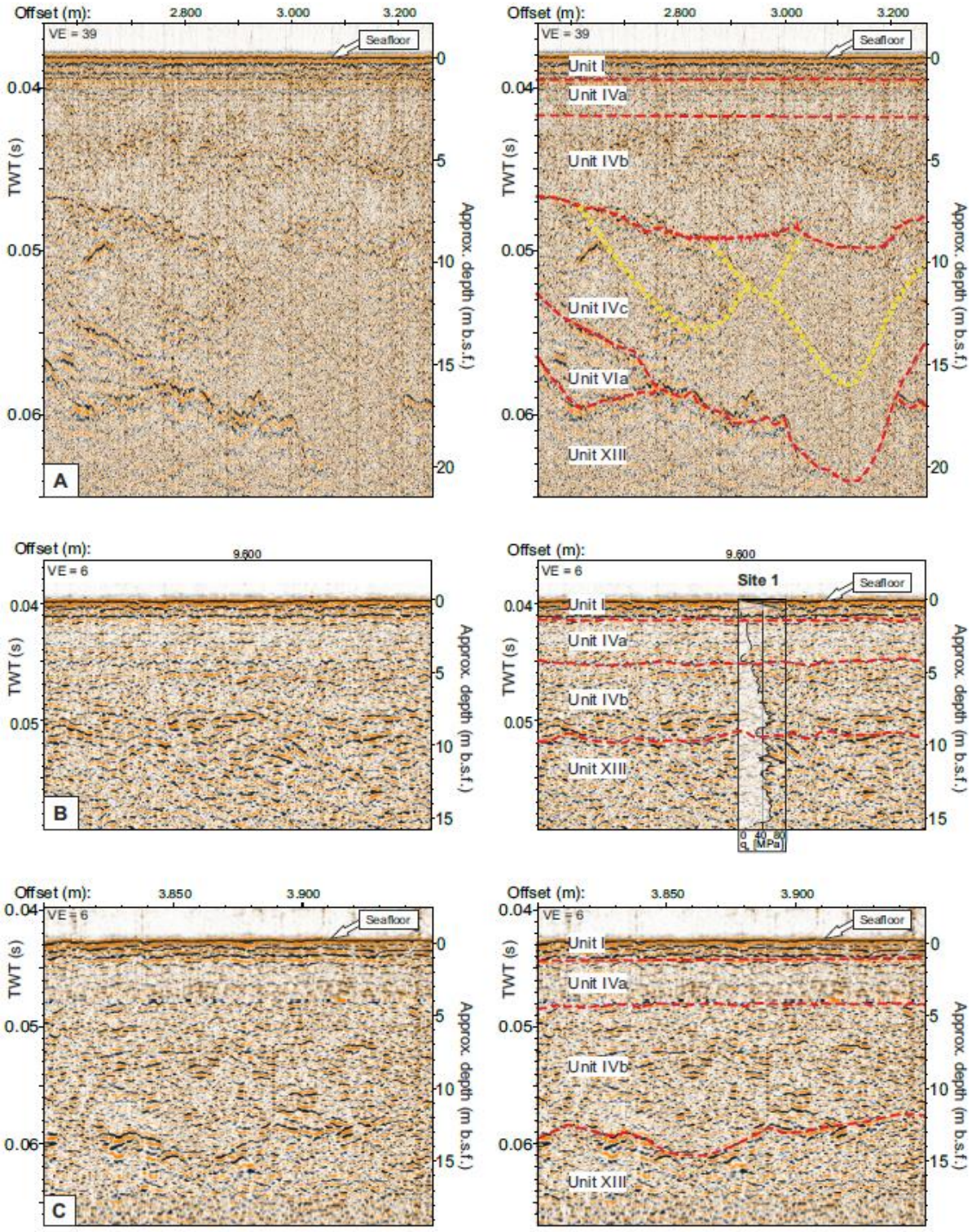

Fig. 5.6. Details from the seismic profiles A-A' and B-B'. The CPT tip resistance curve in (B) was projected on the seismic section (projection distance is less than 5 m). TWT and VE are the two-way-travel-time of the P-wave and the vertical exaggeration of the seismic sections respectively. See the small green lines in Fig. 5.2B for location of the seismic sections. The yellow dotted line in (A) depicts the smaller channels within Unit IVc. CPT and sediment cores were employed in defining stratigraphic surfaces in areas which low impedance contrast.

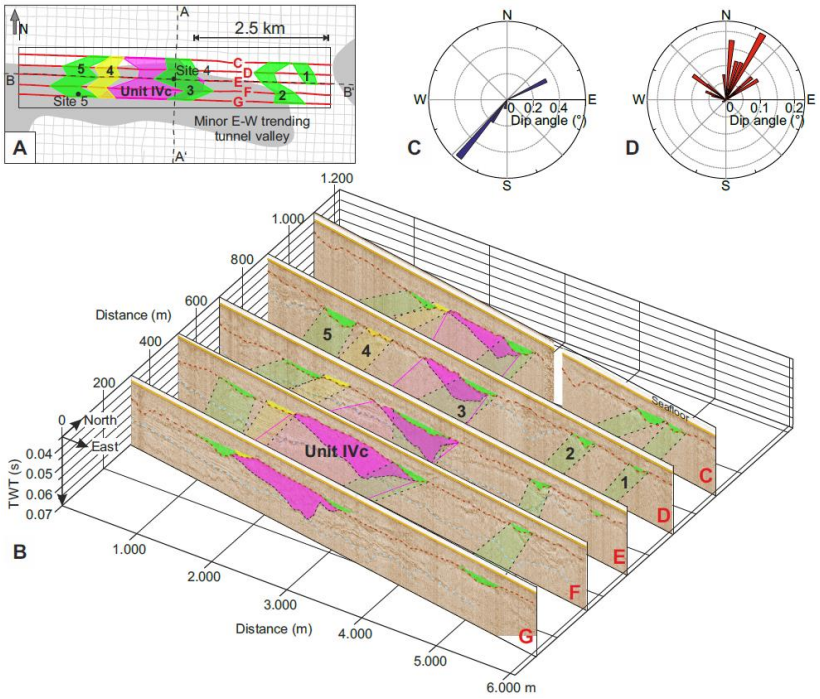

Fig. 5.7. A. Location of seismic profiles C-G used for (B) the three-dimensional view of five seismic sections C-G with five internal channels (1 – 5) within Unit IVb (green and yellow) and the Unit IVc-valley (purple). Dip angle determined from the thalweg between two channel bases of adjacent seismic sections for (C) the Unit IVc-valley and (D) all the internal Unit IVb-channels. Note that the dip angles are measured on sections with good expressions and that the three-dimensional view in (B) has a N-W exaggeration of 1:3.8. See the yellow rectangle in Fig. 5.2B for location of Fig. 7A. Turqoise dashed line = base of the minor E-W trending tunnel valley; red dashed line = base of Unit IVb; thin black dashed line = base of Unit IVc (purple color); thick black dashed line = interpretation of the course of the individual channels and valleys.

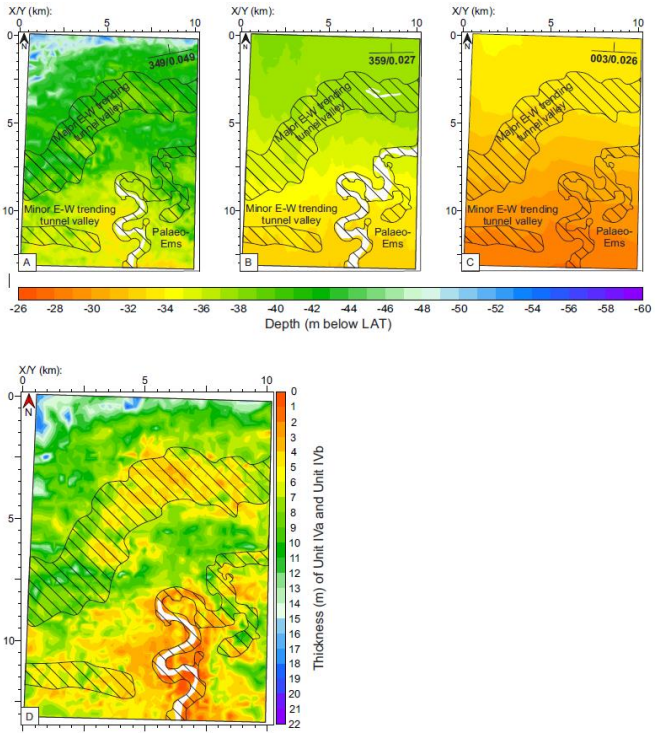

Fig. 5.8. Depth below LAT of (A) the base of the Upper Fluvial Member (Unit IVb) (B), the base of the Aeolian Member (Unit IVa), (C) the seafloor as colour maps, and (D) thickness map of Unit IVa and Unit IVb. The hatched area indicates the locations of buried tunnel and river valleys. The white areas in (A) and (B) mark the region where these units were eroded by the Palaeo-Ems channel. See the purple rectangle in Fig. 5.2B for location of the maps. The strike and dip symbols show the dip direction and angle of the surfaces.

The dip and dip direction of Unit IVb channel thalwegs as determined between the two deepest points of neighbouring profiles is presented in Fig. 5.7D. The thalweg dip direction varies in a range between about 280° and 60° with a mean northward dip direction of about 0° (Fig. 5.7D). The dip and dip direction are consistent to the general dip direction of the Unit IVb base (Fig. 5.8A). The configuration of Unit IVb-channels as well as the Unit IVc-valley are visible above the cohesive infill of the underlying tunnel valleys due to high impedance contrast. Unconformity surfaces which defined the configuration of these units are however less visible in some areas where the units are underlain by deposits with similar lithology and less impedance contrast (Fig. 5.6).

Unit IVa. - Overlying Unit IVb, Unit IVa forms a continuous 3 to 5 m thick interval reaching up to about 1.5 m below sea floor (Fig. 5.3). The base of Unit IVa, as identified on Boomer profiles, is a relatively weak horizontal seismic reflection which is continuous throughout the study area (Figs 5.3, 5.8). The unconformity at the base of Unit IVa was observed to truncate the upper internal reflections of Unit IVb (Fig. 5.3) and forms a laterally consistent surface at a depth of 32-40 m below LAT (Fig. 5.8B). The average dip of 0.027° and dip direction of 349° for this unconformity surface are very similar to the values of the sea floor shown in Fig. 5.8C. Unit IVa is bounded above by the Units II and I (Fig. 5.3). Seismic facies analyses revealed that Unit IVa is characterized by parallel to sub-parallel, continuous to semi-continuous horizontal internal reflections with low to medium amplitude strength over the entire study area (Fig. 5.6).

From the measurements shown in Figs 5.4 and 5.5, it was deduced that Unit IVa consists of medium to mainly fine-grained sands with a relatively homogeneous grain size distribution and d_{50} varying from 0.16 to 0.3 mm compared to Units XIII, IVb and I (Fig. 5.5B). The sands of Unit IVa are moderately well- to moderately-sorted (Fig. 5.5C). Grain size and sorting of Unit IVa shows no lateral trend within the study area. Furthermore, the calcium content of this unit as well as that of Units IVb and IVc revealed that all three units are non-calcareous while units below and above Unit IV are all calcareous (Fig. 5.4, 5.3). Tip resistance of Unit IVa increases with depth from about 10 to 25 MPa (Fig. 5.4) thus revealing predominantly dense competent sands of relative densities (D_R) between 0.6 - 0.9 (Table 5.3). The soil behavior type index varies from 1.7 to 2.3 (Table 5.3).

5.4.1.2. Strata overlying Unit IV

Unit II, the Buried River Valley Formation (Coughlan *et al.* 2018), forms local channel-like incisions into the top of Unit IVa which were subsequently covered by Unit I (Fig. 5.3). Unit II infill consist of calcareous clays, silts and fine sands with varying organic content (Unit IIa, Upper Member) and occasional peat layers (Unit IIb, Peat Member). The base of the Peat Member is inferred to mark the Holocene base (Streif 2004; Schwarzer *et al*. 2008; Coughlan *et al.* 2018; Hepp *et al*. 2019). Tip resistance of Unit II is about 1 MPa while the sandier parts show

local tip resistances which are up to 6 MPa (Fig. 5.4, Sites 3 and 4). The soil behavior type index ranges from 2.7 to 3.9 (Table 5.3).

Unit Ia, the Mobile Sands Member of the Upper Marine Formation (Zeiler *et al*. 2000; Coughlan *et al*. 2018), typically overlies Unit IVa (Fig. 5.3). The Unit Ia basal unconformity is parallel to the sea floor at a depth of about 1.5 m b.s.f. (Fig. 5.3). Unit Ia consists of fine sands with silt, shell and organic material. These sediments have tip resistances of less than 10 MPa and relative densities from very loose to medium dense ($D_R < 0.6$) (Fig. 5.4, Table 5.3). Locally the tip resistance profile shows single sharp peaks up to 80 MPa when the CPT tip hits compact shell layers (Fig. 5.4, Sites 1, 2 and 5).

5.5. Discussion

The integration of lithological, geotechnical and seismic data has allowed for an extensive characterization of the stratigraphic units of parts of the German North Sea sector which is crucial from the perspective of both geological reconstruction of the Quaternary history and engineering design of offshore infrastructures like wind turbine foundations. This data integration allows for a detailed stratigraphic correlation of units within the German North Sea sector and adjoining sectors as well as refinement of specific units of the Coughlan *et al*. (2018) stratigraphy. The correlation is based on identified major seismo-stratigraphic surfaces and the relative stratigraphic succession identified by Rijsdijk *et al*. (2005) as well as geotechnical parameters such as CPT tip resistance and soil behavior type index detailed by Bot *et al*. (2005) and Robertson & Wride (1998). Three major seismo-stratigraphic surfaces are crucial in the stratigraphic correlation within the interval of interest (red texts in Table 5.4). These surfaces which are correlated with the seismo-stratigraphic surfaces of Coughlan *et al*. (2018) includes: (i) the early Saalian glaciogenic unconformity found at the base of the Till Member of the Drenthe Formation and which is older than Unit IV; (ii) the Eemian transgressional unconformity, and (iii) the Holocene base unconformity which formed the upper boundary of the investigated strata. Coughlan *et al*. (2018) also identified and described an older Elsterian glaciogenic surface which marked the top of the Lower Sands Formation (Table 5.4). Based on the current study, two additional surfaces, the base of Unit IVc and the base of Unit IVb, were also recognized as unconformity surfaces which in terms of stratigraphic succession are located between (i) and (ii) as seen Fig. 5.3 and Table 5.4. The newly identified stratigraphic units are placed within the previously established stratigraphic and geotechnical frameworks of Coughlan *et al*. (2018) and Sindowski (1970) as well as the geotechnical sub-division of sub-soil by Schnabel *et al*. (2014) and Naumann *et al*. (2013) for the German North Sea Sector. These units were also correlated with the stratigraphic units in the Dutch and Danish sectors. While the BSH (2021) stratigraphic 'Unit Ib' corresponds to Unit IV identified within the stratigraphic framework of Coughlan *et al*. (2018), the environmental depositional setting of each of the newly identified units are herein discussed.

Table 5.4. A. Updated stratigraphic framework of Coughlan *et al.* (2018) with units identified and described in this study in bold characters and (B) correlation with Sindowski (1970) classification, zones of the geotechnical subsurface model for the German North Sea (Naumann *et al*. 2013; Schnabel *et al*. 2014) and the stratigraphy of the Dutch North Sea (Rijsdijk *et al*. 2005). The most important seismo-stratigraphic surfaces used in this study are shown with grey infill.

A					B		
Period	Unit code (Coughlan *et al*. 2018 and this study)		German North Sea stratigraphic framework (Coughlan *et al*. 2018 and this study)		German North Sea Stratigraphic Framework (Sindowski 1970)	Geotechnical zones defined by the GPDN project (Naumann *et al*. 2013; Schnabel *et al*. 2014)	Quaternary formations of The Netherlands (Laban 1995; Rijsdijk *et al*. 2005)
Holocene	I	a	Upper Marine Formation	Mobile Member	Upper Marine Layer	Zone 1 very loose to loose sands q_c = 0 - 5 MPa	Southern Bight Formation
		b		Lower Member			
	II	a	Buried River Valley Formation	Upper Member			
		b		Peat Member			Nieuwkoop Formation
Holocene base unconformity							
Weichselian	IV	a	Upper Sands Formation	**Aeolian Member**	Limnic Fluvial Layer	Zone 2 Medium dense to dense q_c = 5 - 20 MPa	Boxtel Formation (Wierden Member)
Eemian transgressional unconformity							
Saalian	IV	b	**Fluvial Formation**	**Upper Fluvial Member**		Zone 3 Very dense q_c = 20 – 60 MPa	Kreftenheye Formation (Rhine Meuse)
				Fluvial erosive unconformity			
		c		**Buried Valley Member**			
	Younger early Saalian erosive unconformity						
	VI	a	Drenthe Formation	Upper Member	Basin Deposit		Drente Formation: Schaarsbergen Member
		b		Till Member	Glacial Layer		Drente Formation: Gieten Member
Older early Saalian glaciogenic unconformity							
Elsterian	IX	a	Peelo Formation	Upper Member	Basin Deposits		Peelo Formation
		b		Lower Member	Lower Glaciofluvial Layer		
	Elsterian glaciogenic unconformity						
	XI	a	Middle Tunnel Valley Formation	Upper Member			
		b		Lower Member			
Elsterian glaciogenic unconformity							
Early Pleistocene – Pre-Elsterian	XIII		Lower Sands Formation			Zone 4 Very dense ∅ q_c > 60 MPa	

It is however important to state that a key demerit of seismic and CPT data integration centers around their differences in the level of data resolution and this was highlighted by Vardy *et al*. (2017). In this study for instance, a sub-unit was identified directly above Unit XIII from the CPT profile owning to its higher resolution (Fig. 5.4: Site 6), its lateral extent on seismic section could however not be discerned possibly as a result of a very similar acoustic impedance with the underlying unit (Fig. 5.3BB´; Site 6).

5.5.1. Depositional environment and Quaternary reconstruction

Unit IVc. – The base of the Unit IVc-valley is the lower limit of the newly identified stratigraphic units in this study (Fig. 5.3). Based on the undulating thalweg topography and similarities in shape and infill to known glacial tunnel valleys, Unit IVc is probably the infill of a glacial tunnel valley. These glacial tunnel valleys which developed beneath or adjacent ice-sheets are common in the North Sea and are generally interpreted to have formed by glacial erosion and/or catastrophic outbursts of subglacial meltwater (Huuse & Lykke-Andersen, 2000; Passchier *et al*. 2010; Moreau *et al*. 2012; Stewart *et al*. 2013). Furthermore, the width, depth and stratigraphic position of the Unit IVc-valley are similar to that of the Saalian tunnel valleys in the German and Dutch North Sea sectors and are typically smaller than the Elsterian tunnel valleys (Joon *et al*. 1990; Lutz *et al*. 2009; Passchier *et al*. 2010; Coughlan *et al*. 2018; Abegunrin *et al*. 2020; Lohrberg *et al*. 2020). Unit IVc is thus most likely of Saalian age. The base of the Unit IVc-valley is the youngest marker for ice-sheet cover observed in the study area and it is younger than the early Saalian glaciogenic unconformity at the base of the minor E-W trending tunnel valley since it cuts its infill (Fig. 5.3, Table 5.4). Since the area last experienced glaciation during the early Saalian ice advance (Ehlers 1990), the Unit IVc-base unconformity could represent a second generation of early Saalian tunnel valley incision within the study area forming the younger early Saalian unconformity (Table 5.4; Bendixen *et al*. 2017; Lang *et al*. 2018).

The Unit IVc-valley is filled with dominantly sandy sediments (Fig. 5.4, Sites 3, 4) and shows internal discontinuous stacked channel-like structures on seismic sections (Fig. 5.6A). These channels are mapped as elongate incised feature on seismic sections. Similar features have in other studies been interpreted to be fluvial in origin (Janszen *et al*. 2013; Moreau & Huuse 2014). Similar infill patterns were observed for the upper post-glacial infill of Elsterian tunnel valleys in the Hamburg region (Janszen *et al*. 2013). The infill process is separated from the formation of the tunnel valley itself (Moreau & Huuse 2014) and Unit IVc was deposited post-glacially after the younger early Saalian glacial recession.

Unit IVb. – Unlike Unit IVc, Unit IVb is distributed across the whole study area (Fig. 5.3). The base unconformity of Unit IVb forms an area-wide horizontal erosion surface (Figs 5.3, 5.8). The internal channels found mostly at the base of Unit IVb implies that fluvial erosion constitutes the main process that shaped this unconformity. The

morainic remnants discontinuously coinciding with the base of Unit IVb (Fig. 5.4, Site 6) are remnants of older early Saalian glacial erosion surface which was partly eroded during subsequent fluvial erosion (Coughlan *et al*. 2018). The dip and dip direction of Unit IVb base unconformity and the channels at the base of Unit IVb are similar and show a clear slope in northward direction (Fig. 5.7). This direction indicates a continental river system origin and is different from the meltwater-driven flows in front of the ice sheet which have been shown to flown in a SW direction during the Saalian period. In addition, the northward direction of the Unit IVb base unconformity and Unit IVb base channels compares favourably to the drainage path of the northern German rivers e.g. Elbe, Weser which drained into the periglacial flat plains that were not yet covered by sea water after the retreat of the early Saalian glacier (Gibbard & Lewin 2016; Gibbard *et al*. 1988; Schwarzer *et al*. 2008). Thus, Unit IVb is also believed to be Saalian in age.

Both Unit IVc and Unit VIb show very similar lithological characteristics (Figs 5.4, 5.5A), tip resistance (Fig. 5.4), soil behavior type index (Table 5.3) and seismic reflection patterns (Fig. 5.6) and both units are non-calcareous indicating a similar depositional environment. As opposed to the Weichselian age initially given to both Unit IVc and Unit IVb (Coughlan *et al*. 2018), new evidences described for both units in this study indicate a Saalian age. Based on observed morphological and lithological characteristics, Unit IVc is named the Buried Valley Member while Unit IVb is named the Upper Fluvial Member. The Saalian moraine deposits associated with the older early Saalian glaciogenic unconformity as well as the younger early Saalian glaciogenic unconformity underlying the Buried Valley and Upper Fluvial Members (Table 5.4) are indications that the deposition of these units started post-glacial after Saalian glacial recession.

Unit IVa. – Unit IVa, like Unit IVb (Upper Fluvial Member), is laterally continuous across the study area (Fig. 5.3). In contrast, Unit IVa is composed of homogenous fine and moderately well sorted to moderately sorted sands (Figs 5.4, 5.5C). Based on its grain size distribution (Fig. 5.5A), horizontal cover-like extent deduced from seismic imagery (Figs 5.3, 5.6) and lithological characteristics, Unit IVa is interpreted to be an aeolian deposit typical of periglacial flat plains in the North Sea (Schwan 1988; Cameron *et al*. 1989; Laban 1995; Rijsdijk *et al*. 2005). The morphology of this deposit suggests high wind velocities and low sand availability during deposition (Ehlers 1994). Unit IVa is thus named the Aeolian Member. The later reworking of aeolian sediments by periglacial streams as mentioned by Laban (1995) for parts of the Dutch North Sea was however not observed within the study area. In the south eastern part of the study area, the Aeolian Member was incised by the Palaeo-Ems and other smaller buried river valleys of the Buried River Valley Formation (Unit II of Coughlan *et al.* 2018; Fig. 5.8). On a more general scale, the top of the Aeolian Member is truncated by the Holocene base expressed as autochthonous terrestrial peats or marine transgressional layer (Hepp *et al*. 2017; Coughlan *et al*. 2018). The

Aeolian Member is most likely of Weichselian age deposited between the Eemian hiatus, which is represented by the underlying angular disconformity, and the Holocene onset above (Unit Ia, Table 5.4). The small angular unconformity separating the Upper Fluvial and Aeolian Members (Fig. 5.6) is indicative of an area-wide erosion and levelling, which is in good accordance with the Eemian sea-level high stand. This erosive interpretation is further supported by comparing the similarity in the mapped dip and dip direction of this surface with the marine erosional surface at the base of the Mobile Member (Unit Ia) of the Upper Marine Formation (Coughlan *et al.* 2018; Zeiler *et al*. 2000) and the modern sea floor (Fig. 5.3). The lack of Eemian sediments in the study area was interpreted to be caused by a regional, topographic palaeo-rise which was parallel to the modern coast and allows terrestrial dune formation following a period of abrasion during the Eemian. The existence of Eemian sediments are however well documented more southwards towards the modern coastline in apparent palaeo-trough settings (Menke & Tynni, 1984; Caspers *et al*. 2002; Coughlan *et al*. 2018; Cohen *et al*. 2022).

5.5.2. Stratigraphic correlation

Upper Fluvial Member. – Coughlan *et al*. (2018) reported sediments from the Upper Sands Formation at the entry of the so-called German `Entenschnabel` (Duck's Bill) in the north-eastern part of the German North Sea sector (Fig. 5.2). Lithological characteristics, tip resistance, thickness and stratigraphic position of units above reworked morainic remnants of the Till Member of the Drenthe Formation are similar to the Upper Fluvial Member within the study area. Prins & Andresen (2021) identified corresponding sediments as their ´Unit 3´ in a study area close to the 'Entenschnabel' in the Danish North Sea sector using seismic and CPT data. These sediments which are found in the `Entenschnabel` area are of late Saalian (Coughlan *et al*. 2018) to pre-Weichselian (Prins & Andresen 2021) age and correlate with the Upper Fluvial Member of the Saalian Fluvial Formation (Table 5.4).

West of the study area, in the neighbouring Dutch North Sea sector, fluvial deposits located above the Saalian glaciogenic unconformity (Upper Fluvial Member) are related to the Kreftenheye Formation, which is of Saalian to late Weichselian age (Rijsdijk *et al*. 2005), although the deposits of the Kreftenheye Formation are exclusively defined for sediments of the Rhine-Meuse river (Laban 1995; Rijsdijk *et al*. 2005). The sediments of the Upper Fluvial Member are deduced to be a north-eastern fluvial equivalent of the Kreftenheye Formation with the Upper Fluvial Member consisting of sediments deposited by the Elbe, Weser and Ems palaeo-rivers after the early Saalian ice advance. After the early Saalian glacial retreat, the Elbe, Weser and Ems palaeo-rivers were able to flow through the southern North Sea (Gibbard *et al*. 1988; Schwarzer *et al*. 2008; Naumann *et al*. 2013; Gibbard & Lewin 2016). Subsequently, these rivers most likely joined the Rhine and Meuse rivers since a northward path was blocked by the ice and the region dewatered through the English Channel (Gibbard *et al*. 1988; Schwarzer *et al*. 2008; Gibbard & Lewin 2016).

The study area from where the generalized geotechnical cross-sections of the GPDN project published by Naumann *et al.* (2013) and Schnabel *et al*. (2014) was carried out is close to the present study area. In fact, one seismic line in the GPDN documentation is situated in the near vicinity (<1 km) of the present study area in the region west of the Elbe Palaeovalley. Naumann *et al*. (2013) divided the sandy sub-soil into 4 superimposed zones: (1) very dense (>60 MPa) zone, (2) very dense (>20 MPa) zone, (3) medium dense to dense zone and (4) very loose to loose zone. These zones are characterized by different relative densities and strong bounding seismic reflections (Schnabel *et al*. 2014). The zones 1 to 4 of Naumann *et al*. (2013) classification compare favourably well in grain size, CPT tip resistance, relative density and seismic characteristics with the Lower Sands Formation, Upper Fluvial Member, Aeolian Member and Mobile Member of the Upper Marine Formation (Table 5.4). The zones from this study and that of Naumann *et al*. (2013) also show a similar strong seismic base reflection associated with the early Saalian glaciogenic unconformity in most of the area. The unconformity which marks the base of zone 3 (Upper Fluvial Member) is a major erosional horizon with coarse material such as gravel, cobbles and boulders interpreted to be reworked remnants of till (Coughlan *et al*. 2018). According to Naumann *et al*. (2013), Zone (3) spreads at least west of the Elbe Palaeovalley and as far as the western boundary of the German North Sea Sector. On seismic sections, the thickness of Zone (3) increases in northward direction.

Owning to the foregoing, the Upper Fluvial Member is believed to be distributed in the Western German North Sea Sector, west of the Elbe Palaeovalley (Naumann *et al*. 2013 and Schnabel *et al*. 2014) and as far north as the region of the `Entenschnabel` (Coughlan *et al*. 2018 and Prins & Andresen 2021, Fig.S2). It was however believed that the Upper Fluvial Member is limited/absent in the southward direction as no match was found in the Borkum Riffgrund Area (Coughlan *et al*. 2018). Regarding the stratigraphic position and depositional environment, the Upper Fluvial Member is comparable with the Kreftenheye Formation in the Dutch Sector in the form of a south-west trending delta from the Dutch mainland (Laban 1995; Rijsdijk *et al*. 2005) although a direct connection cannot be established due to gaps in the data coverage. In addition, different river systems which were exposed to the same climatic and glacial conditions during the late Saalian are believed to be responsible for the deposition of the sediments in the individual areas.

Aeolian Member. – Aeolian deposits similar to that found in the Aeolian Member of this study area are widespread in the lowlands of western and central Europe (Schwan 1986; Schwan 1988). In the German North Sea sector, sediments of the Aeolian Member correlate to sediments of the Upper Sands Formation retrieved from cores some 45 km southeast of Borkum Riffgrund area based on similar CPT characteristics and thickness as well as stratigraphic position of the sediments between Eemian deposits and Holocene base (Coughlan *et al*. 2018). However, differences in resolution of seismic sections from this study and that from the Borkum Riffgrund area

(Schnabel *et al*. 2014) hampers a direct comparison of seismic characteristics of the units described in both studies. In most parts, the upper surface of the Aeolian Member is eroded by the most recently deposited Holocene Mobile Member of the Upper Marine Formation (Coughlan *et al*. 2018).

The fact that the occurrence of the aeolian deposits are seldomly identified in the German North Sea sector is probably caused by merging these deposits with other layers into the ´Weichselian periglacial sands unit´ (Laban 1995; Rijsdijk *et al*. 2005; Schaumann *et al*. 2021). Schaumann *et al*. (2021) gave a detailed description of Weichselian periglacial sands identified in the Wadden Sea which is situated south of the Frisian Island of Norderney. Elsewhere, Weichselian periglacial sands known as the Twente Formation have been documented in several cores retrieved near the border of the Dutch sector (Laban 1995) and have been mapped in the most north-western part of the German North Sea sector, south of the Doggerbank (Jeffery *et al*. 1991). Laban (1995) also correlates the Twente Formation to the Weichselian periglacial Limnic-Fluvial Sands of Sindowski (1970) that were found in several cores in the German North Sea sector.

In the Dutch North Sea Sector, aeolian sands occur in the Boxtel Formation (Laban 1995; Rijsdijk *et al*. 2005; Schokker *et al*. 2007). The Boxtel Formation summarizes all local terrestrial deposits of the Cenozoic Era. Aeolian cover sands of Weichselian age, formerly known as part of the Twente Formation (Laban 1995), are now classified as the Wierden Member of the Boxtel Formation (Rijsdijk *et al*. 2005; Schokker *et al*. 2007). The deposition of the Aeolian Member below Holocene strata and above the Eemian erosional surface is consistent to the stratigraphic position of the Wierden Member (Schokker *et al*. 2007). Thus, the Aeolian Member is proposed to correlate with the Wierden Member in the Dutch North Sea Sector (Table 5.4).

The Aeolian Member is also similar in thickness and tip resistances to Zone (2) of Naumann *et al*. (2013) and Schnabel *et al*. (2014) classification with about 5 to 20 MPa (Table 5.4). In Schnabel's seismic sections, the seismic characteristics at the base of the Aeolian Member are defined by weak reflections over a wide area and are similar to that in the study area. An unconformity surface similar to that identified and mapped in this study was recognized at a depth of about 3 m on seismic profiles close to the study area. In general, the thickness of Zone (2) increases northwards. The unconformity surface is in some areas eroded by the incision of Holocene buried river valleys. The Holocene base, which is the upper boundary of the Aeolian Member, is also well defined in the studies of Naumann *et al*. (2013) and Schnabel *et al*. (2014). The thickness of the Holocene strata varies between 1 to 2 m in Naumann *et al*. (2013) and Schnabel *et al*. (2014). This is similar to the thickness found in this study and it is also comparable with that of Coughlan *et al*. (2018) and Zeiler *et al*. (2000).

Therefore, based on findings by Naumann *et al*. (2013), Schnabel *et al*. (2014) and Coughlan *et al*. (2018), the Aeolian Member identified in this study was deduced to be restricted to the area west of the Elbe Palaeovalley in

the southern North Sea sector and as far south as the Borkum Riffgrund area. Following the suggestion of Laban (1995) that Aeolian sands can be correlated to parts of the Weichselian periglacial sands which have been identified in the German North Sea by Sindowski (1970) and Schaumann *et al*. (2021) (Fig. S2), the identified Aeolian deposits from this study could even form a more eastward and southward reaching sheet in the German North Sea Sector. Within the Dutch North Sea sector, the comparable Twente Formation (now classified as the Wierden Member of the Boxtel Formation) is mapped as far west as about 4° E (Fig. 5.2; Jeffery *et al*. 1991; Laban 1995). Similarly, Andresen *et al*. (2022) described Weichselian lacustrine sediments (Unit C) from the eastern part of the Dogger Bank in the Danish North Sea sector which suggests the existence of a large proglacial lake south of the Dogger Bank (Özmaral 2017; Hjelstuen *et al.* 2018; Roberts *et al*. 2018; Hartmut Heinrich, pers. comm. 2022) and a periglacial flat plain with wide areas of aeolian sediment deposition south of the lake. Furthermore, Unit D of Andresen *et al*. (2022) is similar and comparable to Unit IVa of this study in terms of lithology and seismic character. Although, based on analogies to the Eem or Egmond Ground Formations described by Cotterill *et al*. (2017), the authors concluded that Unit D is of Eemian age as opposed to Weichselian age suggested for the equivalent Unit IVa in this study which was mainly based on the angular unconformity and total absence of indications for marine sedimentation. The findings of Andresen *et al*. (2022) thus imply that Unit IVa could represent the link to the "missing Eem" within the study area. There is therefore a strong correlation between major seismo-stratigraphic surfaces found in different studies that can be mapped over large areas of the southern North Sea. The different geotechnical properties of the sediments defined by these surfaces are a result of various depositional environments and over-consolidation due to different glaciations.

5.6. Conclusion

A detailed investigation of the highly competent upper sand units of the uppermost 25 m b.s.f. in the German sector of the North Sea was carried out based on a detailed analysis of seismic reflection data, sediment cores, CPT data and correlation with other published studies. The study refines the upper Quaternary stratigraphy from the early Saalian to the late Weichselian, by introducing the Buried Valley Member, Upper Fluvial Member and Aeolian Member as new stratigraphic units within the established frameworks of Coughlan *et al*. (2018) and BSH (2021). While the Upper Fluvial Member was previously referred to as Weichselian in age based on initial correlation to the stratigraphy in the Borkum Riffgrund area, new evidence from this study indicates a Saalian age for both the Buried Valley Member and Upper Fluvial Member. The distribution of the laterally extensive Aeolian and Upper Fluvial Member were further established by comparing their geotechnical properties to that of published geotechnical sub-surface models. The stratigraphic extent of these units within the German North Sea sector was deduced to be restricted to the area west of the Elbe Palaeovalley up to the area south of the Doggerbank with a

high level of confidence. This study not only updates Coughlan *et al*. 2018 stratigraphic classification, it also complements the BSH 2021 stratigraphic model for the German North Sea sector as well as the overall picture of the North Sea stratigraphy.

In addition to the refinement of the North Sea stratigraphy, the geotechnical parameters deduced for each of the identified units are crucial for future geotechnical investigations before, during and after engineering installations within the German North Sea sector and the Dutch sector by extension. It also provides a first-hand information pertinent to offshore infrastructure development. The Buried Valley, Upper Fluvial and Aeolian Members are all highly competent and generally well-suited for all types of wind farm foundations. However, possible problematic deposits may include shallow buried channels with peat and clayey material infills. In general, the geotechnical properties of all units in the uppermost 50 m are competent and should be considered during subsequent offshore preliminary designs which include but are not limited to offshore wind farm installations. Based on findings from this study, it is recommended that future offshore activities should continuously encompass inter-disciplinary teams including but not limited to geologists and geotechnical engineers in order to benefit from and possibly refine this vital geotechno-stratigraphy framework of the German North Sea Sector.

Acknowledgments. – The study was started within the research funded by the German Federal Ministry for Economic Affairs and Energy – ‘CPT calibration North Sea project’ (FK: 0325407) and followed up the BMWi project ‘‘Restrike-XL’’ (FK: 0324231B). A. Abegunrin received a Ph.D. funding from the Nigeria Petroleum Technology Development Fund (PTDF) in conjunction with the German Academic Exchange Service (DAAD). The authors gratefully acknowledge Lukasz Socko and Sebastian Feldmann for preparing the seismic sections and recognise the effort of Matt J. Ikari who proof read the manuscript. The authors also thank Andrew J. Wheeler, A. Janszen and an anonymous reviewer for comments that improved the manuscript. All science and industry partners that contributed data to the Marine Engineering Geology working group, MARUM – Center for Marine Environmental Sciences, University of Bremen, Germany existing database are appreciated. Special thanks to Geo-Engineering.org GmbH, Bremen, Germany for providing access to the industry data and contacts to Authorities. We also thank RWE Innogy GmbH for providing some of the data sets used for this study. The authors declare no competing interest. Open Access funding enabled and organized by Projekt DEAL.

Author Contributions. – The project was conceived by MF, DAH, SK, MC and TM. MF and AA were involved in the data analysis, writing the full manuscript and incorporated comments and corrections from DAH, SK, MC and TM. AA and MF revised the manuscript with inputs from TM, SK, DAH and MC.

Data Availability Statement. – All data used for this study are available at the existing database of the Marine Engineering Geology working group, MARUM – Center for Marine Environmental Sciences, University of Bremen, Germany.

Supporting Information. – Additional Supporting Information to this article is available at http://www.boreas.dk.

Fig. S1. Complete CPT information and other measured parameters for the selected core sites used in this study.

Fig. S2. Part of the North Sea showing the study areas from previous and present studies.

Chapter 6

Conclusion and Recommendations

This doctoral thesis contributed to broaden the understanding of the landscape architecture and dewatering regime of the German North Sea sector since the Last Glacial Maximum using an integrated tidally corrected geophysical profiles and sedimentology data. The deductions of these important findings which are based on the formulated research questions for this study are summarized as follows.

Using a grid of seismic profiles acquired in the German North Sea sector, the first part of this thesis applied a methodology devised for minimizing the effects of water column variations on seismic profiles acquired especially in shallow waters. While these effects might be negligible in deep reflection seismic data used in oil and gas industry, the correction was crucial in identifying and distinguishing various sub-surface morphological structures. In complex geological terrain, these morphological structures have similar apparent stratigraphic depths and originated from different processes over different time scales. This modern approach and easy recipe for correcting water column height variation using co-recorded information from dGPS is a less time-consuming methodology which can be applied to all sorts of reflections seismic data and requires only a small budget which is important for offshore data acquisition and processing.

The second part unraveled the evolution, morphology and valley infill successions of the EPV since the late Weichselian using an integrated seismo-stratigraphic approach. The methodology employed involves a detailed analysis of sediment echo sounder data, shallow drill cores, physical property measurements on these cores and age datings. The result revealed a minimum of a five-stage model for the EPV evolution. The first phase, represented by the FU unit, formed a braided river system at the base of the EPV. This phase depicts a classic ice marginal valley infill which developed as a result of water collected from the retreating ice. This was followed by the LU phase which was formed in a low energy aggradation system setting as the EPV re-adjusted to a new hydrodynamic regime. The OU, SU and TU units constitute the EPV main infill and accounted for the bulk of the EPV stratigraphic history. This approximately 210 km long shallow geomorphological trough played a major role in the late Weichselian and early Holocene palaeo-drainage network of the Northwest Europe as the meltwater and sediment flux from these areas were collected by it through a network of palaeo rivers.

In fact, the Palaeo Ems, the submerged extension of the modern Ems river, is one of the major tributaries that fed the southern head of the EPV. This tributary which was discussed in subsequent section formed an important part of the dewatering system that drained the unglaciated hinterland of the continental NW Europe between the more western Rhein and eastern Weser/Elbe system. Using the tide corrected seismic profiles and drill cores, the overall

course and the stratigraphic infill of the Palaeo Ems was decipher. The last phase of the Palaeo-Ems was mapped as a buried, low gradient and meandering channel spanning a length of over 100 m. In its downstream direction, the channel branched into two major pathways as it approaches the western flank of the EPV where it formed a unified depositional system with the late stage of the EPV LU unit. This study thus revealed the EPV/Palaeo Ems morpho-stratigraphic relationship for the very first time. The EPV/Palaeo Ems unified depositional system was later drowned due to the fast rising sea-level which overwhelmed the adaptation capabilities of the joint system and their infills reflect changes in the hydrodynamic conditions which occurred over time.

An understanding of these drowned palaeo-drainage network and subsequent infill descriptions is crucial for various reasons. Firstly, continental shelves and river banks are sought after settlement areas for Mesolithic people and thus hold cultural heritage which are buried in ancient sediments. Furthermore, continental shelves that are exposed during periods of low sea level are usually incised by flowing rivers. These incisions are then filled with sediments during subsequent sea level rise and thus serves as archives for palaeo-climate, palaeo-environmental and past sea level changes reconstructions. In more recent times, a good knowledge of stratigraphic infill of these drainage networks is key in siting various offshore structures such as windfarm, platforms amongst others.

The last part of the thesis focused on the refined stratigraphic units and geotechnical parameters of the uppermost 50 m below the sea floor within the German North Sea sector. By focusing on the less well understood, regionally dominant sand units which were deposited after the retreat of the last glaciers, two sandy units, the Aeolian Member and the Upper Fluvial Member, were identified as dominant deposits in the late- to post-Saalian geology within the study area. In addition, a Saalian Buried Valley Member consisting of fluvial deposits was identified. Based on the integration of seismic facies analysis with core and CPT data, a detailed geotechnical parameter set for each identified stratigraphic unit within the study area was developed and correlated with those of the neighbouring sectors. The findings complement and detailed the geotechnical and stratigraphic framework of the study area which was revised by Coughlan *et al*. (2018) as well as the stratigraphic framework which was recently developed by the German Federal Maritime and Hydrographic Agency (BSH) 2021. The deductions offer a new insight about the sub-surface sub-soil competency of an interval that is becoming increasingly important for geotechnical-engineering purposes as part of the ongoing energy transition

Further works should center on the EPV morpho-stratigraphic extension in the Danish and Norwegian sectors of the North Sea. Future research works should also investigate the predicted late Weichselian North Sea Lake believed to exist morphologically in the north western part of the EPV. These recommendations will not only provide a detailed understanding of the full hydrodynamic regime and drainage systems that developed in the North Sea since the Last Glacial Maximum but will also shed light on the existence of an ice connection between

the British – Irish Ice Sheet and the Scandinavian Ice Sheet which has continue to be a subject of subtle debate in recent past.

Lastly, it is worthy to note that the gateway function of river channels in allowing proceeding from marine hinterland transgression is a reminder and example that the past is a warning key to the future of NW European lowlands under the conditions of the accelerating man-made sea-level rise.

References

The numberings refer to references in Chapter 2.

1. Lacombe, C., Butt, S., Mackenzie, G., Schons, M. & Bornard, R. Correcting for water-column variations. *Leading Edge* **28(2),** 198–201(2009).
2. Cox, M. Static corrections for seismic reflection surveys. *Society of Exploration Geophysicists*, Tulsa, 546 p (1999).
3. Kim, H., Lee, G. H., Yi, B. Y., Yoon, Y., Kim, K. O., Kim, H. J. & Lee, S. H. A simple method of correction for profile-length water-column height variations in high-resolution, shallow-water seismic data. *Ocean Sci J.* **52,** 283-292 (2017).
4. Ong, B. S., Hembd, J., Srinivasam, A., Chu, D. & Johnston, D. H. Estimation of water layer correction in shallow time-lapse streamer data sets. *SEG New Orleans Annual Meeting* p. 5394 – 5398 (2015).
5. Toffoli, A. & Bitner-Gregersen, E. M. Types of ocean surface waves, wave classification. *Encyclopedia of Maritime and Offshore Eng.* 1-8. doi: 10.1002/9781118476406.emoe077 (2017).
6. Ellmer, W. & Goffinet, P. Tidal correction using GPS - determination of the chart datum. Shaping the Change XXIII FIG Congress Munich, Germany, October 8-13, 2006 (2006).
7. Balak, P. R., Pal, A. & Pande, K. K. Determination of tidal corrections and application to 3D marine data: a case study. In: Proceedings of the 5th Conference and Exposition on *Pet. Geophysics*, Hyderabad, 15–17 Jan 2004, pp 234 – 237 (2004).
8. Wardell, N., Diviacco, P. & Sinceri, R. 3D pre-processing technique for marine VHR seismic data. *First Break* **20,** 7 (2002).
9. Xu, S. & Pham, D. Global solution to water column statics: a new approach to an old problem. 73rd Internatiouni mensanal meeting of *Society of Exploration Geophysicists* (1997).
10. Kelletat, D. Coastal geomorphology and tourism on the German North Sea coast. In: Wong P.P. (eds) Tourism vs Environment: The case for coastal areas. The *Geo J. Library,* **26,** Springer, Dordrecht (1993).
11. Piotrowski, J. A. Tunnel-valley formation in northwest Germany: geology, mechanisms of formation and subglacial bed conditions for the Bornhöved tunnel valley. *Sedimentary Geology* **89,** 107–141 (1994).
12. Schwab, G. & Ludwig, A. O. Zum relief der Quartärbasis in Norddeutschland: Bemerkungen zu einer neuen Karte. *Zeitschrift für Geologische Wissenschaften* **24,** 343–349 (1996).
13. Winsemann, J., Koopmann, H., Tanner, D. C., Lutz, R., Lang, J., Brandes, C. & Gaedicke, C. Seismic interpretation and structural restoration of the Heligoland glaciotectonic thrust-fault complex:

Implications for multiple deformation during (pre-) Elsterian to Warthian ice advances into the southern North Sea Basin. *Quaternary Sci Rev.* **227,** 106068 (2020).

14. Stackebrandt, W., Ludwig, A. O. & Ostaficzuk, S. Base of Quaternary deposits of the Baltic Sea depression and adjacent areas (map 2). *Brandenburgische Geowissenschaftliche Beiträge*, 13–19 (2001).
15. Hepp, D. A., Hebbeln, D., Kreiter, S., Keil, H., Bathmann, C., Ehlers, J. & Mörz, T. An east – west-trending Quaternary tunnel valley in the south-eastern North Sea and its seismic – sedimentological interpretation. *J. of Quaternary Sci.* **27,** 844–853 (2012).
16. Hepp, D. A., Warnke, U., Hebbeln, D. & Mörz, T. Tributaries of the Elbe-Palaeovalley: features of a hidden palaeolandscape in the German Bight, North Sea. In Bailey, G. N., Harff, J. and Salkellariou, D. (eds.): Under the Sea: Archaeology and Palaeolandscapes. *Coastal Research Library, Springer*, Dordrecht. 211 – 222 (2017).
17. Coughlan, M., Fleischer, M., Wheeler, A. J., Hepp, D. A., Hebbeln, D., & Mörz, T. A revised stratigraphical framework for the Quaternary deposits of the German North Sea sector: a geological-geotechnical approach. *Boreas*, **10.1111**/bor.12253. ISSN 0300-9483 (2018).
18. Zeiler, M., Schulz-Ohlberg, J. & Figge, K. Mobile sand deposits and shoreface sediment dynamics in the inner German Bight (North Sea). *Marine Geology***, 170,** 363 – 380 (2000).
19. Özmaral, A. Climatically controlled sedimentary processes on continental shelves. Ph.D thesis. University of Bremen, Bremen, Germany (2017).
20. Behre, K. Coastal development, sea-level change and settlement history during the later Holocene in the Clay District of Lower Saxony (Niedersachsen), northern Germany. *Quaternary International*, **112,** 37-53. 10.1016/S1040-6182(03)00064-8 (2004).
21. Schuerch, M., Dolch, T., Reise, K. & Vafeidis, A. T. Unravelling interactions between salt marsh evolution and sedimentary processes in the Wadden Sea (south-eastern North Sea), Progress in *Physical Geography*, **38(6),** 691-715 (2014).
22. Reise, K. Coast of change: habitat loss and transformations in the Wadden Sea. Helgoland *Marine Research* **59,** 9-12 (2005).
23. Leroy, C. C., Robinson, S. P. & Goldsmith, M. J. A new equation for the accurate calculation of sound speed in all oceans. *The J. of the Acoustical Society of America*, **124(5),** 2774-2782 (2008).
24. Loewe, P. North Sea SST anomalies in October 2017. Retrieved from ftp://ftp.bsh.de/outgoing/SST-Products/NS_Archive/Anomalies/A201710.pdf (2017).

25. Klein, H., Frohse, A., Schulz, A. Salzgehalt 2016 and 2017. Retrieved from https://www.bsh.de/DE/PUBLIKATIONEN/Meer_und_Umwelt/Nordseezustand_Aktuell/nordseezustand-aktuell_node.html (2018).
26. Bailey, R. T. Sound velocity corrections for the North Sea Surveyor. *International Hydrographic Review*, Monaco, LV **1,** 123 – 133(1978).
27. Rosgen, D. L. A classification of natural rivers. *CATENA*, **22(3),** 169–199. doi:10.1016/0341-8162(94)90001-9 (1994).
28. Lutz, R., Kalka, S., Gaedicke, C., Reinhardt, L. & Winsemann, J. Pleistocene tunnel valleys in the German North Sea: spatial distribution and morphology. *Zeitschrift der Deutschen Gesellschaft für Geowissenschaften* **160,** 225–235 (2009).
29. Holthuijsen, L. H. Waves in oceanic and coastal waters. Cambridge University Press, Cambridge (2007).

Abegunrin, A., Hepp, D.A., Mörz, T., 2020. Correction of water column height variation on 2D grid high resolution seismic data using dGPS based methodology. Scientific Report 10: 18760. doi:10.1038/s41598-020-75740-z.

Andresen, K.J., Hepp, D.A., Keil, H., Spiess, V., 2022. Seismic morphologies of submerged late glacial to early Holocene landscapes at the eastern Dogger Bank, central North Sea Basin-implications for geo-archaeological potential. Geological Society, London, Special Publications, 525. doi:10.1144/SP525-2021-155.

API RP 2A-WSD 2014. Recommended practice for planning, designing and constructing fixed offshore platforms –working stress design. vol 22. American Petroleum Institute (API), Washington, D.C.

Backhaus, J.O., 1989. The North Sea and the climate. Dana 8, 69–82.

Bailey, G., Galanidou, N., Peeters, H., Jöns, H., Mennenga, M., (Eds.) 2020. The Archaeology of Europe's Drowned Landscapes. Coastal Research Library 35, Springer Cham, 561 pp. doi:10.1007/978-3-030-37367-2.

Behre, K.E., 2007. A new Holocene sea-level curve for the southern North Sea. Boreas 36(1), 82–102. doi:10.1111/j.1502-3885.2007.tb01183.x.

Bendixen, C., Lamb, R.M., Huuse, M., Boldreel, L.O., Jensen, J.B., Clausen, O.R., 2017. Evidence for a grounded ice sheet in the central North Sea during the early Middle Pleistocene Donian Glaciation. Journal of the Geological Society, 175(2), 291–307. doi:10.1144/jgs2017-073.

Blott, S.J., Pye, K., 2001. GRADISTAT: a grain size distribution and statistics package for the analysis of unconsolidated sediments. Earth Surf Proc Land 26:1237-1248.

Blum, M., Martin, J., Milliken, K., Garvin, M., 2013. Paleovalley systems: Insights from Quaternary analogs and experiments. Earth-Science Reviews 116, 128–169. doi:10.1016/j.earscirev.2012.09.003.

Blum, M.D., Törnqvist, T.E., 2000. Fluvial responses to climate and sea-level change: A review and look forward. Sedimentology 47(745), 2–48. doi:10.1046/j.1365-3091.2000.00008.x.

Böse, M., Lüthgens, C., Lee, J.R., Rose, J., 2012. Quaternary glaciations of northern Europe. Quaternary Science Reviews 44, 1–25.

Bot, S.L., Van Lancker, V., Deleu, S., De Batist, M., Henriet J.P., Haegeman W., 2005. Geological characteristics and geotechnical properties of Eocene and Quaternary deposits on the Belgian continental shelf: synthesis in the context of offshore wind farming. Netherlands J Geosci-Geol Mijnbouw 84:147-160. doi:10.1017/S0016774600023027.

Bourillet, J.F., Reynaud, J.Y., Baltzer, A., Zaragosi, S., 2003. The 'Fleuve Manche': the submarine sedimentary features from the outer shelf to the deep-sea fans. Journal of Quaternary Science 18(3-4), 261–282. doi:10.1002/jqs.757.

Bradwell, T., Stoker, M., Golledge, N.R., Wilson, C.K., Merritt, J.W., Long, D., Everest, J., Hestivk, O.B., Stevenson, A.G., Hubbard, A.L., Finlayson, A.G., Mathers, H.E., 2008. The northern sector of the last British Ice Sheet: maximum extent and demise. Earth Science Reviews 88, 207-226.

Buckley, F.A., 2017. A glaciogenic sequence from the Early Pleistocene of the Central North Sea. Journal of Quaternary Science, 32, 145–168.

Buckley, F.A., 2012. An Early Pleistocene grounded ice sheet in the Central North Sea. In: Huuse, M., Redfern, J., Le Heron, D.P., Dixon, R.J., Moscariello, A. & Craig, J. (eds.) Glaciogenic Reservoirs and Hydrocarbon Systems. Geological Society, London, Special Publications, 368, 185–209. doi:10.1144/SP368.8

BSH 2021. Datenportal Flächenvoruntersuchung. https://pinta.bsh.de last accessed on October 12th, 2021.

BSH 2014. Ground Investigation for Offshore Wind Energy. vol 2. Federal Maritime and Hydrographic Agency (BSH), Hamburg and Rostock, Germany.

Cameron, D., van Doorn, D., Laban, C., Streif, H.J., 1993. Geology of the Southern North Sea Basin. In: Hillen, R., Verhagen, H.J. (Eds.), Coastlines of the southern North Sea. Coastlines of the world. American Society of Civil Engineers, New York, N.Y.

Cameron, T.D.J., Crosby, A., Balson, P.S., Jeffrey, D.H., Lott, G.K., Bulat, J., Harrison, D.J., 1992. The geology of the southern North Sea, BGS United Kingdom Offshore Regional Report, 152 pp.

Cameron, T.D.J., Schüttenhelm, R., Laban, C., 1989. Middle and Upper Pleistocene and Holocene stratigraphy in the southern North Sea between 52 and 54 N, 2 to 4 E. In: Henriet, J.P., De Moor, G., De Batist, M. (eds.) The

Quaternary and Tertiary geology of the Southern Bight, North Sea. Belgian Geological Survey, Brussel, pp 119-135.

Cameron, T.D.J., Stoker, M.S., Long, D., 1987. The history of Quaternary sedimentation in the UK sector of the North Sea Basin. Journal of the Geological Society 144, 43–58.

Carr, S.J., 2004. The North Sea basin. In: Quaternary Glaciations Extent and Chronology - Part I: Europe. Developments in quaternary sciences. Elsevier, pp. 261–270 eBook ISBN: 9780080540146.

Caspers, G., Merkt, J., Müller, H., Freund, H., 2002. The Eemian Interglaciation in Northwestern Germany. Quaternary Research, 58(01), 49–52. doi:10.1006/qres.2002.2341.

Caston, G.F., 1981. Potential gain and loss of sand by some sand banks in the Southern Bight of the North Sea. Marine Geology 41(3-4), 239–250.

Caston, V.N.D., 1979. The Quaternary Sediments of the North Sea. In: Banner FT, Collins MB, Massie KS (eds) The North-West European shelf seas: the sea bed and the sea in motion, Part I: Geology and Sedimentology. vol 1. Elsevier, Amsterdam, pp 195-270.

Caston, V.N., 1977. Quaternary deposits of the central North Sea, 2: The Quaternary deposits of the Forties field, northern North Sea. Natural Environment Research Council Report, 77/11. HMSO, London.

Caston, V., 1972. Linear sand banks in the southern North Sea. Sedimentology 18(1-2), 63–78.

Church, J.A., Aarup, T., Woodworth, P.L., Wilson, W.S., Nicholls, R.J., Rayner, R., Lambeck, K., Mitchum, G.T., Steffen, K., Cazenave, A., Blewitt, G., Mitrovica, J.X., Lowe, J.A., 2010. Sea-Level Rise and Variability: Synthesis and Outlook for the Future. In: Church, J. (Ed.), Understanding sea-level rise and variability. Blackwell Pub, Hoboken, NJ, 402–419.

Cohen, K.M., Cartelle, V., Barnett, R., Busschers, F.S., Barlow, N.L.M., 2022. Last Interglacial sea-level data points from Northwest Europe, Earth Syst. Sci. Data Discuss 14, 2895–2937. doi:10.5194/essd-2021-390.

Cohen, K.M., Gibbard, P.L., Weerts, H., 2014. North Sea palaeogeographical reconstructions for the last 1 Ma. Netherlands Journal of Geosciences - Geologie en Mijnbouw 93(1-2), 7–29. doi:10.1017/njg.2014.12.

Coles, B.J., 2000. Doggerland: The cultural dynamics of a shifting coastline. Geological Society, London, Special Publications 175(1), 393–401. doi:10.1144/GSL.SP.2000.175.01.27.

Coles B.J., 1998. Doggerland: a Speculative Survey, Proceedings of the Prehistoric Society, 64, 45–81, https://doi.org/10.1017/S0079497X00002176.

Corbetta, G., Mbistrova, A., 2015. The European Offshore Wind Industry – Key Trends and Statistics 2014. European Wind Energy Association (EWEA). http://www.ewea.org. Accessed 10 June, 2015.

Cotterill, C.J., Phillips, E., James, L., Forsberg, C.F., Tjelta, T.I., Carter, G., Dove, D., 2017a. The evolution of the Dogger Bank, North Sea: a complex history of terrestrial, glacial and marine environmental change. Quat. Sci. Rev. 171, 136–153. doi:10.1016/j.quascirev.2017.07.006.

Cotterill, C., Phillips, E., James, L., Forsberg, C.F., Tjelta, T.I., 2017b. How understanding past landscapes might inform present-day site investigations: a case study from Dogger Bank, southern Central North Sea. Near Surf. Geophys. 15, 403–414. doi:10.3997/1873-0604.2017032.

Coughlan, M., Fleischer, M., Wheeler, A.J., Hepp, D.A., Hebbeln, D., Mörz, T., 2018. A revised stratigraphical framework for the Quaternary deposits of the German North Sea sector: a geological-geotechnical approach. Boreas 47, 80-105. doi:10.1111/bor.12253.

Cronin, T.M., 2012. Rapid sea-level rise. Quaternary Science Reviews 56, 11–30.

Davis, R.A., Balson, P.S., 1992. Stratigraphy of a North Sea Tidal Sand Ridge. SEPM Journal of Sedimentary Research 62(1), 116–121.

Deleu, S., van Lancker, V., van den Eynde, D., Moerkerke, G., 2004. Morphodynamic evolution of the kink of an offshore tidal sandbank: the Westhinder Bank (Southern North Sea). Continental Shelf Research 24(15), 1587–1610.

DIN 18123 1996. Baugrund, Untersuchung von Bodenproben - Bestimmung der Korngrößenverteilung. Deutsches Institut für Normung, Berlin.

DIN 18125-2 2011. Baugrund, Untersuchung von Bodenproben - Bestimmung der Dichte des Bodens - Teil 2: Feldversuche. Deutsches Institut für Normung, Berlin.

DIN 18135 1999. Baugrund, Untersuchung von Bodenproben - Eindimensionaler Kompressionsversuch. Deutsches Institut für Normung, Berlin.

DIN 18137-3 2002. Baugrund, Untersuchung von Bodenproben - Bestimmung der Scherfestigkeit, Teil 3: Direkter Versuch. Deutsches Institut für Normung, Berlin.

DIN EN 1997-2 2010. Eurocode 7: Geotechnical design - Part 2: Ground investigation and testing.

DIN EN ISO 14688-2 2020. Geotechnische Erkundung und Untersuchung - Benennung, Beschreibung und Klassifizierung von Boden - Teil 2: Grundlagen für Bodenklassifizierungen. Deutsches Institut für Normung, Berlin.

DIN EN ISO 22476-1 2009. Geotechnische Erkundung und Untersuchung - Felduntersuchungen - Teil 1: Drucksondierung mit elektrischen Messwertaufnehmern und Messeinrichtungen für Porenwasserdruck. Deutsches Institut für Normung, Berlin.

Ehlers, J., 1990. Reconstructing the dynamics of the north-west european Pleistocene ice sheets. Quatern Sci Rev 9:71-83. doi:10.1016/0277-3791(90)90005-U.

Ehlers, J., 1994. Allgemeine und historische Quartärgeologie. Enke Verlag, Stuttgart.

Ehlers, J., Gibbard, P.L, Hughes, P.D., 2011. Quaternary Glaciations - Extent and Chronology: A closer look, 15. Elsevier.

Ehlers, J., Eissmann, L., Lippstreu, L., Stephan, H.J., Wansa, S., 2004. Pleistocene glaciations of North Germany. In: Ehlers, J., Gibbard, P.L. (Eds.), Quaternary Glaciations Extent and Chronology - Part I: Europe. Developments in quaternary sciences. Elsevier, pp. 135–146. doi:10.1016/B978-0-444-53447-7.00013-1.

Ehlers, J., Meyer, K.D., Stephan, H.J., 1984. The pre-Weichselian glaciations of north-west Europe. Quaternary Science Reviews 3, 1–40.

Ehlers, J., Gibbard, P.L., 2004. Quaternary Glaciations - Extent and Chronology. Elsevier.

Ehlers, J., Linke, G., 1989. The origin of deep buried channels of Elsterian age in Northwest Germany. Journal of Quaternary Science 4, 255–265.

Ehlers, J., Wingfield, R., 1991. The extension of the Late Weichselian/Late Devensian ice sheets in the North Sea Basin. Journal of Quaternary Science 6(4), 313–326.

Eissmann, L., 2002. Quaternary geology of eastern Germany (Saxony, Saxon–Anhalt, South Brandenburg, Thüringia), type area of the Elsterian and Saalian Stages in Europe. In: Quaternary Science Reviews 21 (11), S. 1275–1346. doi:10.1016/S0277-3791(01)00075-0.

Ellmer, W., Goffinet, P., 2006. Tidal correction using GPS - determination of the chart datum. Shaping the Change XXIII FIG Congress Munich, Germany, October 8-13, 2006.

Emery, A.R., Hodgson, D.M., Barlow, N.L.M., Carrivick, J.L., Cotterill, C.J., Richardson, J.C., Ivanovic, R.F., Mellett, C.L., 2020. Ice sheet and palaeoclimate controls on drainage network evolution: an example from Dogger Bank, North Sea, Earth Surf. Dynam., 8, 869–891. doi:10.5194/esurf-8-869-2020.

Emery, A.R., Hodgson, D.M., Barlow, N.L.M., Carrivick, J.L., Cotterill, C.J., Phillips, E., 2019. Left High and Dry: Deglaciation of Dogger Bank, North Sea, Recorded in Proglacial Lake Evolution. Frontiers in Earth Science, 7. doi:10.3389/feart.2019.00234

Figge, K., 1983. Morainic deposits in the German Bight area of the North Sea. In: Ehlers, J. (Ed.), Glacial deposits in North-West Europe. Balkema, Rotterdam, pp. 299–304.

Fitch, S., Thomson, K., Gaffney, V., 2005. Late Pleistocene and Holocene depositional systems and the palaeogeography of the Dogger Bank, North Sea. Quaternary Research 64(2), 185–196. doi:10.1016/j.yqres.2005.03.007.

Frisch, W., Meschede, M., Blakey, R.C., 2011. Plate Tectonics Continental Drift and Mountain Building, Springer Berlin Heidelberg. doi:10.1007/978-3-540-76504-2.

Gaffney, V., Fitch, S., 2022. Europe's Lost Frontiers: context and development. In Gaffney V, Fitch S. (eds.) Europe's Lost Frontiers: Context and Methodology Vol. 1, 1-15 doi: 10.32028/9781803272689

Gaffney, V., Fitch, S., Bates, M., Ware, R.L., Kinnaird, T., Gearey, B., *et al*. 2020. Multi-Proxy Characterisation of the Storegga Tsunami and Its Impact on the Early Holocene Landscapes of the Southern North Sea. Geosciences 10, 270. doi:10.3390/geosciences10070270.

Gaffney, V., Fitch, S., Smith, D., 2009. Europe's lost world: the rediscovery of Doggerland. Council for British Archaeology Research (York): 202 pp. doi:10.1017/S0003598X00100377.

Gaffney, V.L., Thomson, K., Fitch, S., 2007. Mapping Doggerland: The Mesolithic Landscapes of the Southern North Sea. Archaeopress, Oxford.

Gatliff, R.W., Richards, P.C. et al. 1994. The geology of the central North Sea, United Kingdom Offshore Regional Report. HMSO for the British Geological Survey, London.

Germanischer Lloyd 2012. Rules and Guidelines - IV, Industrial Services, Part 2: Guideline for the Certification of Offshore Wind Turbines. GL Renewables Certification, Hamburg, Germany.

Gibbard, P.L., 1988. The history of the great Northwest European rivers during the past three million years. Philosophical Transactions of the Royal Society, Series B, 318, 559–602.

Gibbard, P.L., Cohen, K.M., 2008. Global chronostratigraphical correlation table for the last 2.7 million years. Episodes 31, 243–247.

Gibbard, P.L., Lewin, J., 2016. Filling the North Sea Basin: Cenozoic sediment sources and river styles (André Dumont medallist lecture 2014). Geol Belgica 19. doi:10.20341/gb.2015.017.

Gibbard, P.L., Rose, J., Bridgland, D.R., 1988. The History of the Great Northwest European Rivers During the Past Three Million Years [and Discussion]. Philosophical Transactions of the Royal Society of London. Series B, Biological Sciences 318(1191), 559–602. doi:10.1098/rstb.1988.0024.

GPDN 2022: Datenportal deltaentwicklung. https://www.gpdn.de/wilma.aspx?pgId=177. Accessed on November 8th, 2022.

Graham, A.G.C., Stoker, M.S., Lonergan, L., Bradwell, T., Stewart, M.A., 2011. The Pleistocene glaciations of the North Sea Basin. In: Ehlers, J., Gibbard, P.L., Philip, D.H. (eds.) Quaternary glaciations, extent and chronolgy, part 4: a closer look, vol 15. Developments in Quaternary sciences. Elsevier, Amsterdam, pp 261-278. doi:10.1016/b978-0-444-53447-7.00021-0.

Graham, A.G.C., Lonergan, L., Stoker, M.S., 2009. Seafloor glacial features reveal the extent and decay of the last British Ice Sheet, east of Scotland. Journal of Quaternary Science 24, 117–138.

Grube, F., Christensen, S., Vollmer, T., Duphorn, K., Klostermann, J., Menke, B., 1986. Glaciations in north west Germany. Quaternary Science Reviews 5, 347–358.

Hepp, D.A., Romero, O.E., Mörz, T., De Pol-Holz, R., Hebbeln, D., 2019. How a river submerges into the sea: a geological record of changing a fluvial to a marine paleoenvironment during early Holocene sea level rise. J. Quatern. Sci. 34, 581-592. doi:10.1002/jqs.3147.

Hepp, D.A., Warnke, U., Hebbeln, D., Mörz, T., 2017. Tributaries of the Elbe-Palaeovalley: features of a hidden palaeolandscape in the German Bight, North Sea. In Bailey, G.N., Harff, J., Salkellariou, D. (eds.): Under the Sea: Archaeology and Palaeolandscapes. Coastal Research Library, Springer, Dordrecht. 211 – 222. doi:10.1007/978-3-319-53160-1_14.

Hepp, D.A., Hebbeln, D., Kreiter, S., Keil, H., Bathmann, C., Ehlers, J., Mörz, T., 2012. An east – west-trending Quaternary tunnel valley in the south-eastern North Sea and its seismic – sedimentological interpretation. Journal of Quaternary Science 27, 844–853. doi:10.1002/jqs.2599.

Hinz, P., Lesny, K., Richwien, W., 2007. Prognose des Langzeitverhaltens von Monopilegründungen. In: 5. Symposium Offshore-Windenergie - Bau- und Umwelttechnische Aspekte, Hannover, 2007.

Hjelstuen, B.O., Sejrup, H.P., Valvik, E., Becker, L.W.M., 2018. Evidence of an ice-dammed lake outburst in the North Sea during the last deglaciation. *Marine Geology*, *402*, 118-130. doi:10.1016/j.margeo.2017.11.021.

Hughes, A.L.C., Gyllencreutz, R., Lohne, Ø.S., Mangerud, J., Svendsen, J.I., 2016. The last Eurasian ice sheets - a chronological database and time-slice reconstruction, DATED-1. Boreas 45(1), 1–45. doi:10.1111/bor.12142.

Huuse, M., 2002. Late Cenozoic palaeogeography of the eastern North Sea Basin: Climatic vs tectonic forcing of basin margin uplift and deltaic progradation. Bulletin of the Geological Society of Denmark, 49, 145–170.

Huuse, M., Kristensen, T.B., 2016. Pleistocene tunnel valleys in the North Sea Basin. Geological Society, London, Memoirs, 46: (1), 207–208. doi:10.1144/m46.129.

Huuse, M., Lykke-Andersen, H., 2000. Overdeepened Quaternary valleys in the eastern Danish North Sea: Morphology and origin. Quaternary Science Reviews 19(12), 1233–1253. doi:10.1016/S0277-3791(99)00103-1.

Huuse, M., Lykke-Andersen, H., Michelsen, O., 2001. Cenozoic evolution of the eastern Danish North Sea. Marine Geology 177(3-4), 243–269.

Janszen, A., Moreau, J., Moscariello, A., Ehlers, J., Kröger, J., 2013. Time-transgressive tunnel-valley infill revealed by a three-dimensional sedimentary model, Hamburg, north-west Germany. Sedimentology 60:693-719. doi:10.1111/j.1365-3091.2012.01357.x.

Jeffery, D.H., Laban, C., Mesdag, C.S., Schüttelhlem, R.T.E., 1991. Doggersheet 55°N/02°E, Quarternary Geology. British Geological Survey and Geological Survey of The Netherlands.

Jenyon, M.K., 1988. Overburden deformation related to the pre-piercement development of salt structures in the North Sea. In: Journal of the Geological Society 145 (3), S. 445–454. doi:10.1144/gsjgs.145.3.0445.

Joon, B., Laban, C., van der Meer, J.J.M., 1990. The Saalian glaciation in the Dutch part of the North Sea. Geol Mijnbouw 69:151-158.

Kiden, P., Denys, L., Johnston, P., 2002. Late Quaternary sea-level change and isostatic and tectonic land movements along the Belgian-Dutch North Sea coast: Geological data and model results. Journal of Quaternary Science 17(5-6), 535–546.

Kluiving, S.J., Aleid Bosch, J., Ebbing, J.H., Mesdag, C.S., Westerhoff, R.S., 2003. Onshore and offshore seismic and lithostratigraphic analysis of a deeply incised Quaternary buried valley system in the Northern Netherlands. Journal of Applied Geophysics 53, 249–271.

Knudsen, K.L., 1988. Marine interglacial deposits in the Cuxhaven Area, N W Germany: a comparison of Holsteinian, Eemian and Holocene foraminiferal faunas. Eiszeitalter und Gegenwart 38, 69–77.

Konradi, P.B., Larsen, B., Sørensen, A.B., 2005. MarineEemianin the Danish eastern North Sea. Quaternary International 133/134, 21–31.

Kristensen, T.B., Huuse, M., Piotrowski, J.A., Clausen, O.R., 2007. A morphometric analysis of tunnel valleys in the eastern North Sea based on 3D seismic data. Journal of Quaternary Science, 22: (8), 801–815. doi:10.1002/jqs.1123.

Kuhlmann, G., 2004. High resolution stratigraphy and paleoenvironmental changes in the southern North Sea during the Neogene. An integrated study of Late Cenozoic marine deposits from the northern part of the Dutch offshore area, cummulativ thesis, 209 pp, Utrecht University, Utrecht.

Kuhlmann, G., Langereis, C., Munsterman, D., Jan van Leeuwen, R., Verreussel, R., Meulenkamp, J., Wong, T., 2006. Chronostratigraphy of Late Neogene sediments in the southern North Sea Basin and paleoenvironmental interpretations. Palaeogeography, Palaeoclimatology, Palaeoecology 239, 426–455.

Laban, C., 1995. The Pleistocene glaciations in the Dutch sector of the North Sea: a synthesis of sedimentary and seismic data. Ph.D. thesis, University of Amsterdam.

Lambeck, K., 1995. Late Devensian and Holocene shorelines of the British Isles and North Sea from models of glacio-hydro-isostatic rebound. Journal of the Geological Society 152(3), 437–448. doi:10.1144/gsjgs.152.3.0437.

Lang, J., Lauer, T., Winsemann, J., 2018. New age constraints for the Saalian glaciation in northern central Europe: Implications for the extent of ice sheets and related proglacial lake systems. Quaternary Science Reviews 180, 240-259. doi:10.1016/j.quascirev.2017.11.029.

Lee, A.J., 1980. Chapter 14 North Sea: Physical Oceanography. Elsevier Oceanography Series, 467–493. doi:10.1016/s0422-9894(08)71359-x.

Lee, J.R., Busschers, F.S., Sejrup, H.P., 2012. Pre-Weichselian Quaternary glaciations of the British Isles, The Netherlands, Norway and adjacent marine areas south of 68°N: implications for long-term ice sheet development in northern Europe. Quaternary Science Reviews, 44, 213–228.

Litt, T., Behre, K.E., Meyer, K.D., Stephan, H.J., Wansa, S., 2007. Stratigraphische Begriffe für das Quartär des norddeutschen Vereisungsgebietes (E&G – Quaternary Science Journal; Vol. 56 No 1-2; 7-65; ISSN 0424-7116).

Littke, R., Bayer, U., Gajewski, D., Nelskamp, S., 2008. Dynamics of complex intracontinental basins: the central European basin system. Springer Science & Business Media.

Lohrberg, A., Schwarzer, K., Unverricht, D., Omlin, A., Krastel, S., 2020. Architecture of tunnel valleys in the southeastern North Sea: New insights from high-resolution seismic imaging. Journal of Quaternary Science: Vol. 35 No. 892 - 906. doi:10.1002/jqs.3244.

Long, D., Laban, C., Streif, H., Cameron, T., Schuttenhelm, R.T.E., Paepe, R., 1988. The Sedimentary Record of Climatic Variation in the Southern North Sea [and Discussion]. Philosophical Transactions of the Royal Society B: Biological Sciences 318(1191), 523–537. doi:10.1098/rstb.1988.0022.

Lunne, T., Robertson, P.K., Powell, J.J.M., 1997. Cone penetration testing in geotechnical practice. Blackie Academic & Professional/Routledge, New York.

Lutz, R., Kalka, S., Gaedicke, C., Reinhardt, L., Winsemann, J., 2009. Pleistocene tunnel valleys in the German North Sea: Spatial distribution and morphology [Pleistozäne Rinnen in der deutschen Nordsee: Verbreitung und Morphologie]. Zeitschrift der Deutschen Gesellschaft für Geowissenschaften 160(3), 225–235. doi:10.1127/1860-1804/2009/0160-0225.

Madsen, T.M., Piotrowski, J.A., 2012. Genesis of the glaciotectonic thrust–fault complex at Halk Hoved, southern Denmark. Bulletin of the Geological Society of Denmark, 60, 61–80.

Marcott, S.A., Shakun, J.D., Clark, P.U., Mix, A.C., 2013. A reconstruction of regional and global temperature for the past 11,300 years. Science (New York, N.Y.) 339(6124), 1198–1201.

Martin, J., Sheets, B., Paola, C., Hoyal, D., 2009. Influence of steady base-level rise on channel mobility, shoreline migration, and scaling properties of a cohesive experimental delta. Journal of Geophysical Research, **114**, F03017. doi:10.1029/2008JF001142.

Maystrenko, Y., Bayer, U., Brink, H.J., Littke, R., 2008. The Central European basin system–an overview. In Dynamics of complex intracontinental basins, 16–34. Springer.

Maystrenko, Y., Bayer, U., Scheck-Wenderoth, M., 2005. Structure and evolution of the Glueckstadt Graben due to salt movements. International Journal of Earth Sciences, 94(5-6):799–814.

McCann, T., 2008. The geology of central Europe. Geological Society of London.

McCann, T., Pascal, C., Timmerman, M.J., Krzywiec, P., López-Gómez, J., Wetzel, L., Krawczyk, C.M., Rieke, H., Lamarche, J., 2006. Post-Variscan (end Carboniferous-Early Permian) basin evolution in western and central Europe. Geological Society, London, Memoirs, 32(1):355–388.

Meijer, X.D., 2002. Modelling the drainage evolution of a river-shelf system forced by Quaternary glacio-eustasy. Basin Research 14(3), 361–377. doi:10.1046/j.1365-2117.2002.00187.x.

Menke, B., Tynni, R., 1984. Das Eeminterglazial und das Weichselfrühglazial von Rederstall/Dithmarschen und ihre Bedeutung für die mitteleuropäische Jungpleistozän-Gliederung. Geologisches Jahrbuch A 76, 3–120.

Michelsen, O., Danielsen, M., Heilmann-Clausen, C., Jordt, H., Laursen, G.V., 1998. Cenozoic sequence stratigraphy in the eastern North Sea. In: Society for Sedimentary Geology (60).

Michelsen, O., Danielsen, M., Heilmann-Clausen, C., Jordt, H., Laursen, G.V., Thomsen, E., 1995. Occurrence of major sequence stratigraphic boundaries in relation to basin development in Cenozoic deposits of the southeastern North Sea. In: Norwegian Petroleum Society Special Publications (5), S. 415–427.

Mittelstaedt, E., Lange, W., Brockmann, C., Soetje, K.C., 1983. Die StroÈmungen der Deutschen Bucht. Deutsches Hydrographisches Institut, Nr. 2347. 141 pp.

Mohrig, D, Heller, P.L., Paola, C., Lyons, W.J., 2000. Interpreting avulsion process from ancient alluvial sequences: Guadalope-Matarranya system (northern Spain) and Wasatch Formation (western Colorado). GSA Bulletin, **112**(12), 1787–1803. doi:10.1130/0016-7606(2000)112<1787:IAPFAA>2.0.CO;2.

Moossen, H., Bendle, J., Seki, O., Quillmann, U., Kawamura, K., 2015. North Atlantic Holocene climate evolution recorded by high-resolution terrestrial and marine biomarker records. Quaternary Science Reviews 129, 111–127.

Moreau, J., Huuse, M., 2014. Infill of tunnel valleys associated with landward-flowing ice sheets: The missing Middle Pleistocene record of the NW European rivers? Geochem, Geophys, Geosyst 15. doi:10.1002/2013GC005007.

Moreau, J., Huuse, M., Janszen, A., van Der Vegt, P., Gibbard P.L., Moscariello, A., 2012. The glaciogenic unconformity of the southern North Sea. Geological Society, London, Special Publications 368. doi:10.1144/sp368.5.

Müller, P.J., Schneider, R., Ruhland, G., 1994. Late Quaternary PCO_2 Variations in the Angola Current: Evidence from Organic Carbon $\delta^{13}C$ and Alkenone Temperatures. In: Zahn, R., Pedersen, T.F., Kaminski, M.A., Labeyrie, L. (Eds.), Carbon Cycling in the Glacial Ocean: Constraints on the Ocean's Role in Global Change. NATO ASI Series, vol 17. Springer, Berlin, Heidelberg. https://doi.org/10.1007/978-3-642-78737-9_15

Naumann, M., Schnabel, C., Fritz, J., Djuren, D., 2013. Erstellung von Baugrundschnitten in der deutschen Nordsee - Dokumentation Nr. 9, Geopotenzial Deutsche Nordsee - Modul B. BGR, LBEG, BSH. http://www.gpdn.de. Accessed October 12th, 2021.

Neill, S.P., Scourse, J.D., Uehara, K., 2010. Evolution of bed shear stress distribution over the northwest European shelf seas during the last 12,000 years. Ocean Dynamics 60(5), 1139–1156.

Nielsen, S.B., Gallagher, K. et al. 2009. The evolution of western Scandinavian topography: A review of Neogene uplift versus the ICE (isostasy–climate–erosion) hypothesis. Journal of Geodynamics, 47, 72–95. doi:10.1016/j.jog.2008.09.001.

Nittrouer, C.A., Austin, J.A., Field, M.E., Kravitz, J.H., Syvitski, J.P.M., Wiberg, P.L., 2007. Writing a Rosetta Stone: Insights into Continental-Margin Sedimentary Processes and Strata. In: Nittrouer, C.A., Austin, J.A., Field, M.E., Kravitz, J.H., Syvitski, J.P.M., Wiberg, P.L. (Eds.), Continental Margin Sedimentation. Blackwell Publishing Ltd, Oxford, UK, pp. 1–48.

O´Cofaigh C., 1996. Tunnel valley genesis. Progress in Physical Geography 20: 1–19. doi:10.1177/030913339602000101.

Oele, E., Schüttenhelm, R.T.E., 1979. Development of the North Sea after the Saalian glaciation. In: Oele, E., Schüttenhelm, R.T.E., Wiggers, A.J. (eds.) The Quaternary history of the North Sea, vol 2. Acta Universitatis Upsaliensis, vol Symposia Universitatis Upsaliensis annum quingentesimum celebrantis. Almqvist and Wiksell, Uppsala, pp 191-216.

Ottesen, D., Stewart, M., Brönner, M., Batchelor, C.L., 2020. Tunnel valleys of the central and northern North Sea (56°N to 62°N): Distribution and characteristics. Marine Geology, 425, 106199. doi:10.1016/j.margeo.2020.106199.

Ottesen, D., Dowdeswell, J.A., Bugge, T., 2014. Morphology, sedimentary infill and depositional environments of the Early Quaternary North Sea Basin (56–62°N). Marine and Petroleum Geology, 56, 123–146.

Overeem, I., Weltje, G.J., Bishop-Kay, C., Kroonenberg, S.B., 2001. The Late Cenozoic Eridanos delta system in the Southern North Sea Basin: a climate signal in sediment supply?. Basin Research, 13: 293-312. doi:10.1046/j.1365-2117.2001.00151.x

Özmaral, A., Abegunrin, A., Keil, H., Hepp, D.A., Schwenk, T., Lantzsch, H., Mörz, T., Spiess, V., 2022. The Elbe Palaeovalley: evolution from an ice-marginal valley to a sedimentary trap (SE North Sea). Quaternary Science Reviews 282, 107453. doi:10.1016/j.quascirev.2022.107453.

Özmaral, A., 2017. Climatically controlled sedimentary processes on continental shelves. Ph.D Thesis. University of Bremen, Bremen, Germany.

Papenmeier, S., Hass, H.C., 2020. Revisiting the Paleo Elbe Valley: Reconstruction of the Holocene, Sedimentary development on basis of high-resolution grain size data and shallow seismics. Geosciences, 10:(12), 505. doi:10.3390/geosciences10120505.

Passchier, S., Laban, C., Mesdag, C.S., Rijsdijk, K.F., 2010. Subglacial bed conditions during Late Pleistocene glaciations and their impact on ice dynamics in the southern North Sea. Boreas 39:633-647. doi:10.1111/j.1502-3885.2009.00138.x.

Passeri, D.L., Hagen, S.C., Medeiros, S.C., Bilskie, M.V., Alizad, K., Wang, D., 2015. The dynamic effects of sea level rise on low-gradient coastal landscapes: A review. Earth's Future 3(6), 159–181.

Pedersen, S.A.S., 2014. Architecture of glaciotectonic complexes. Geosciences, 4, 269–296.

Pedersen, S.A.S., 2005. Structural analysis of the Rubjerg Knude Glaciotectonic Complex, Vendsyssel, northern Denmark. Geological Survey of Denmark and Greenland Bulletin, 8.

Pedersen, S.A.S., 2000. Superimposed deformation in glaciotectonics. Bulletin of the Geological Society of Denmark, 46, 125–144.

Pedological mapping guide, KA5 (manual of soil mapping, 5th Ed.) published by the German Federal Institute for Geosciences and Natural Resources in cooperation with the State Geological Services. ISBN 978-3-510-95920-4.

Pharaoh, T.C., 1999. Palaeozoic terranes and their lithospheric boundaries within the Trans-European Suture Zone (TESZ): a review. Tectonophysics, 314(1-3):17–41.

Phillips, E., Hodgson, D.M., Emery, A.R., 2017. The Quaternary geology of the North Sea basin. Journal of Quaternary Science, 32(2), 117–126. doi:10.1002/jqs.2932.

Piotrowski, J.A., 1994. Tunnel-valley formation in northwest Germany: geology, mechanisms of formation and subglacial bed conditions for the Bornhöved tunnel valley. Sedimentary Geology 89, 107–141.

Pisarska-Jamroży, M., 2015. Factors controlling sedimentation in the Toruń-Eberswalde ice-marginal valley during the Pomeranian phase of the Weichselian glaciation: An overview. Geologos 21(1), 1–29. doi:10.1515/logos-2015-0001.

Prins, L.T., Andresen, K.J., 2021. A geotechnical stratigraphy for the shallow subsurface in the Southern Central Graben, North Sea. Engineering Geology, 286, 106089. doi:10.1016/j.enggeo.2021.106089.

Prins, L.T., Andresen, K.J., 2019. Buried late Quaternary channel systems in the Danish North Sea – Genesis and geological evolution. Quatern. Sci. Rev. 223, 105943.

Prins, L.T., Andresen, K.J., Clausen, O.R., Piotrowski, J.A., 2020. Formation and widening of a North Sea tunnel valley - The impact of slope processes on valley morphology. Geomorph. 368.

Rasmussen, E.S., Vejbæk, O.V., Bidstrup, T., Piasecki, S., Dybkjær, K., 2005. Late Cenozoic depositional history of the Danish North Sea Basin: implications for the petroleum systems in the Kraka, Halfdan, Siri and Nini fields. In: Doré, A.G., Vining, B.A. (eds.) Petroleum Geology: North-West Europe and Global Perspectives – Proceedings of the 6th Petroleum Geology Conference. Geological Society, London, 1347–1358. dpoi:10.1144/0061347

Richter, H.P., 1962. Geschiebekundliche Gliederung der Elster-Kaltzeit in Niedersachen.

Rijsdijk, K., Passchier, S., Weerts, H., Laban, C., Van Leeuwen, R., Ebbing, J., 2005. Revised Upper Cenozoic stratigraphy of the Dutch sector of the North Sea Basin: towards an integrated lithostratigraphic, seismostratigraphic and allostratigraphic approach. Netherlands Journal of Geosciences/Geologie en Mijnbouw 84.

Roberts, D.H., Evans, D.J.A., Callard, S.L., Clark, C.D., Bateman, M.D., Medialdea, A., *et al*. 2018. Ice marginal dynamics of the last British-Irish Ice Sheet in the southern North Sea: Ice limits, timing and the influence of the Dogger Bank. Quaternary Science Reviews, 198, 181–207. doi:10.1016/j.quascirev.2018.08.010.

Robertson, P K., Wride, C.E., 1998. Evaluating cyclic liquefaction potential using the CPT. Can. Geotech. J. 35(3):442—459.

Rodrigues, S., Restrepo, C., Kontos, E., Teixeira Pinto, R., Bauer, P., 2015. Trends of offshore wind projects. Renewable and Sustainable Energy Reviews 49:1114-1135. doi:10.1016/j.rser.2015.04.092.

Roskosch, J., Winsemann, J., Polom, U., Brandes, C., Tsukamoto, S., Weitkamp, A., Bartholom€aus, W.A., Henningsen, D., Frechen, M., 2015. Luminescence dating of ice-marginal deposits in northern Germany: evidence for repeated glaciations during the Middle Pleistocene (MIS 12 to MIS 6). Boreas 44, 103-126.

Schack-Pedersen, S.A., Boldreel, L.O., 2016. Glaciotectonic deformations in the Jammerbugt and glaciodynamic development in the eastern North Sea. Journal of Quaternary Science, 32(2), 183–195. doi:10.1002/jqs.2887.

Schaumann, R.M., Capperucci, R.M., Bungenstock, F., McCann, T., Enters, D., Wehrmann, A., Bartholomä, A., 2021. The Middle Pleistocene to early Holocene subsurface geology of the Norderney tidal basin: new insights from core data and high-resolution sub-bottom profiling (Central Wadden Sea, southern North Sea). Netherlands Journal of Geosciences, 100. doi:10.1017/njg.2021.3.

Scheder, J., Bungenstock, F., Haynert, K., Pint, A., Schlütz, F., Frenzel, P., Wehrmann, A., Brückner, H., Engel, M., 2021. Insights into Holocene relative sea-level changes in the southern North Sea using an improved microfauna-based transfer function. Journal of Quaternary Science. doi:10.1002/jqs.3380.

Schieber, J., 2016. Mud re-distribution in epicontinental basins – Exploring likely processes. Marine and Petroleum Geology 71, 119–133.

Schnabel, C., Reinhardt, L., Laurer, U., Zeiler, M., 2014. Bearbeitung und Interpretation hochauflösender Reflexionsseismik aus dem deutschen Nordsee-Sektor - Geopotenzial Deutsche Nordsee. LBEG, BSH, BGR. http://www.gpdn.de. Accessed 25th Nov., 2021.

Schokker, J., Weerts, H., Westerhoff, W., Berendsen, H., Otter, C.D., 2007. Introduction of the Boxtel Formation and implications for the Quaternary lithostratigraphy of the Netherlands. Netherlands Journal of Geosciences/Geologie en Mijnbouw 86.

Schupp, M.F., Kafas, A., Buck, B.H., Krause, G., Onyango, V., Stelzenmüller, V., Davies I., Scott, B.E., 2021. Fishing within offshore wind farms in the North Sea: Stakeholder perspective for multi-use from Scotland and Germany. Journal of Environmental Management, 279: 1-10. doi:10.1016/j.jenvman.2020.111762.

Schwan, J., 1986. The origin of horizontal alternating bedding in Weichselian aeolian sands in Northwestern Europe. Sediment Geol 49:73-108. doi:10.1016/0037-0738(86)90016-3.

Schwan, J., 1988. The structure and genesis of Weichselian to early Holocene aeolian sand sheets in western Europe. Sediment Geol 55:197-232. doi:10.1016/0037-0738(88)90132-7.

Schwarzer, K., Ricklefs, K., Bartholomä, A., Zeiler, M., 2008. Geological development of the North Sea and the Baltic Sea. Die Küste 74:1-17.

Shennan, I., Lambeck, K., Flather, R., Horton, B., McArthur, J., Innes, J., Lloyd, J., Rutherford, M., Wingfield, R., 2000. Modelling western North Sea palaeogeographies and tidal changes during the Holocene. Geological Society, London, Special Publications 166(1), 299–319. doi:10.1144/GSL.SP.2000.166.01.15.

Sindowski, K.H., 1970. Das Quartär im Untergrund der Deutschen Bucht (Nordsee). Eiszeitalter u Gegenwart 21:33-46. doi:10.3285/eg.21.1.03.

Slingerland, R., Smith, N.D., 2004. River avulsions and their deposits. Annual Review of Earth and Planetary Sciences, 32(1), 257–285. doi:10.1146/annurev.earth.32.101802.120201.

Smed, P., 1998. Die Entstehung der dänischen und norddeutschen Rinnentäler (Tunneltäler) - Glaziologische Gesichtspunkte. Eiszeitalter und Gegenwart 48, 1–18.

Smith, D.E., Harrison, S., Firth, C.R., Jordan, J.T., 2011. The early Holocene sea level rise. Quaternary Science Reviews 30(15-16), 1846–1860.

Somme, J., 1979: Quaternary coastlines in northern France. In Oele, E. (ed.): The Quaternary History of the North Sea, 147–158. Symposia Universitatis Upsaliensis, Annum Quingentesimum Celebrantis 2, Uppsala.

Sørensen, J.C., Gregersen, U., Breiner, M., Michelsen O., 1997. High-frequency sequence stratigraphy of Upper Cenozoic deposits in the central and southeastern North Sea areas, Marine and Petroleum Geology, 14 (2), 99-123.

Spinney, L., 2008. The lost world. Nature 454: 151–153. doi:10.1038/454151a.

Steffen, H., Kaufmann, G., 2005. Glacial isostatic adjustment of Scandinavia and northwestern Europe and the radial viscosity structure of the Earth's mantle. Geophysical Journal International, 163(2):801–812.

Steffen, H., Wu, P., 2011. Glacial isostatic adjustment in Fennoscandia: A review of data and modeling. Journal of Geodynamics 52, 169–204.

Stewart, M.A., Lonergan, L., Hampson, G., 2012. 3D seismic analysis of buried tunnel valleys in the Central North Sea: tunnel valley fill sedimentary architecture. In: Huuse, M., Redfern, J., Le Heron, D.P., Dixon, R.J., Moscariello, A., Craig, J. (eds) Glaciogenic Reservoirs and Hydrocarbon Systems. Geological Society, London, Special Publications, 368, 173–184. doi:10.1144/SP368.9.

Stewart, M.A., Lonergan, L., Hampson, G., 2013. 3D seismic analysis of buried tunnel valleys in the central North Sea: morphology, cross-cutting generations and glacial history. Quaternary Science Reviews, 72, 1–17. doi:10.1016/j.quascirev.2013.03.016.

Stewart, S. A., Coward, M. P., 1995. Synthesis of salt tectonics in the southern North Sea, UK. In: Marine and Petroleum Geology 12 (5), S. 457–475. doi:10.1016/0264-8172(95)91502-G.

Stoker, M.S., Balson, P.S., Long, D., Tappin, D.R., 2010. An Overview of the Lithostratigraphical Framework for the Quaternary Deposits on the United Kingdom Continental Shelf, p. 48. British Geological Survey Research Report, RR/00/00.

Streif, H., 2004. Sedimentary record of Pleistocene and Holocene marine inundations along the North Sea coast of Lower Saxony, Germany. Quaternary International, 112(1), 3–28. doi:10.1016/s1040-6182(03)00062-4.

Strozyk, F., Reuning, L., Scheck-Wenderoth, M., Tanner, D.C., 2017. The Tectonic History of the Zechstein Basin in the Netherlands and Germany. In: Permo-Triassic Salt Provinces of Europe, North Africa and the Atlantic Margins: Elsevier, S. 221–241.

Törnqvist, T.E., 1994. Middle and late Holocene avulsion history of the River Rhine (Rhine-meuse delta, Netherlands). Geology, 22(8), 711–714.

Toucanne, S., Zaragosi, S., Bourillet, J.F., Cremer, M., Eynaud, F., van Vliet-Lanoë, B., Penaud, A., Fontanier, C., Turon, J.L., Cortijo, E., 2009. Timing of massive 'Fleuve Manche' discharges over the last 350kyr: İnsights into the European ice-sheet oscillations and the European drainage network from MIS 10 to 2. Quaternary Science Reviews 28(13-14), 1238–1256. doi:10.1016/j.quascirev.2009.01.006.

van der Molen, J., 2002. The influence of tides, wind and waves on the net sand transport in the North Sea. Continental Shelf Research 22(18-19), 2739–2762.

van der Molen, J., Swart, H.E., 2001. Holocene tidal conditions and tide-induced sand transport in the southern North Sea. Journal of Geophysical Research: Oceans 106(C5), 9339–9362. doi:10.1029/2000jc000488.

van der Vegt, P., Janszen, A., Moscariello, A., 2012. Tunnel valleys: current knowledge and future perspectives. In Huuse, M., Redfern, J., Dixon, R.J., Craig, J., Moscariello, A., Le Heron, D.P. (eds). Glaciogenic Reservoirs and Hydrocarbon Systems, 75–97, Geological Society, London, Special Publications 368. doi:10.1144/SP368.13.

Vardy, M.E., Vanneste, M., Henstock, T.J., Clare, M.A., Forsberg, C.F., Provenzano, G., 2017. State-of-the-art remote characterization of shallow marine sediments: the road to a fully integrated solution. Near Surf. Geophys. 15, 387–402. doi:10.3997/1873-0604.2017024.

Vejbæk, O.V., 1997. Dybe strukturer i danske sedimentære bassiner. In: Geologisk Tidsskrift (4), S. 1–31.

Vink, A., Steffen, H., Reinhardt, L., Kaufmann, G., 2007. Holocene relative sea-level change, isostatic subsidence and the radial viscosity structure of the mantle of northwest Europe (Belgium, the Netherlands, Germany, southern North Sea). Quaternary Science Reviews 26(25-28), 3249–3275. doi:10.1016/j.quascirev.2007.07.014.

Ward, S.L., Neill, S.P., Scourse, J.D., Bradley, S.L., Uehara, K., 2016. Sensitivity of palaeotidal models of the northwest European shelf seas to glacial isostatic adjustment since the Last Glacial Maximum. Quaternary Science Reviews 151, 198–211.

Wedel-Heinen, J., Ronold, K.O., Madsen, P.H., 2007. *Revision of DNV Design Standard for Offshore Wind Turbine Structures.* Vol. 5: Ocean Space Utilization; Polar and Arctic Sciences and Technology; The Robert

Dean Symposium on Coastal and Ocean Engineering; Special Symposium on Offshore Renewable Energy. doi:10.1115/omae2007-29118.

Weihrauch, S., Balthes, R., van der Zwaag, G., 2009. Pfahlgründungen für Offshore-Windparks - neue Entwicklungen bei der Baugrunderkundung und bei der Pfahlbemessung. In: Stahlmann J (ed) Pfahlsymposium 2009 - Mitteilung des Instituts für Grundbau und Bodenmechanik - Heft Nr. 88. Technische Universität Braunschweig, Braunschweig, Germany, pp 213-230.

Wiemann, J., Lesny, K., Richwien, W., 2002. Gründung von Offshore-Windenergieanlagen - Gründungskonzepte und geotechnische Grundlagen. Mitteilungen aus dem Fachgebiet Grundbau und Bodenmechanik, vol 29. Verlag Glückauf GmbH, Essen.

WindEurope 2018. Offshore wind in Europe – Key trends and statistics. WindEurope Business Intelligence. doi:10.1016/S1471-0846(02)80021-X.

Wingfield, R., 1990. The origin of major incisions within the Pleistocene deposits of the North Sea. Marine Geology, 91, 31–52.

Winsemann, J., Koopmann, H., Tanner, D.C., Lutz, R., Lang, J., Brandes, C., Gaedicke, C., 2020. Seismic interpretation and structural restoration of the Heligoland glaciotectonic thrust-fault complex: Implications for multiple deformation during (pre-) Elsterian to Warthian ice advances into the southern North Sea Basin. Quaternary Science Reviews, 227**,** 106068. doi:10.1016/j.quascirev.2019.106068.

Woodroffe, C.D., Murray-Wallace, C.V., 2012. Sea-level rise and coastal change: The past as a guide to the future. Quaternary Science Reviews 54, 4–11.

Wright, L.D., 1995. Morphodynamics of inner continental shelves. Marine science series. CRC Press, Boca Raton, London.

Zeiler, M., Schulz-Ohlberg, J., Figge, K., 2000. Mobile sand deposits and shoreface sediment dynamics in the inner German Bight (North Sea). Mar Geol 170:363-380. doi:10.1016/S0025-3227(00)00089-X.

Ziegler, P.A., 1990. Geological Atlas of Western and Central Europe. Shell Internationale Petroleum Maatshappij BV, The Hague.

Appendix

(The Appendix belongs to Chapter 5)

Fig. S1. Complete CPT information and other measured parameters for the selected core sites used in this study

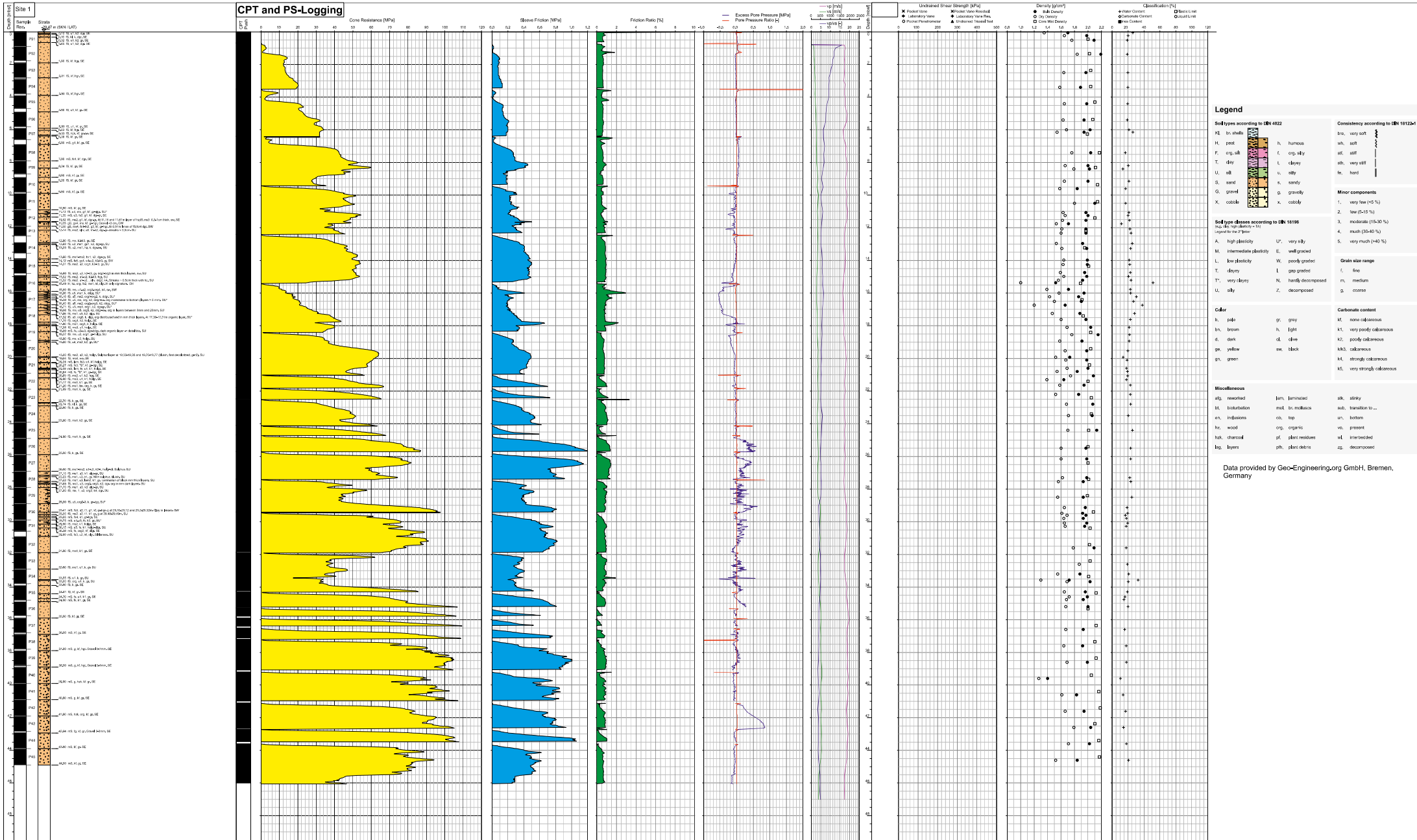

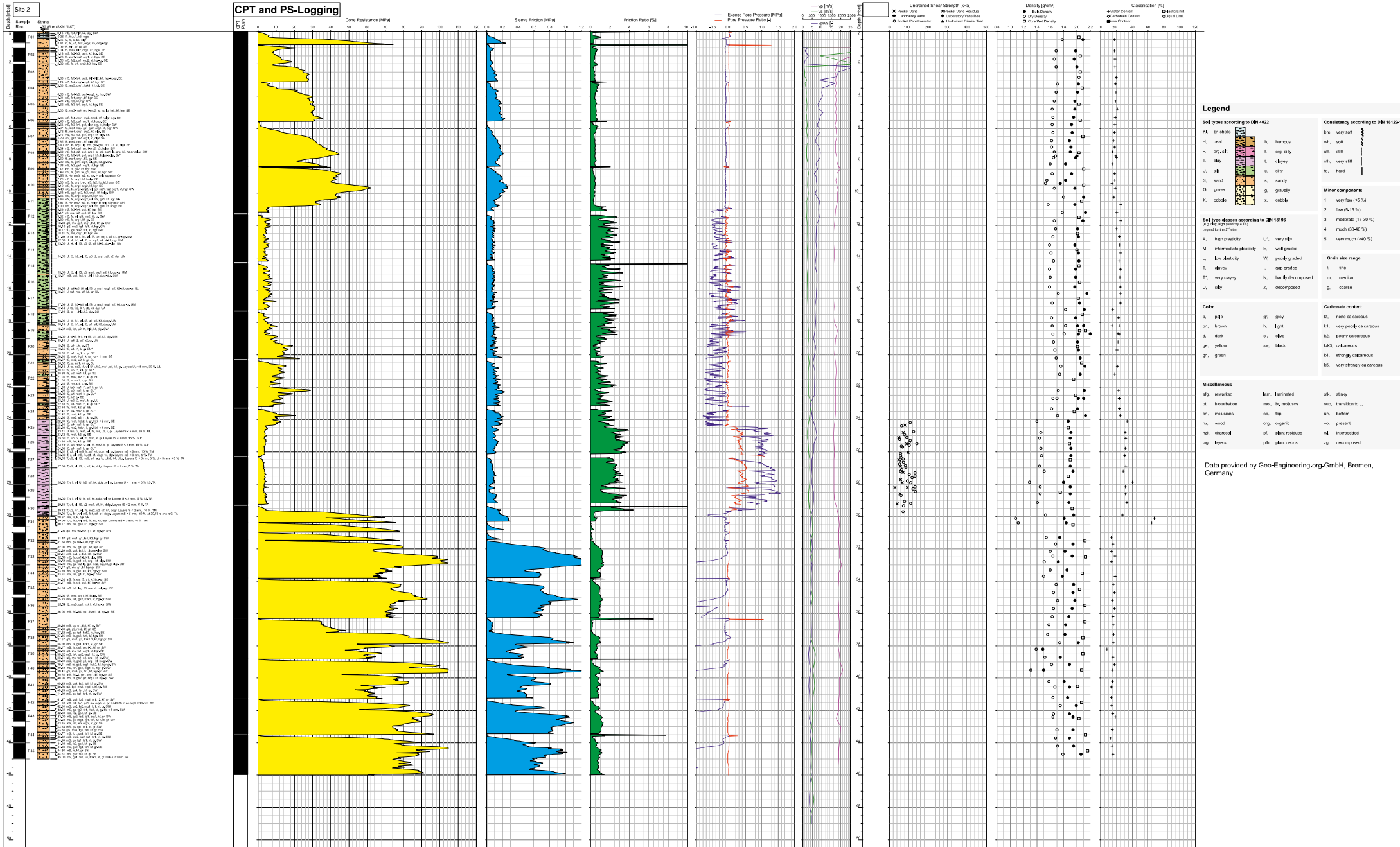

Legend

Soil types according to DIN 4022

Xt,	br. shells		
H,	peat	h,	humous
F,	org. silt	f,	org. silty
T,	clay	t,	clayey
U,	silt	u,	silty
S,	sand	s,	sandy
G,	gravel	g,	gravelly
X,	cobble	x,	cobbly

Consistency according to DIN 18123+1

vs,	very soft
sft,	soft
stf,	stiff
sth,	very stiff
fe,	hard

Soil type classes according to DIN 18196
(xg/x, clay: high plasticity = TA)
Legend for the 2nd letter:

A,	high plasticity	U*,	very silty
M,	intermediate plasticity	E,	well graded
L,	low plasticity	W,	poorly graded
T,	clayey	I,	gap graded
T*,	very clayey	N,	hardly decomposed
U,	silty	Z,	decomposed

Minor components

1,	very few (<5 %)
2,	few (5-15 %)
3,	moderate (15-30 %)
4,	much (30-40 %)
5,	very much (>40 %)

Color

b,	pale	gr,	grey
bn,	brown	h,	light
d,	dark	ol,	olive
ge,	yellow	sw,	black
gn,	green		

Grain size range

f,	fine
m,	medium
g,	coarse

Carbonate content

kf,	none calcareous
k1,	very poorly calcareous
k2,	poorly calcareous
kk3,	calcareous
kf,	strongly calcareous
k5,	very strongly calcareous

Miscellaneous

afg,	reworked	lam,	laminated
bt,	bioturbation	mol,	bi, molluscs
en,	inclusions	co,	top
hz,	wood	org,	organic
hzk,	charcoal	pf,	plant residues
lag,	layers	pfh,	plant debris
slk,	slinky		
sub,	transition to ...		
un,	bottom		
vo,	present		
wl,	interbedded		
zg,	decomposed		

Data provided by Geo-Engineering.org.GmbH, Bremen, Germany

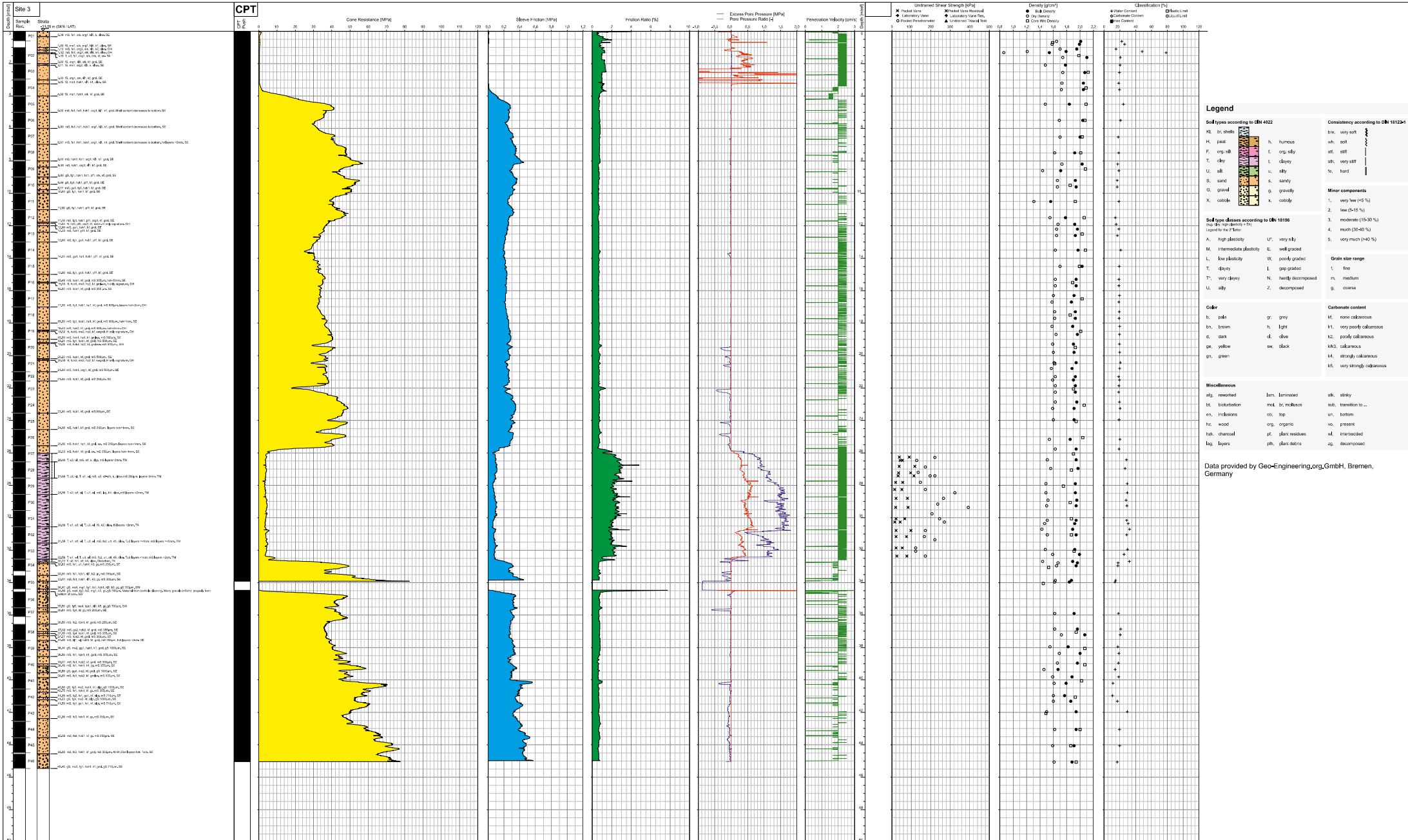
Site 3
Depth (mbsf)
Sample
Rec.
Strata
CPT
Cone Resistance [MPa]
Sleeve Friction [MPa]
Friction Ratio [%]
Excess Pore Pressure [MPa]
Pore Pressure Ratio [-]
Penetration Velocity (cm/s)
Undrained Shear Strength [kPa]
Density [g/cm³]
Classification [%]
Legend
Soil types according to DIN 4022
Consistency according to DIN 18123+1
Soil type classes according to DIN 18196
Minor components
Grain size range
Color
Carbonate content
Miscellaneous
Data provided by Geo-Engineering.org.GmbH, Bremen, Germany

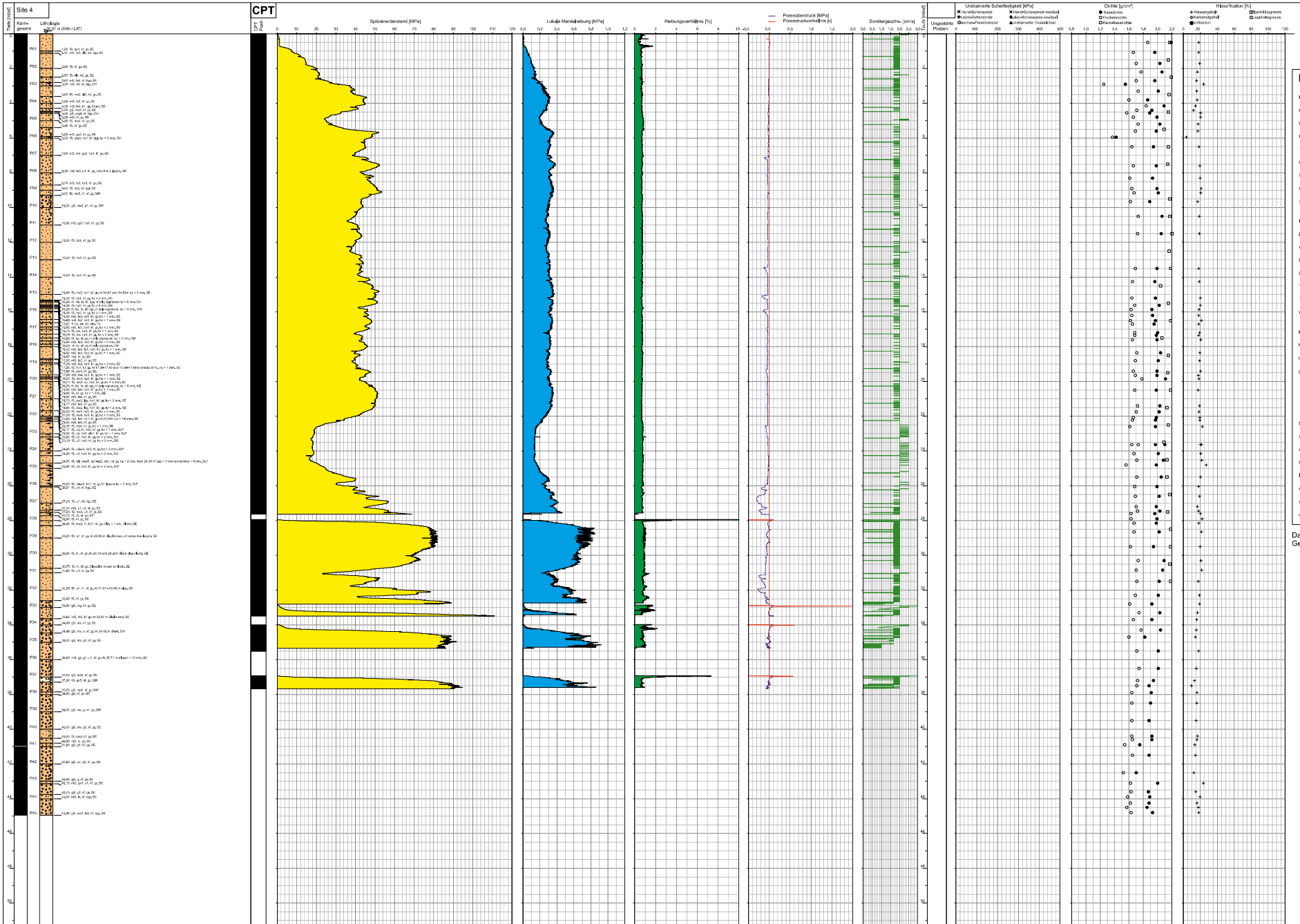

Legende

Bodenarten nach DIN 4022:

Kd, Schlick		
H, Torf	h, humos	
F, Mudde	f, muddig	
T, Ton	t, tonig	
U, Schluff	u, schluffig	
S, Sand	s, sandig	
G, Kies	g, kiesig	
X, Stein	x, steinig	

Konsistenzen nach DIN 18122-1:

breiig	
weich	wh
steif	stf
halbfest	sth
fest	fe

Bodengruppen nach DIN 18196: z.B. Ton, ausgeprägt plastisch, TA

Bedeutung des 2. Buchstabens:

A, ausgeprägt plastisch	U*, stark schluffig
M, mittel plastisch	E, enggestuft
L, leicht plastisch	W, weitgestuft
T, tonig	I, intermittierend
T*, stark tonig	N, kaum zersetzt
U, schluffig	H, zersetzt

Korngrößenbereich:	Nebenanteile:	Kalkgehalt:
f, fein	1, sehr schwach (< 5 %)	kf, kalkfrei
m, mittel	2, schwach (5 – 15 %)	k1, sehr schwach kalkhaltig
g, grob	3, mittel (15 - 30 %)	k2, schwach kalkhaltig
	4, stark (30 – 40 %)	k, kalkhaltig
	5, sehr stark (> 40 %)	k4, stark kalkhaltig
		k5, sehr stark kalkhaltig

Sonstige Bezeichnungen:		Farbe:	
afg, aufgearbeitet	pfh, Pflanzenhäcksel	b, blass	h, hell
en, Einschlüsse	stk, stinkt	bn, braun	ol, olive
hz, Holz	sub, Übergang zu	d, dunkel	sw, schwarz
lag, Lagen	un, unten	ge, gelb	
mol, Molluskenschill	vo, vorhanden	gn, grün	
ob, oben	wl, wechsellagernd	gr, grau	
org, organisch	zg, zersetzt		

Data provided by Geo-Engineering.orgGmbH, Bremen, Germany

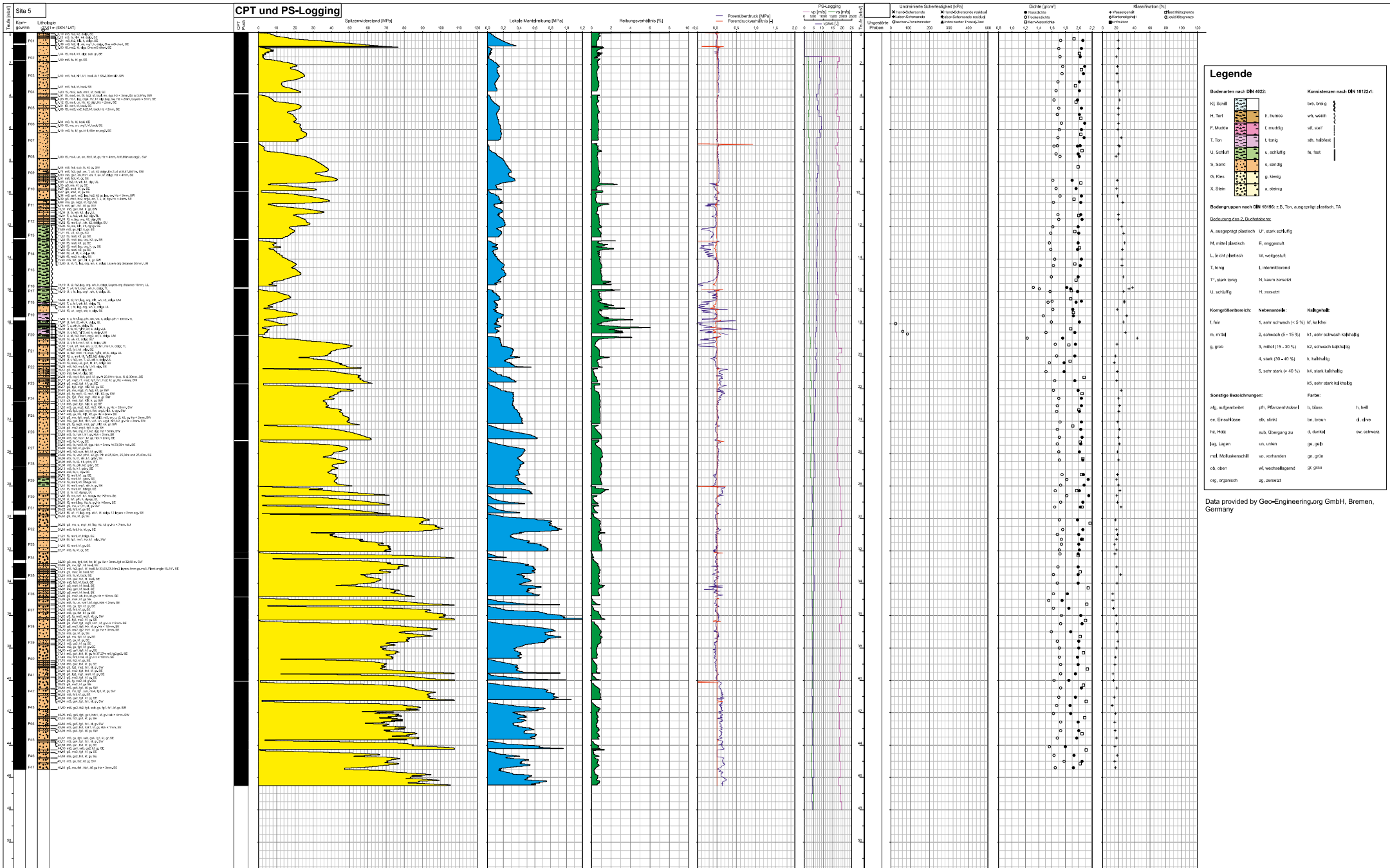
Site 5
CPT und PS-Logging
Kern-gewinn
Lithologie
22.81 m (SKN / LAT)
Tiefe [mod]
CPT
Push
Spitzenwiderstand [MPa]
Lokale Mantelreibung [MPa]
Reibungsverhältnis [%]
Porenüberdruck [MPa]
Porendruckverhältnis [-]
PS-Logging
vp [m/s]
vs [m/s]
vp/vs [-]
Ungestörte Proben
Bohrlochdurchm.
Undrainierte Scherfestigkeit [kPa]
Dichte [g/cm³]
Klassifikation [%]
Legende
Bodenarten nach DIN 4022:
Konsistenzen nach DIN 18122-1:
Bodengruppen nach DIN 18196: z.B. Ton, ausgeprägt plastisch, TA
Bedeutung des 2. Buchstabens:
Korngrößenbereich:
Nebenanteile:
Kalkgehalt:
Sonstige Bezeichnungen:
Farbe:
Data provided by Geo-Engineering.org GmbH, Bremen, Germany

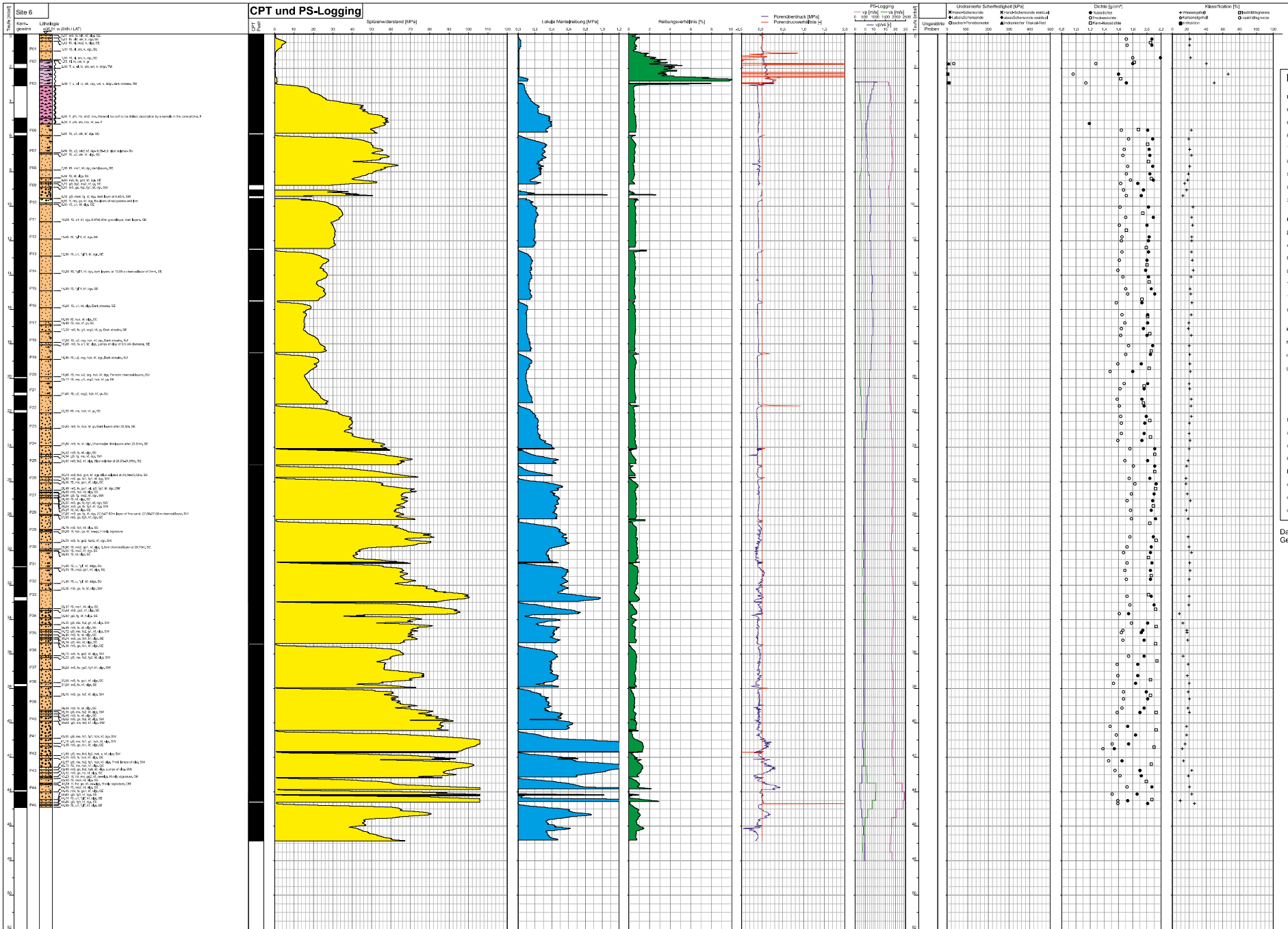

Legende

Bodenarten nach DIN 4022:

Kl, Schill	
H, Torf	h, humos
F, Mudde	f, muddig
T, Ton	t, tonig
U, Schluff	u, schluffig
S, Sand	s, sandig
G, Kies	g, kiesig
X, Stein	x, steinig

Konsistenzen nach DIN 18122-1:

breiig	bre, breig
weich	wh, weich
steif	stf, steif
halbfest	sth, halbfest
fest	fe, fest

Bodengruppen nach DIN 18196: z.B. Ton, ausgeprägt plastisch, TA

Reduzierung des 2. Buchstabens:

A, ausgeprägt plastisch	U*, stark schluffig
M, mittel plastisch	E, enggestuft
L, leicht plastisch	W, weitgestuft
T, tonig	I, intermittierend
T*, stark tonig	N, kaum zersetzt
U, schluffig	H, zersetzt

Korngrößenbereich:

f, fein	
m, mittel	
g, grob	

Nebenanteile:

1, sehr schwach (< 5 %)	kf, kalkfrei
2, schwach (5 - 15 %)	k1, sehr schwach kalkhaltig
3, mittel (15 - 30 %)	k2, schwach kalkhaltig
4, stark (30 - 40 %)	k, kalkhaltig
5, sehr stark (> 40 %)	k4, stark kalkhaltig
	k5, sehr stark kalkhaltig

Kalkgehalt:

Sonstige Bezeichnungen:

afg, aufgearbeitet	
en, Einschlüsse	
hz, Holz	
lag, Lagen	
mol, Molluskenschill	
ob, oben	
org, organisch	
pfh, Pflanzenhäcksel	
stk, stinkt	
sub, Übergang zu	
un, unten	
vo, vorhanden	
wl, wechsellagernd	
zg, zersetzt	

Farbe:

b, blass	h, hell
bn, braun	ol, olive
d, dunkel	sw, schwarz
ge, geb	
gn, grün	
gr, grau	

Data provided by Geo-Engineering.org GmbH, Bremen, Germany

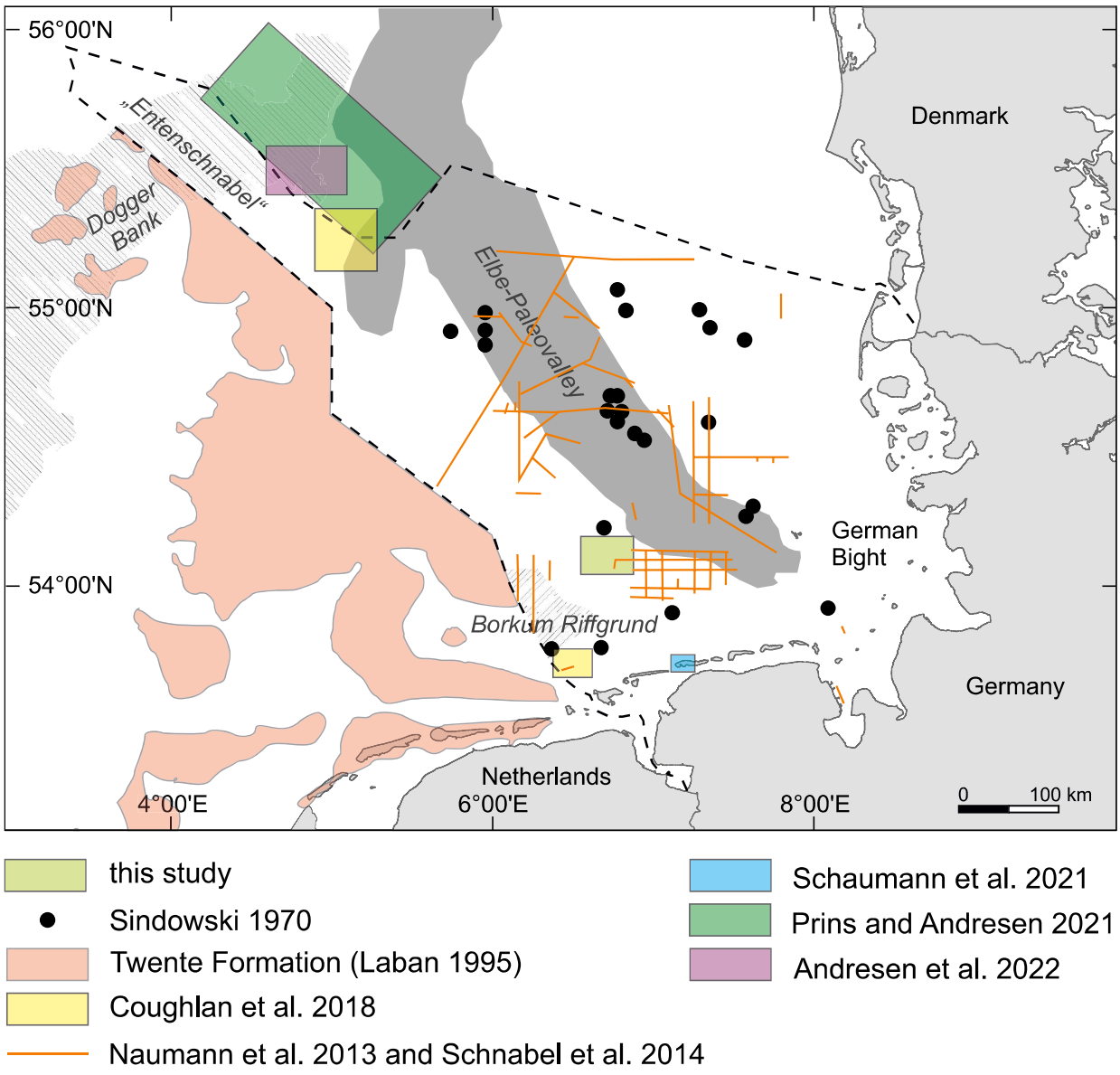

Fig. S2. Part of the North Sea showing the study areas from previous and present studies